INFORMATION TO USERS

This manuscript has been reproduced from the microfilm master. UMI films the text directly from the original or copy submitted. Thus, some thesis and dissertation copies are in typewriter face, while others may be from any type of computer printer.

The quality of this reproduction is dependent upon the quality of the copy submitted. Broken or indistinct print, colored or poor quality illustrations and photographs, print bleedthrough, substandard margins, and improper alignment can adversely affect reproduction.

In the unlikely event that the author did not send UMI a complete manuscript and there are missing pages, these will be noted. Also, if unauthorized copyright material had to be removed, a note will indicate the deletion.

Oversize materials (e.g., maps, drawings, charts) are reproduced by sectioning the original, beginning at the upper left-hand corner and continuing from left to right in equal sections with small overlaps.

Photographs included in the original manuscript have been reproduced xerographically in this copy. Higher quality 6" x 9" black and white photographic prints are available for any photographs or illustrations appearing in this copy for an additional charge. Contact UMI directly to order.

Bell & Howell Information and Learning
300 North Zeeb Road, Ann Arbor, MI 48106-1346 USA
800-521-0600

Experimental Investigation of Noise Reduction In Supersonic Jets due to Jet Rotation and to Nozzle Geometry Changes

By

Said S. AlGattus

A thesis

in

The Department

of

Mechanical Engineering

Presented in Partial Fulfillment of the requirements

for the degree of Doctor Philosophy

Concordia University

Montreal, Quebec, Canada

APRIL 1999

Abstract

Experimental Investigation of Noise Reduction In Supersonic Jets due to Jet Rotation and Nozzle Geometry Changes

Said S. Algattus

The present work deals with two different methods used for noise reduction in supersonic jets. The first method employed consisted of a swirl chamber, which produced axisymmetric jets with a tangential velocity component. This component was found to affect the structure of the jet cell and the internal oblique shocks formed inside. In the second method, the nozzle exit plane of the cylindrical chamber was perturbed such that the nozzle's exit lip was not lying in one plane perpendicular to the axis of symmetry of the nozzle.

These two methods were investigated experimentally via spark Schlieren photography, static, Pitot and sound pressure measurements. Schlieren photography was employed to visualize the flow and shock structure associated with any of the above changes. Static and pitot pressure measurements were carried out to obtain the velocity distribution whereas sound pressure measurements were used to determine the resulting gain in noise reduction. The introduction of a small flow rotation was found to weaken the internal shock strength and to reduce the cell length and screech noise generated.

Increasing the flow rotation beyond a certain limit was found to effect the shock structure without any noticeable noise reduction. Sinusoidal perturbation was found to affect the symmetry and strength of the oblique shocks in the supersonic cells. A considerable noise reduction was also noted with perturbation amplitude equal to 12.5% of the nozzle inside diameter. Larger perturbation did not result in a further noise reduction. In the first and second methods, a maximum noise reduction of 12 dB and 8 dB were measured, respectively.

ACKNOWLEDGMENTS

The author would like to thank his thesis supervisor Dr. R. A. Neemeh for his constant guidance and help through the course of this investigation.

The author would like to thank Ms. Laura Neemeh for her assistance and help during the course of the present investigation.

The author would like to thank Mr. John Elliot and Mr. Paul Scheuiller and his associates in their numerous help in the experimental phase of this work.

Special thanks are due to his wife and children for their understanding and support throughout the course of this investigation.

This study is financially supported by Libyan Secretary of Education, and administered by Canadian Bureau for International Education (CBIE) No 1396.

Table of Contents

List of Figures

Nomenclature

a	Speed of sound
D	Nozzle exit diameter
f_s	Screech frequency
L	Shock cell length
M	Flow Mach number
M_ϕ	Swirl Mach number
P	Pressure
St	Strouhal number
T	Temperature
V	Flow velocity
x_o, z_o	Tool coordinates
β	$\sqrt{[M_j^2 - 1]}$
θ	Flow angle
ρ	Density
γ	Specific heat ratio (C_p/C_v)

Subscripts

c	Critical conditions (M = 1)
j	Fully expanded jet property
o	Stagnation property
r	Radial component
θ	Tangential component

Chapter 1

Introduction

The development of large transport airplanes using jet engines with supersonic exhaust velocities has made the problem of jet exhaust noise during take off critical around the airports. In order to suppress this noise, the noise generation mechanism, its location, as well as the source both for the near and far fields must be understood. The suppression of the noise will increase the comfort of both the aircraft passengers and the neighboring communities while decreasing the structural fatigue on buildings. Furthermore, some of the proven noise reduction techniques are not yet fully understood and are still under investigation. The objectives of the current work are to find methods capable of reducing screech noise in supersonic jets and to have a better understanding of the reasons of such noise reduction. Before these methods are introduced a literature survey about the different mechanisms of noise generation and suppression will be presented in the following two sections.

1.1 Types of noise and generation mechanism

Community noise is a major technological challenge facing future supersonic transports, such as the High-Speed Civil Transport (HSCT). The hot supersonic jets exhausting from the engines of such aircraft are powerful noise generators and propagate with a convective velocity, which is supersonic with respect to the surrounding air stream, especially during take-off. Untreated, they create noise levels, which are environmentally unacceptable. Existing techniques, like mixer-ejectors, reduce noise but inflict serious thrust and weight penalties.

Supersonic flow can be obtained using either a converging or a converging-diverging nozzle. In the latter case, both under and over-expanding jet conditions take place while convergent nozzles can only produce an under expanded jet. When a converging nozzle is choked and is operating at an ambient pressure less than the critical pressure ratio, expansion fans will occur at the lip of the nozzle and a system of quasi-periodic shock cells appear in the jet plume. The structure and length of each cell depends on the operating and design conditions. It is constituted of a series of shock waves and expansion fans reflecting at the jet boundary thus generating the various types of sound radiated noise, that are illustrated in figure 1.1.

The noise generated by imperfectly expanded supersonic jets consists of two principal components: turbulent mixing noise and shock associated noise. The latter can be either broadband or screech tone and can only be present in jet flow if it is operating at off design conditions, as shown in figure 1.1. Turbulent mixing noise is known to exist in both subsonic and supersonic flows and is directly generated by turbulence that exists in

jet flow. At design conditions, the jet is shock free and turbulence mixing noise is dominant. At off design conditions, large-scale turbulence occurs and generates shock noise in supersonic jet [1].

1.1.1 Noise from Subsonic Air Jet

In the past few decades, both theoreticians and experimentalists have been engaged into the production of noise from turbulent jets. The aim of investigation was mainly focused on the relationship between the far field jet noise and the activities of the large-scale orderly structures within the turbulent shear layer of the jet. The dynamics of the coherent structures in the shear layer have been studied extensively by numerous workers using the technique of conditional sampling and flow visualization [2, 3, 4]. It is now a well known fact that the major activities in the jet are the pairings of vortex rings to form the coherent structures and their eventual break down. Their results clearly demonstrate that large rate of change of vortex ring velocities occurs during the pairing process. Experimentally, Kibens [5] used acoutic excitation to establish the relationship of the jet noise and the vortex pairing process. However, this method did not determine the actual mechanism involved in the sound generation. Laufer and Yen [6], with the instability wave approach, suggested that the rapid amplitude change of the convective instability waves within the first diameter of the jet is responsible for the jet noise emission. Bridges and Hussain [7] showed how the initial condition of a jet affected the pairing noise while Hussain [8], based on turbulent jet noise results, argued that the break

down of vortex rings into substructures and the interaction of these azimuthally spaced structures produced most of the noise. Flow visualization clearly illustrated [3, 9, 10] the process of vortex ring pairing development, thus showing that it is highly probable that these are the major noise source in the jet. Tang and Ko [11] investigated the noise production mechanism in a subsonic jet under controlled acoustic excitation. They also concluded that the sound generated by vortices is correlated with the acceleration and deceleration of the vortical elements of both the thin vortex rings in the pairing stage and the thicker vortex rings during the breakdown process. This clarifies the role of the rate of change of velocities of the vortical elements on the generation of jet noise.

1.1.2 Noise from Supersonic Air Jets

Shock associated noise is believed to be a result of the interaction of the turbulent structures, created at the nozzle exit plane, with the internal shock created in each cell. Such an interaction and its spectra is characterized by a steep rise, on the low frequency side, to the dominant peak, followed by a gentle decrease on the high frequency side. Broadband shock associated noise and screech tones are both forms of shock noise. The broadband shock noise arises as a result of interaction of turbulent eddies with shock waves. The screech tones are special cases of the broadband noise; namely, the results of the interaction between large-scale turbulence structure and the instability waves originating at the nozzle lip with the quasi-periodical shock cell structure. The interaction occurs at the edge of the jet in the region of the fourth and fifth shock cells. The screech tone noise propagates outside the jet and upstream towards the nozzle lip, further exciting

the instability waves thus completing an acoustic feedback loop. Two modes of screech tones (axisymmetric / toroidal and helical/flapping) are known to exist, although not occurring simultaneously [12]. Helical modes become increasingly dominant at high-pressure ratios.

Various investigators using small-scale jets have studied the noise generated from a supersonic jet. Powell [13] was able to determine the cause of the loud screech obtained from room temperature supersonic jets using Schlieren photography. He concluded that initial flow disturbances issuing from the nozzle exit caused jet screech and propagated downstream, interacting with the shock cell system thereby generating noise. The resulting noise was assumed to radiate upstream outside the supersonic flow, thereby producing a resonant loop resulting in the screech tone and associated harmonics. Davies and Oldfield [14] investigated the shock cell system in circular jets. Based on their findings, they concluded that screech tones varied with changes in screech tone frequency and pressure ratio. Photographic evidence of Powell's feedback loop mechanism was obtained by Poldervaart et al [15]. Their results showed that when the screech tone impinges on the nozzle exit, it causes a vortex to develop and convect downstream. The vortex interaction with the shock cells perpetuates the screech. Lighthill [16] derived an analytical method for acoustic noise based on dimensional analysis and experimental acoustic data. The work of Harper-Bourne and Fisher [17] is one of the most important contributions to the theory of shock associated noise. Their primary interest was in supersonic jets discharged from converging nozzles. They were able to identify a broadband noise component having spectral and directional characteristics, which are different from that of turbulent mixing noise. They adopted a simple model consisting of

an array of point sources spaced at a length nearly equal to that of the shock cells. These sources are then set into oscillatory motion. In order to make the screech tones steadier, they placed a reflecting surface at the nozzle exit plane resulting in an improvement of the stationary quality of the tones. However, an increase in screech amplitude was also noted. Covering the surface with acoustically absorbent foam, resulted in a reduced screech tone amplitude which was still greater than the tones from the jet without the reflecting surface.

Since then a good number of theoretical and experimental investigations on this subject have been carried out. Seiner and Norum [18] 1980, Tam 1982 [19] and Tam and Chen [20] 1985 adopted different approaches and found very satisfactory agreement with previous studies.

1.2 Methods of noise suppression

A considerable number of experiments have been conducted on noise suppression. Some of these studies tackled the noise generation mechanism and others isolated the factors causing it.

In subsonic and supersonic jets, disturbances are created due to the interaction of the jet and the surrounding atmospheric air. Furthermore, the thrust formula shows that the thrust is proportional to the square of the relative velocity, while the turbulent component of noise is related to the eighth power of the speed. In gas turbines, this led to

the study of what is called bypassing [21]. A reduction in noise can be achieved by larger by-pass ratio with rapid mixing of secondary flow and the main jet before leaving the nozzle. This method is never without disadvantages since more by-pass ratio means higher compressor work and more intake noise. Based on the above principle similar methods were employed using ejectors, which by-pass the exhaust using ducts with diameters greater than that of the exit. Although this method was found to be very effective, it had limited applications in aircraft engines due to its higher drag, weight and its unpractical length. It could be used on the ground to reduce fan noise. In addition, the noise generated from engine test rigs projected the velocity profile modification by modifying the exit geometry. For example by comparing the flow from the squared velocity profile and parabolic one, it was found that the noise generated from the former one is less than that of the latter. The investigation of turbulent noise generated when two jets were in close proximity showed that the interference of two jets reduces the turbulent noise [22]. It appears from the above discussion that the requirement for turbulent mixing noise reduction is introducing a secondary flow rapidly mixed with the main flow. Due to this fact many studies have been initiated to use this phenomena and reduce the turbulent noise.

Most of the studies to suppress the shock-associated noise were directed to screech tone repression, which was believed to cause structural damage if its amplitude increased beyond a certain level. Methods used include porous plug, where the shocks are canceled at the plug surface, inverted velocity profile as an active suppression of the noise [23], coaxial jet Kuhlman [24], lip projection and nozzle wrapping Powell [13], nozzle asymmetry and notches. The above mentioned methods basically alter the nozzle

geometry and flow conditions. Ahuja and Brown [25] conducted a series of experiments on the effect of tabs on supersonic jets and found the importance of this simple concept in suppression of the screech tone. Bradbury et al [26] where the first to conduct a study on jets under the influence of tabs with the use of various arrangements of rectangular tabs. They correlated the number of tabs used to the velocity decay at jet centerline.

Tanna [1] used a converging nozzle with tabs (lip projection) at the exit to cancel the screech tone. He suggested that flow symmetry at the nozzle exit was required to establish the screech tone feedback loop between the shock cells and nozzle lip which was disrupted by the tabs resulting in screech tone elimination. In 1993, Samimy [27] experimentally investigated the effect of a vortex generator in the form of small tabs at the nozzle exit thereby eliminating the screech tone and distorting the shock cell structure in the entire jet cross section.

When two jets are closely spaced the screech tone is found to be higher due to the coupling process between the two plumes. In the last decade many investigators studied this phenomena. Seiner [28] and Shaw [29] deduced that the amount of screech may be increased up to 6 dB. The suppression methods of single jets are also valid for twin jets since suppression of one jet results in coupling of the two jets and the screech amplitude is reduced below the fatigue level or even eliminated.

Recent work conducted at Concordia University by Neemeh and Roshanzamir [30] employed combinations of rectangular tabs in the choked nozzle both for single and twin jets and variation of lateral spacing of the two jets using acoustical and optical observations. Screech tone suppression was found to be most effective when three tabs and a small spacing of S/D were used.

In 1992, Longmir, Eaton and Elkins [31] investigated the downstream flow structure of crown-shaped nozzles with a variable number of peaks (teeth) and lengths of a scale model of a jet using smoke seeded flow. It was shown that these nozzles can cause significant deviation from axisymmetry and this tends to inject longitudinal vorticity into downstream flow, which increases the entrainment of ambient air into the jet core. They have also concluded that a longer tooth does not increase the deviation from the axisymmetry but does increase the entrainment in the jet core. Reynolds [32], Rose [33] and others have investigated subsonic and supersonic swirling jets. Their conclusion includes the facts that swirling jets mix more rapidly than axial jets. The swirl component of the velocity is found to decay more rapidly than the axial component as the jet mixes with surrounding air.

Smith [34] investigated supersonic swirling flow using the method of characteristics. From the Schlieren photographs, he found that the cellular structure of the core region does not extend as far downstream as in the corresponding jet without swirl, and generalized the result that all swirling jets are mixing more rapidly than their non-swirling counterpart. He added that the shock cell length, for all the pressure ratios, do not change much for $M_{swirl} \leq 0.5$. This is not the case, as it will be clearly demonstrated in this investigation. He suggested that the exit flow is rotating almost as a solid body with a small annular region of fluid. In 1973, Smith [34] investigated both theoretically and experimentally, the effect of swirl on a supersonic jet. He concluded that an increase in swirl results in a shortening of the cell length, the formation of shocks nearer to the nozzle and may cause, in some cases, reversed flow of air in the core when they increase in strength.

In 1985, Carpenter [35] used a linearized theory to examine the effect of swirling supersonic jets and its application to shock-cell noise. His results sowed that for certain types of swirl, shock-associated noise was greatly reduced and sometimes even eliminated at higher swirl levels. However, a very small thrust loss was also obtained.

In 1996, Carvalho and Heitor [36] conducted a series of experiments to observe the response changes in the flow structure to changes in swirl and outer Reynolds number using laser light sheet visualisation. The swirl was produced using either a swirler with 40 flat vanes or a cylindrical chamber with 12 tangential slots. The results showed that at low swirl, normal jet behavior was obtained but with an increasing spreading rate and entrainment. By increasing the swirl level, a spiral flow type was formed. The period of the spiral was also found to decrease with higher swirl.

In 1997, Yu and Chen [37] examined the effect of swirl on screech tone noise in supersonic jets by injecting various strengths of swirl in the path of axial flow in order to induce it, using a scale model of 1 cm exit diameter. They concluded that swirl did not eliminate the screech tone and that its presence is due to the quasi-periodic shock structure and the inherent instability waves propagating downstream of the nozzle jet boundary. Their results also showed that increasing swirl had no effect noise reduction. This could be explained by the fact that the injected tangential swirl has enough inertia to drag the axial jet to swirl.

1.3 Scope of Thesis

The suppression of the jet noise is very complicated. Various suppresser configurations have been investigated as was stated above. Most of the methods surveyed suppressed the jet noise after it had been generated from the source. For example, the use of tangential jets to induce flow rotation, just before the nozzle exit plane introduces large-scale turbulence resulting from their mixing with the main jet. The use of triangular peaks and rectangular tabs are found to reduce screech noise but are not based on any particular foundation other than it works under certain conditions.

Swirling flow is found to effect the jet structure and the noise emitted from the jet. The results obtained previously are very confusing. Some researchers claim that fluid rotation does not have any effect on the jet structure or noise emitted from it and some claim the contrary. The results are therefore contradictory and the reason is the apparatus used to produce the swirl in the jet. Tangential jets, placed just upstream the nozzle exit, introduce an additional turbulence noise that is added to the equation. The proper way to determine the effect of swirl is to introduce it to the flow without perturbing it (i.e. well upstream of the nozzle exit).

The primary objective of the present work is to experimentally determine the effect of swirling flow on jet noise suppression using a small-scale, 12 mm inside diameter nozzle and 32 mm long. A swirling chamber is used to allow the variation in the swirl velocity for any given jet pressure ratio without adding any additional disturbances to the flow. This chamber will be introduced in chapter 3. The flow structure inside the vortex chamber and that exiting the nozzle will be determined via detailed pressure

measurements and spark schlieren photography to the flow exiting the nozzle. The second approach used in our investigation was to modify the nozzle exit by perturbing it in a wavy shape. As noted from the literature survey, part of the shock-associated noise is a result of feed back from sound radiation at the nozzle exit plane. This inspired the initiation of the second method for noise suppression where the exit plane of the nozzle is perturbed in a sinusoidal fashion with two different amplitudes. Such a perturbation results in non-symmetric and weaker internal shocks, the main source for the screech noise. The ability of the two methods in suppressing the noise will be determined by means of a microphone, placed near the nozzle exit, connected to signal frequency analyzer. The results obtained from these two methods will be presented and analyzed in chapter 4 and conclusions will be drawn in chapter 5.

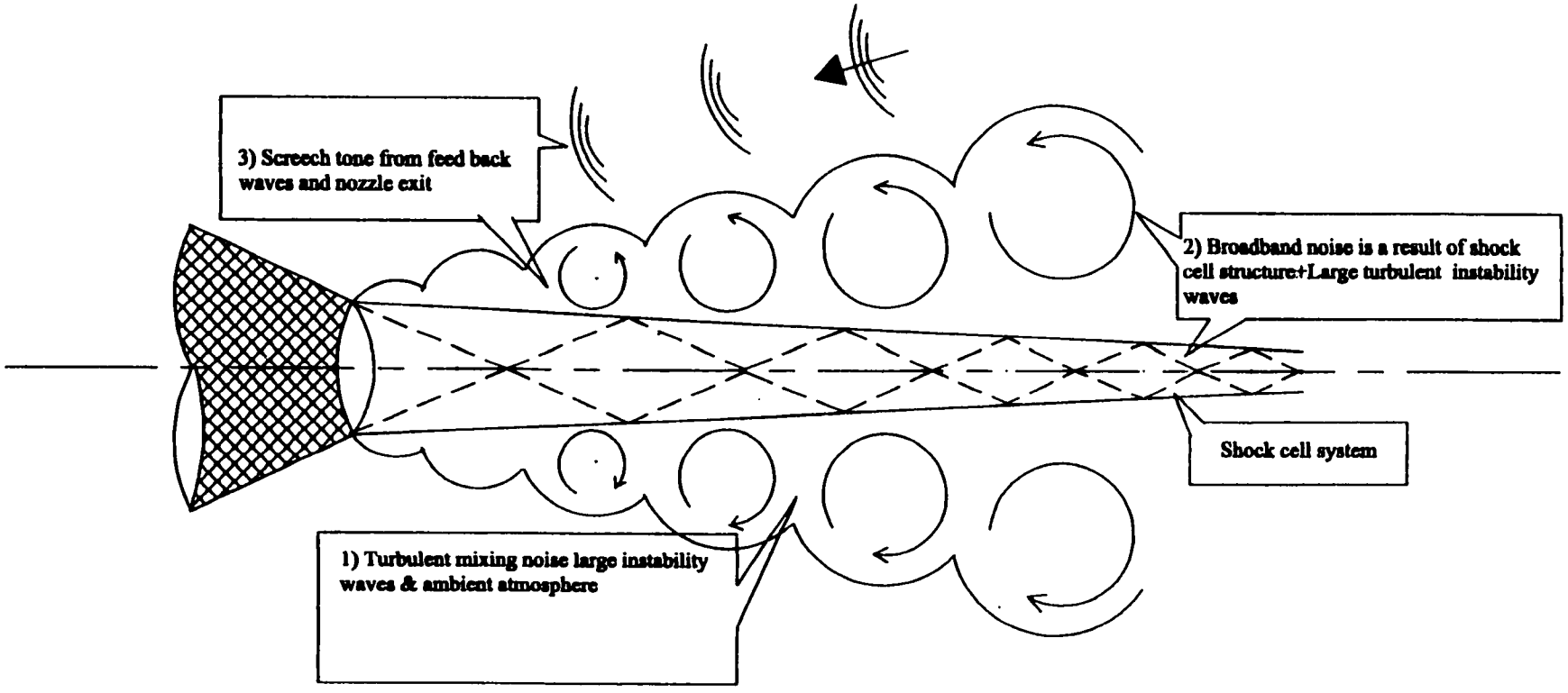

Figure 1.1 Schematic diagram of a converging nozzle operating off design conditions. (1) turbulent mixing noise; (2) and (3), shock associated noise

Chapter 2

Theoretical Analysis

2.1 Underexpanded Supersonic Jets without Swirl

In underexpanded jets, a system of expansion and compression waves form. The compression waves coalesce and form oblique shocks. The flow structure and the conditions under which the jet becomes underexpanded will first be presented followed by the Method of Characteristics which is used to theoretically demonstrate the structure of the first shock cell in a two dimensional jet.

At the end of each shock cell, oblique shock waves form. Shock waves are defined as an abrupt change in flow properties [38]. There are two types of shock waves: normal and oblique. A normal shock is a plane shock occurring normal to the direction of flow whereas for an oblique shock it occurs at an angle to the flow direction. Figure 2.1 demonstrates this

phenomenon.

The type of nozzle used can control the shock properties to a certain extent. There are two possible nozzle configurations: convergent and convergent-divergent. In the present work, a convergent nozzle was used. Figure 2.2 shows a typical convergent nozzle.

If the back pressure is equal to the reservoir pressure, there is no flow through the nozzle (Point A). Slightly reducing the back pressure allows some flow through the nozzle (points B & C). If the back pressure is further reduced until sonic velocity is reached at the exit plane of the nozzle, the nozzle is said to be choked (Point D). This occurs because further reduction in back pressure would only result in an increase of flow. Therefore, decreasing the back pressure beyond this critical point results in the formation of expansion waves at the exit plane of the nozzle and the nozzle is said to be underexpanded.

The expansion waves obtained reach the jet boundary, reflect and return towards the centre compressing the flow back to its original state. A second cell is formed and the process repeats, until shock cell formation is no longer possible. The process of expansion-compression creates a shock cell. Figure 2.3 illustrates this process.

A shock cell is defined as a segment of the jet plume between two consecutive intersections between a shock and the jet boundary. The first shock cell begins at the nozzle exit lip.

2.2 Method of Characteristics

The Method of Characteristics is used to obtain solutions to supersonic flow with a hyperbolic system of equations. This method is based on the assumption that the flow is irrotational and isentropic. The method of characteristics yields the properties of a compressible fluid in which the flow is continuous and isentropic [39]. These properties are the Prandtl-Meyer angle, ν, and the flow direction, θ, which can be obtained using either the point-to-point method or the region-to-region method. Both methods take into consideration the fact that certain properties remain constant along characteristic curves. The region-to-region method is applied by dividing the field of flow into uniform regions of flow. The properties obtained correspond to the average values of the region under consideration. To travel from region to region, only the properties that remain constant along the characteristic curves are used.

In the point-to-point method, the characteristic curves propagate downstream from the given initial conditions. The intersection of these waves yields new points in the flow field. By determining all the characteristics of the flow at the various points the shape of the weak oblique shock can then be obtained. The calculations are performed as follows. Given points a, b (figure 2.4), point d is calculated using the following two equations:

$$C_I = \theta_a + \nu_a = \theta_d + \nu_d$$
$$C_{II} = \theta_b - \nu_b = \theta_d - \nu_d$$

By adding and subtracting the above two equations, the flow angle and the Prandtl Meyer angle are determined as follows:

$$\theta_d = \frac{(\upsilon_a - \upsilon_b) + (\theta_a + \theta_b)}{2} = \frac{C_I + C_{II}}{2}$$

$$\upsilon_d = \frac{(\upsilon_a + \upsilon_b) + (\theta_a - \theta_b)}{2} = \frac{C_I - C_{II}}{2}$$

The shock cell structure for a 2D-flow system with a jet total pressure of 273.6 kPa is shown in figure 2.4. As noted in the figure, the shock cell is represented by the system of characteristic curves.

Points 1 & 4 were obtained using the following initial conditions:

- The exit Mach number, $M_1 = 1$
- The exit pressure is equal to 0.528 times the jet total pressure (i.e. 144.45 kPa)
- The ambient pressure is 101.3

The pressure ratio of P_4/P_0 was obtained using the following relation:

$$\frac{P_4}{P_0} = \frac{P_4}{P_1}\frac{P_1}{P_0}$$

where - P_o is the jet total pressure

- P_1/P_0 is the pressure ratio obtained from isentropic tables at M = 1 [38]

The flow and Prandtl Meyer angles of each point in figure 2.5 are tabulated in

table 2.1. At the end of each cell the compression waves coalesce and form a weak oblique shock wave. When the oblique shock reaches the jet boundary, another cell is created and another shock is formed.

When the jet pressure exceeds a certain value (~ 342.5 kPa), the oblique shock intersection at the centreline transforms to Mach reflection. In jet noise, and in particular shock noise, two important parameters are important: The cell length and the strength of the internal shock. These parameters will be measured experimentally via spark schlieren photography, as will be demonstrated in the next chapter.

2.2 Underexpanded Jets with Swirl

For non-swirling supercritical flows it is generally assumed that one-dimensional theory is equally applicable to convergent and convergent-divergent nozzles. The theory is found to give good results when the area change is gradual and the nozzle curvature is small. There has been considerable difficulty in defining a suitable choking criterion for swirling nozzle flows. For axisymmetric swirling flows, the sonic line is defined with reference only to the velocity component in the meridian plane; i.e., to the axial velocity. Thus, it is quite possible for the flow to be locally supersonic (based on the total velocity magnitude) but at the same time subcritical. To support a pressure difference between the exit of a convergent nozzle and ambient conditions, a finite curvature must exist at nozzle exit. The slope of the free jet boundary is no longer equal to that of the wall curvature immediately upstream of the nozzle exit. This streamline curvature is presumed to be sufficient to ensure that the sonic

line intersects the nozzle lip [35]. Using tangential jets to produce swirling flows [40] is found to produce tangential velocities that vary linearly with the radial coordinate. Previous theoretical analysis did not yield quantitative results. For example, the linearized theory by Carpenter is only qualitative which shows that swirls decrease the maximum height of the jet boundary. Smith [21] demonstrated the same result using the method of characteristics.

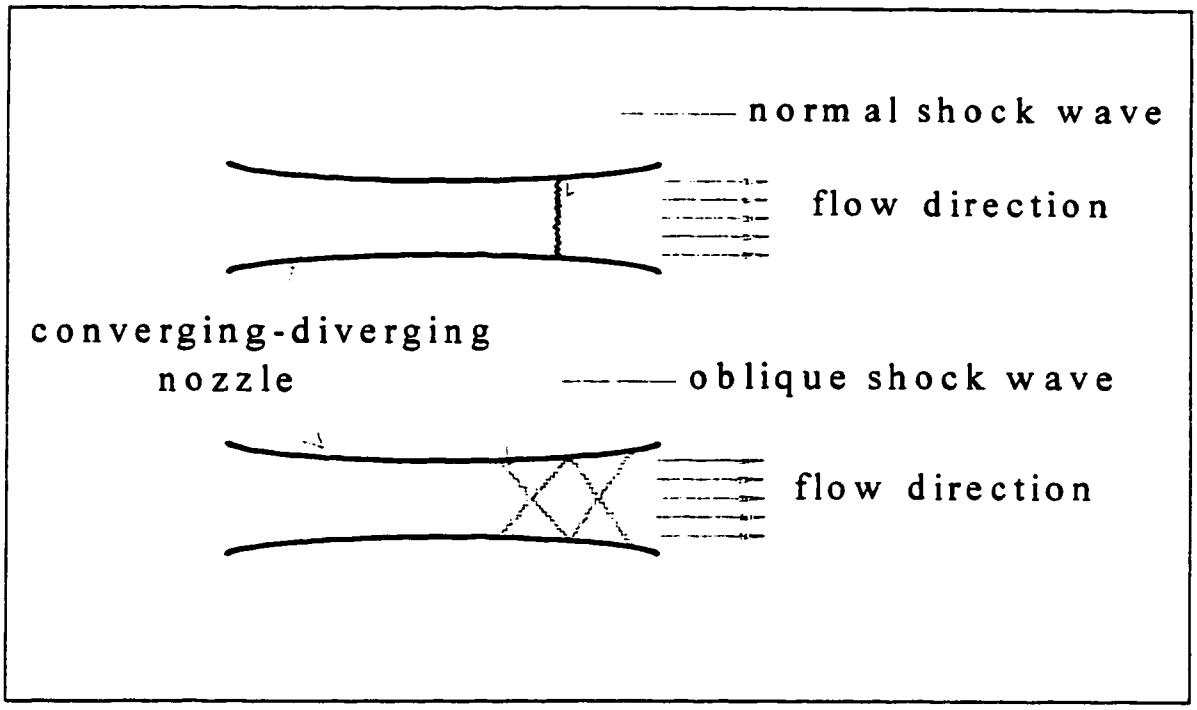

Figure 2.1. Types of shock waves in supersonic flow

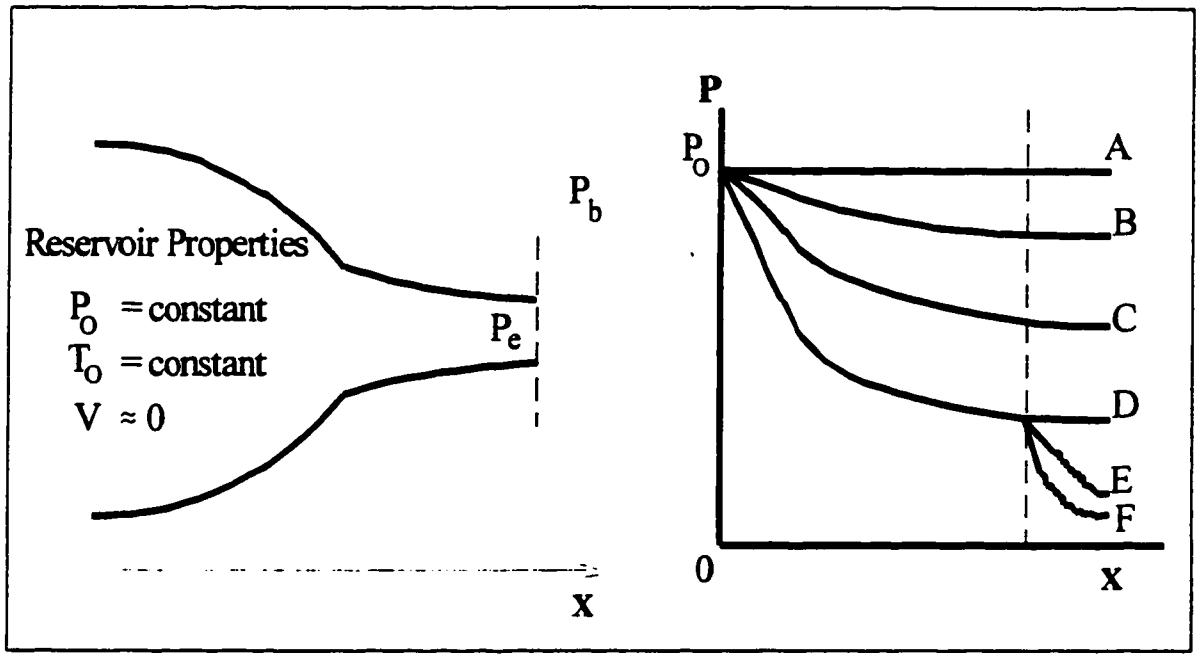

Figure 2.2. Operation of converging nozzle at various back pressures

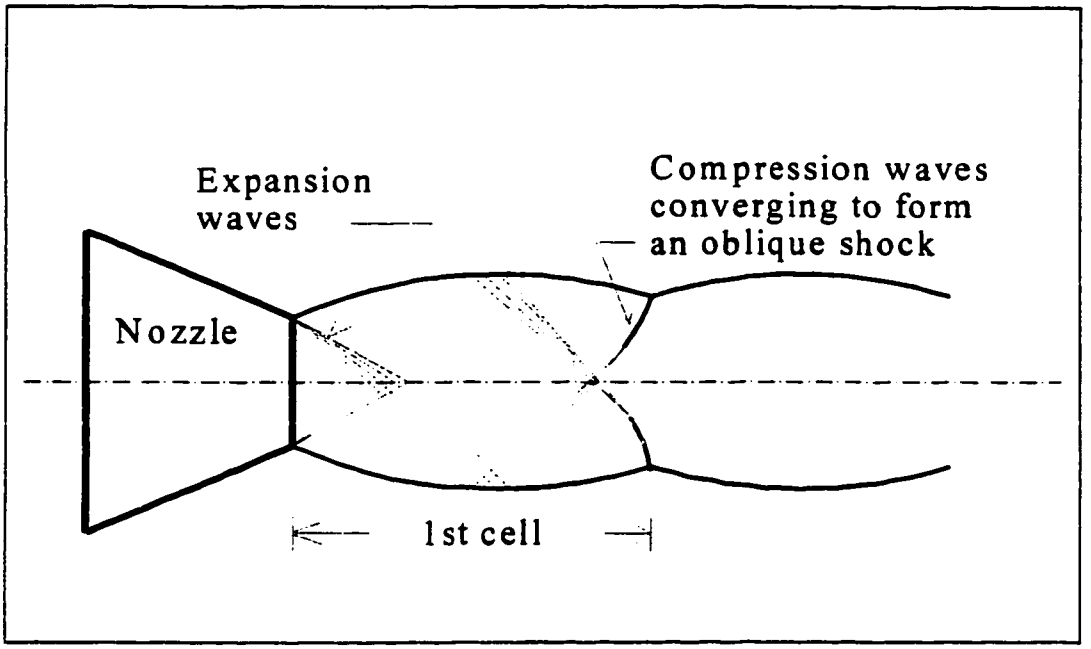

Figure 2.3. Shock cell formation in the jet wake

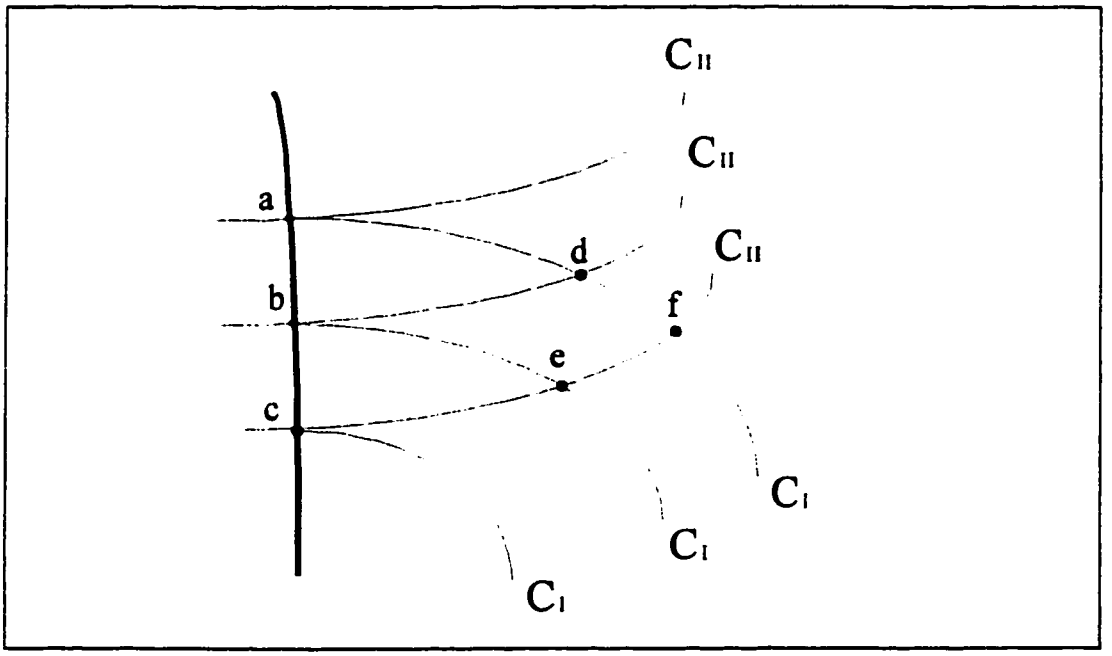

Figure 2.4 Schematic diagram showing positive and negative characteristics of supersonic irrotational isentropic flow.

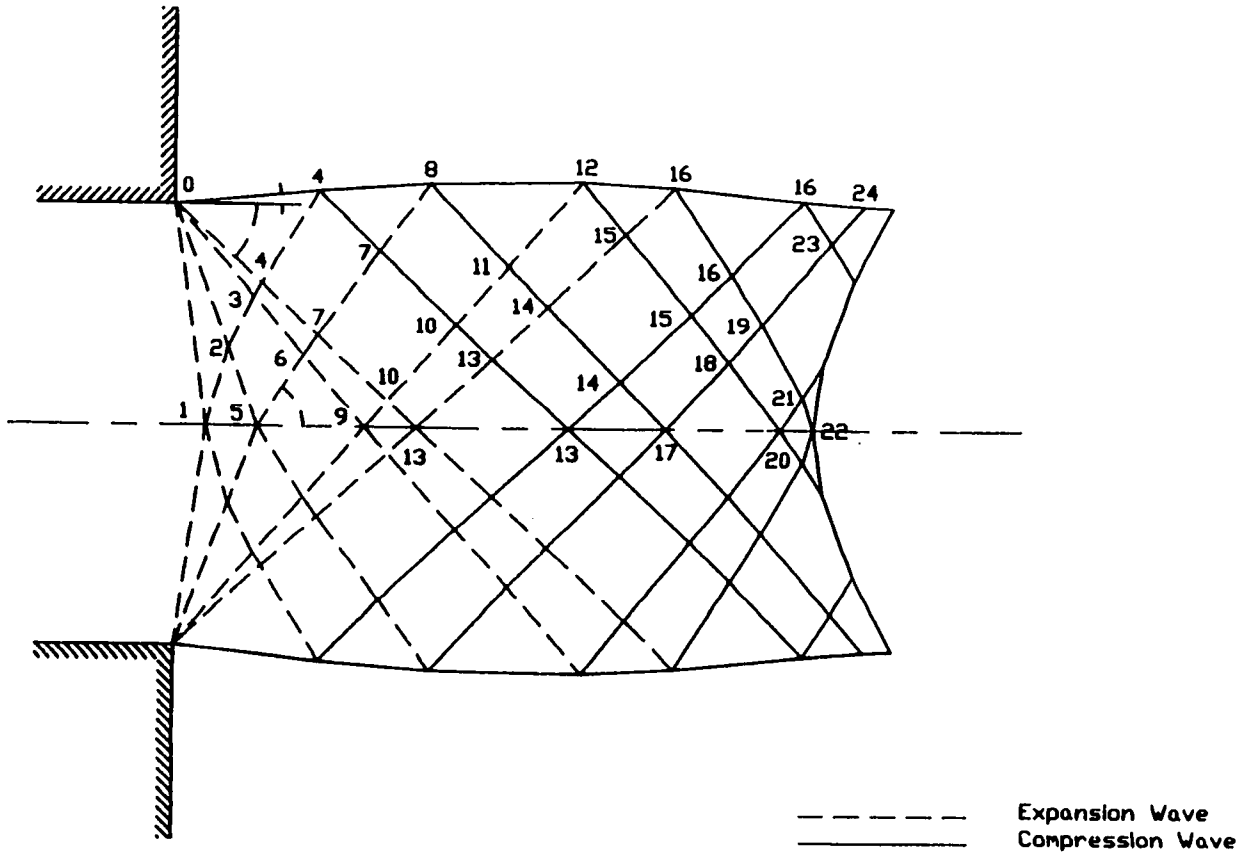

Figure 2.5 Detailed point to point flow properties inside the shock cell structure

Table 2.1 Numerical Analysis of a 2-D Underexpanded Jet

Flow Characteristics						
Point	$\theta + \nu$	$\nu - \theta$	ν	θ	M	μ
1	0.045	0.045	0.045	0.000	1.01	81.930
2	2.627	0.045	1.336	1.291	1.10	65.380
3	6.583	0.045	3.314	3.269	1.19	57.180
4	11.209	0.045	5.627	5.582	1.28	51.380
5	2.627	2.627	2.627	0.000	1.16	59.480
6	6.583	2.627	4.605	1.978	1.24	53.660
7	11.209	2.627	6.918	4.291	1.33	48.900
8	8.627	2.627	5.627	3.000	1.28	51.380
9	6.583	6.583	6.583	0.000	1.32	49.605
10	11.209	6.582	8.895	2.313	1.40	45.710
11	8.627	6.583	7.605	1.022	1.35	47.720
12	4.671	6.583	5.627	-0.956	1.28	51.380
13	11.209	11.209	11.209	0.000	1.48	42.640
14	8.627	11.209	9.918	-1.291	1.43	44.290
15	4.671	11.209	7.940	-3.269	1.36	47.180
16	0.045	11.209	5.627	-5.582	1.28	51.380
17	8.627	8.627	8.627	0.000	1.39	46.120
18	4.671	8.627	6.649	-1.978	1.32	49.430
19	0.045	8.627	4.336	-4.291	1.23	54.330
20	4.671	4.671	4.671	0.000	1.24	53.510
21	0.045	4.671	2.358	-2.313	1.15	60.500
22	0.045	0.045	0.045	0.000	1.01	81.930
23	0.045	8.627	4.336	-4.291	1.23	54.330
24	2.627	8.627	5.627	-3.000	1.28	51.380
25	1.336	2.357	1.847	-0.510	1.13	62.750

Chapter 3

Experimental Apparatus and Procedures

The apparatus used in the present study was essentially the same in all tests. Compressed air was supplied from a large reservoir connected to the university high-pressure air system, which is continuous, and large enough to maintain the required jet pressure ratios for sufficient time to acquire the necessary data. Three separate sets of experiments were carried out for each jet pressure and setup conditions. One set for pressure and velocity measurements, the second set for schlieren photography and the third set for acoustic measurements. In the next sections, the apparatus used to produce various degrees of swirl and the nozzle shapes used to perturb the flow will be described. Following these, a full description of the schlieren system and the acoustic setup will be presented.

3.1 The Vortex Chamber

3.1.1 Background

Vortex flow can be accomplished by various methods [41] (see figure 3.1). One method employs rotating porous surface at the inlet and a stationary one at the outlet. In the second method, the air is injected through guiding vanes at the inlet. The vanes in this case are used to control both the mass flow rate and the flow direction. A third method, which is employed in the present study, is injecting air through tangential ports evenly distributed over the circumferential surface. To control the strength of the vortex flow in the chamber, the port width was increased or decreased by moving the vanes radially outwards or inwards, respectively. The compressed air is supplied to the vanes by means of four flexible rubber hoses connected to a large plenum chamber.

When the flow enters the vortex chamber it experiences high centrifugal force. The flow may then follow one of the following patterns: vortex motion, rotating motion, or curved motion. The vortex motion may be divided into confined or free. In our investigation the flow is clearly confined where the flow is allowed to rotate within solid boundaries whereas at the exit the flow is free to rotate and expand to the ambient air. Generally the confined part of the flow is governed by the equation $V_\theta = k\, r^{n}$. Confined vortex may be free at the entrance of the vortex chamber, and n=-1. As the flow

approaches the axis of rotation, the flow becomes a forced vortex and n=1. A typical velocity distribution of a confined vortex flow is as shown in figure 3.2.

3.1.2 Experimental Apparatus

The experimental apparatus used in the present investigation was designed with the following objectives:

- Design of a small-sized experimental vortex chamber with low aspect ratio in order to generate a swirling flow of different magnitudes (strength).
- Easy to assemble and disassemble.
- Has a wide range of operating conditions.
- An echoic chamber or large space free from any sound reflecting surfaces.
- Strong enough to withstand high pressures (up to 700 kPa) and perfectly sealed.
- The total inlet area to the vortex chamber should be much larger than the exit area to prevent early choking of the apparatus.
- The end part of the exit nozzle must be replaceable to allow exit plane modification in later stages of noise investigation.

With this in mind, a small-scale chamfered jet nozzle of exit diameter 12 mm and 32 mm long was connected via a converging section to a vortex generator chamber made of aluminum (figure 3.3). The chamber has an overall diameter of 279 mm, a height of 64

mm and is capable of producing swirling flow with variable intensity by using four movable slabs that are internally assembled to provide the circulatory motion (see figure 3.3). The slabs have different settings in order to be able to change the magnitude of the swirl to the desired value and can also be removed to produce a jet without flow rotation. The air at normal conditions is temporarily stored in a large reservoir connected to the testing facility via four identical high pressure rubber hoses of 13 mm internal diameter and having a total area of 506 mm^2, which is four times greater than the nozzle exit area. This condition insures that the nozzle always chokes before the inlets for all operating pressures. The supply pressure and the mass flow rate to the plenum chamber are controlled by a means of a pressure-regulating valve.

For static pressure measurements, three pressure-taps were drilled along the radial direction. These pressure taps are 2 mm in diameter. This diameter was carefully chosen to avoid any disturbances to the flow and yield accurate readings. The static pressure taps were located at radial locations r_1= 75 mm, r_2= 53 mm and r_3= 36 mm corresponding to static pressures P_1, P_2, and P_3, respectively. In addition to the static pressure taps, a pitot tube was inserted in the chamber to read the total pressure of the flow entering the chamber from the four ports. The pitot and static pressure readings were used to determine the flow velocities at the three radii mentioned above.

3.2 The perturbed nozzle

For the perturbed nozzle exit case, the same cylindrical chamber, shown in figure 3.3, was used. The four slabs were removed and the three different nozzles a, b and c, shown in figure 3.4, were added to the nozzle flat exit and were held tight by a small (1.6 mm) screw. Figure 3.4 (a), corresponds to a nozzle with plane exit, while in (b) the perturbation amplitude is equal to .125 the nozzle diameter and in (c) the amplitude equal to 0.25 the nozzle diameter. The shape of the nozzle lip was chosen to be sinusoidal and varies according to the following relation:

$$y_0 = y - \frac{d}{2}\sin\theta_1$$
$$z_0 = z + d/2\cos\theta_1$$

where,

y_0 and z_0 are the tool coordinates, d is the tool diameter and $\theta_1 = \tan^{-1}(dz/dy)$.

In the present work (z) was chosen to vary sinusoidally according to the following relation:

$$z = z_m \cos(2\cos^{-1}(y/(D/2))$$

Where z_m represent the maximum amplitude and D the nozzle diameter. Note that y varies from – D/2 to + D/2 which give two maxima along the nozzle perimeter.

The perturbed nozzle shapes were machined using an N/C machine located at Concordia University's machine shop .

Based on a nozzle inside diameter of 12 mm and maximum perturbation of D/8 and D/4 the tool coordinates (y_0, z_0) are illustrated in figure 3.5 a and b.

3.2 The Schlieren system

A schematic of the schlieren system used in the present work is shown in figure 3.6. It consists of two parabolic mirrors, 1230 mm in focal length. The light source is a 2 kV spark with a duration time of less than one microsecond. The light source is located in front of the condenser lenses. These lenses and the first knife edge are used to obtain a light source, 1 mm^2 in area. The knife-edge was positioned at the focal point of the first parabolic mirror to yield parallel light beams, which pass through the test section. The light rays then reflect from the second parabolic mirror and converge at the focal point where another knife-edge is used to cut part of the light, producing the schlieren effect on the image of the test section where a camera is placed. An open shutter camera is used to take the instantaneous photograph. A continuous video camera was also employed to determine the behavior of the flow in the jet as well as the flow exit angle at the nozzle exit plane.

3.3 Acoustics Setup

The acoustical results were determined using a signal frequency analyzer. The microphone is first calibrated using the calibration instrument provided with the analyzer, such that it records a 94 dB at a frequency of 1 kHz when the instrument is operated. The condenser microphone is then aligned with the nozzle exit plane at a distance equal to half the inside diameter of the nozzle and connected to a signal frequency analyzer (Bruel & Kjœr 2035) equipped with a scan screen to display the signals in frequency domain. The operating valve is then opened to allow air from a pressure reservoir into the settling chamber to cover a wide range of stagnation pressures.

The pressure of the settling chamber is monitored from a gauge connected to it (see figure 3.6). The microphone is isolated from all vibrating objects to ensure the reading is that of the nozzle noise only. The output data is stored in ASCII delimited format to be analyzed using any spread sheet software (in this study MS Excel, is used). For acoustical measurements, 1/4" and 1/8" (Brüel & Kjœr 4181 and 4138 respectively) microphones are placed at the exit plane of the nozzle at a distance equal to half the inside diameter of the nozzle. This microphone is connected to the interface to convert the sound signals to electrical ones which are then fed to a signal analyzer unit of type (B&K 2035) equipped with a scan screen to display the signals. Data is then stored on a computer diskette for later analysis.

For the perturbed nozzle, acoustic measurements were carried out at eight different angular positions as shown in figure 3.7.

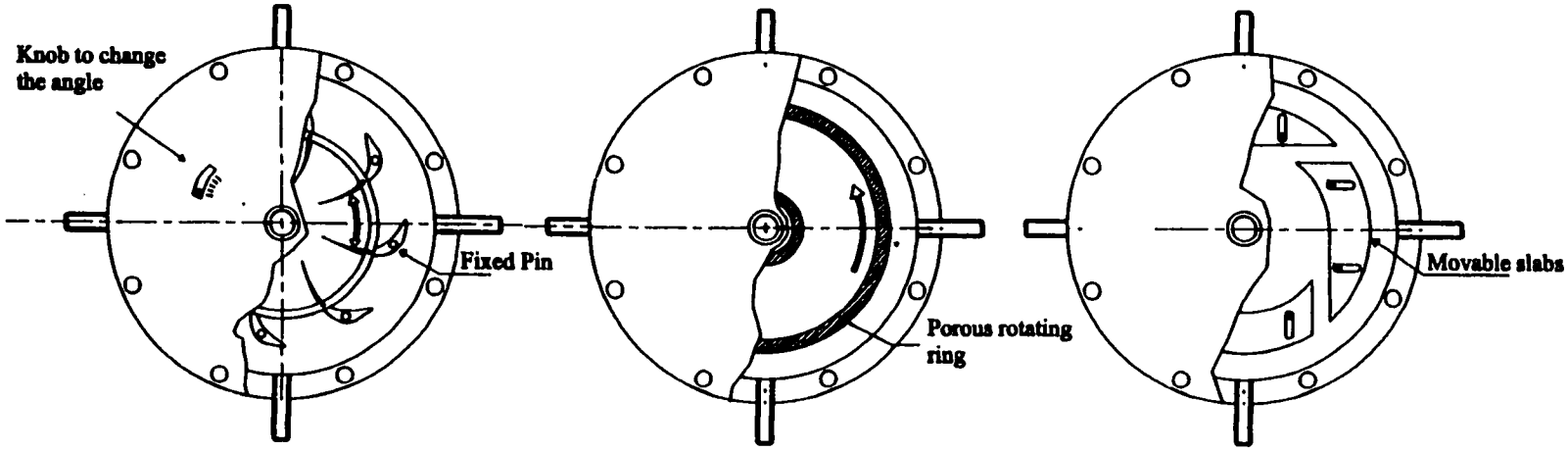

Figure 3.1. Methods of creating swirl in a confined chamber

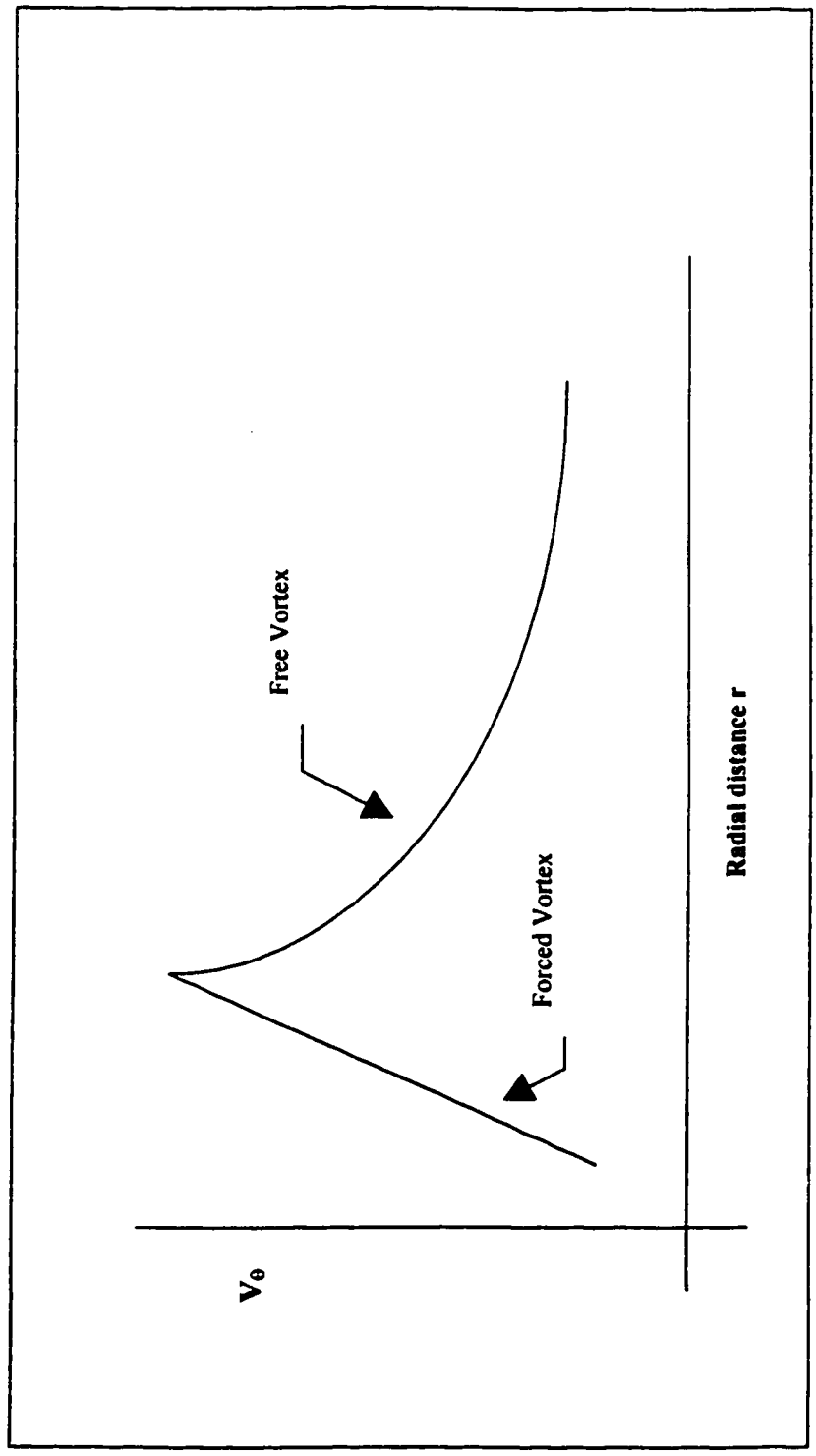

Figure 3.2. Sketch of radial distribution of tangential velocity component.

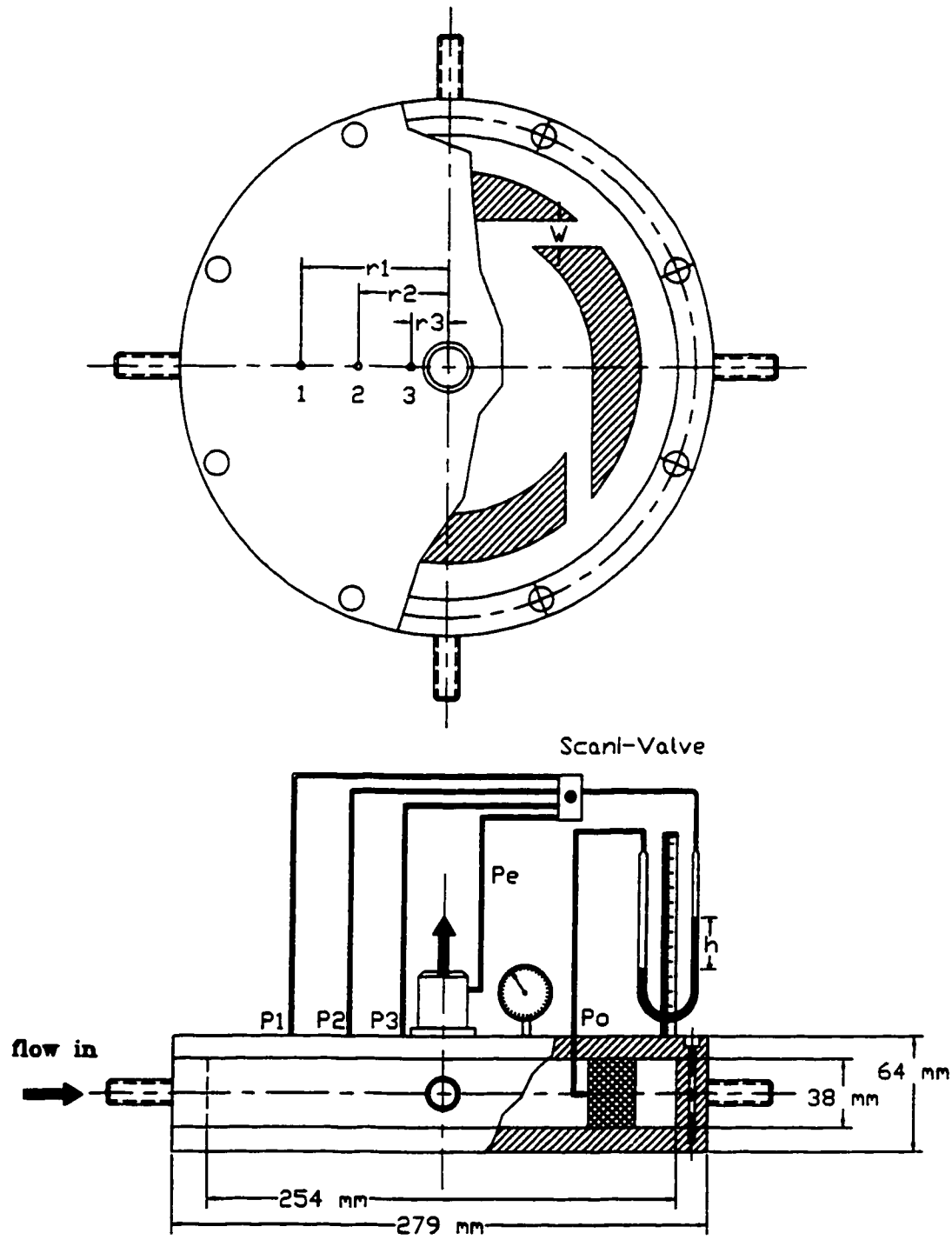

Figure 3.3 The vortex chamber apparatus

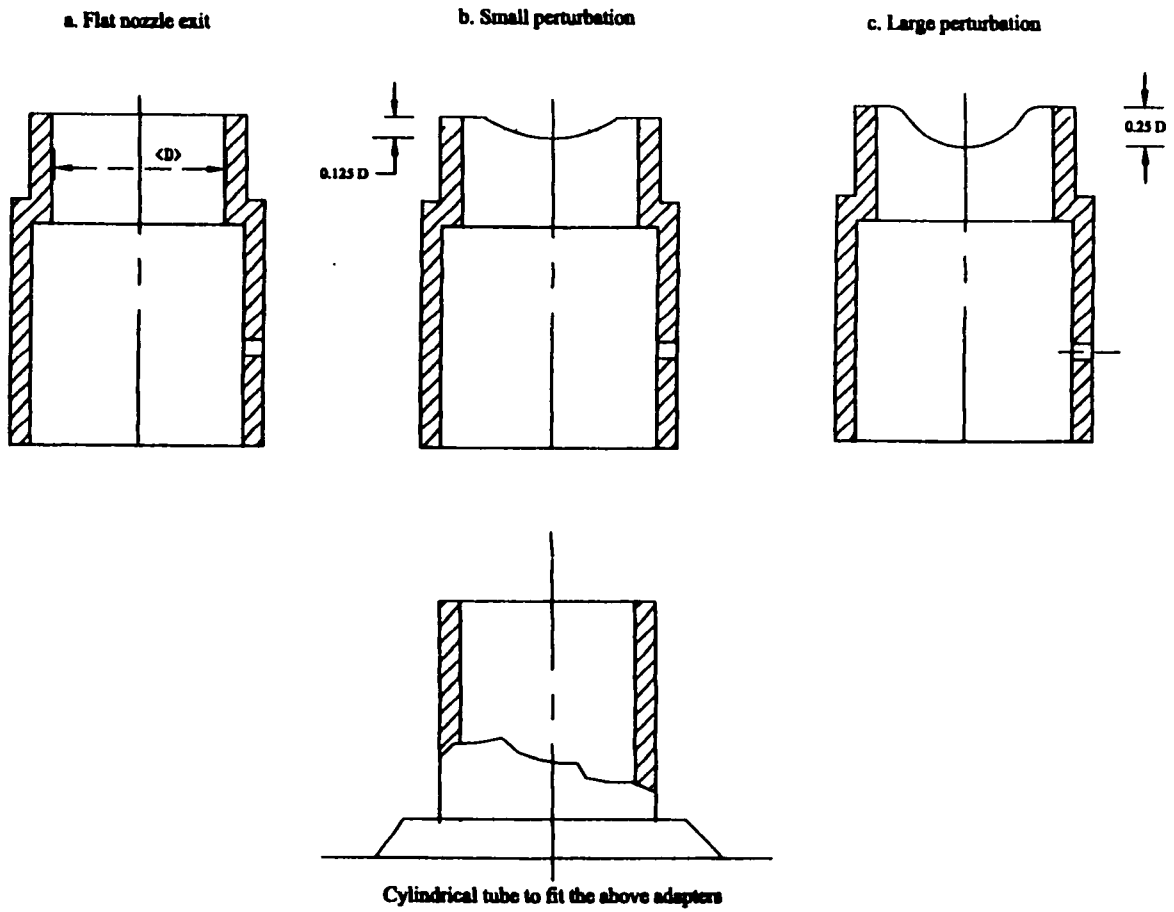

Figure 3.4 The Three types of nozzle surfaces tested

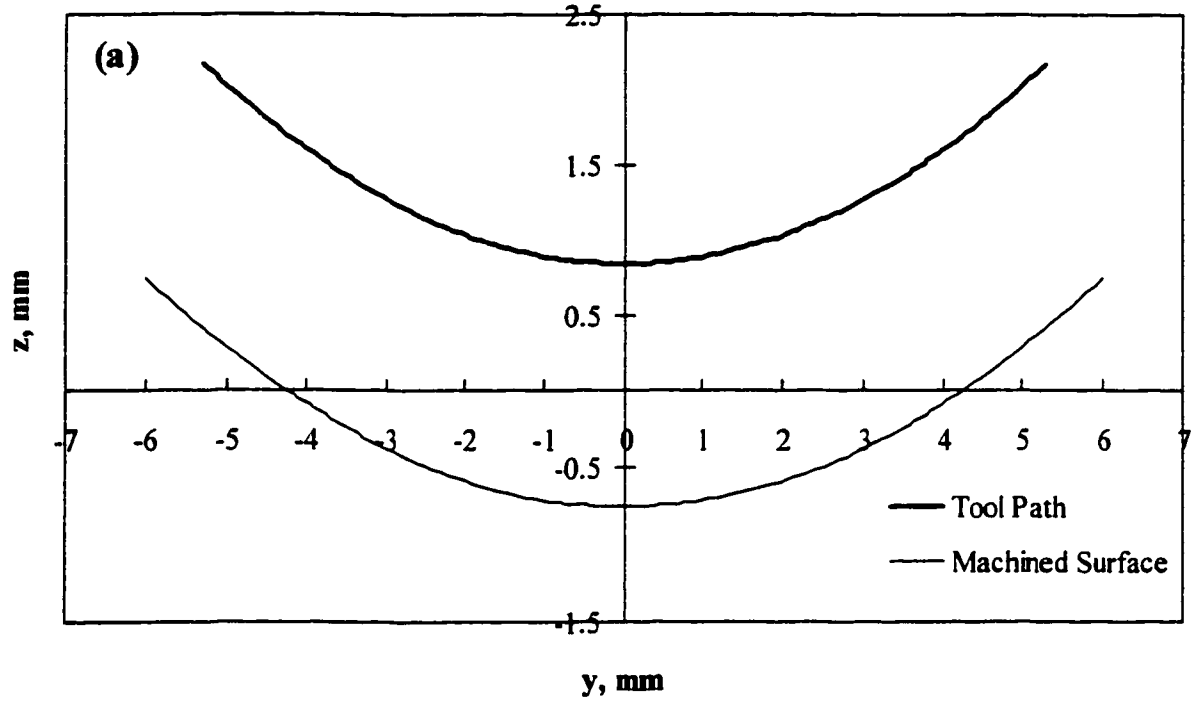

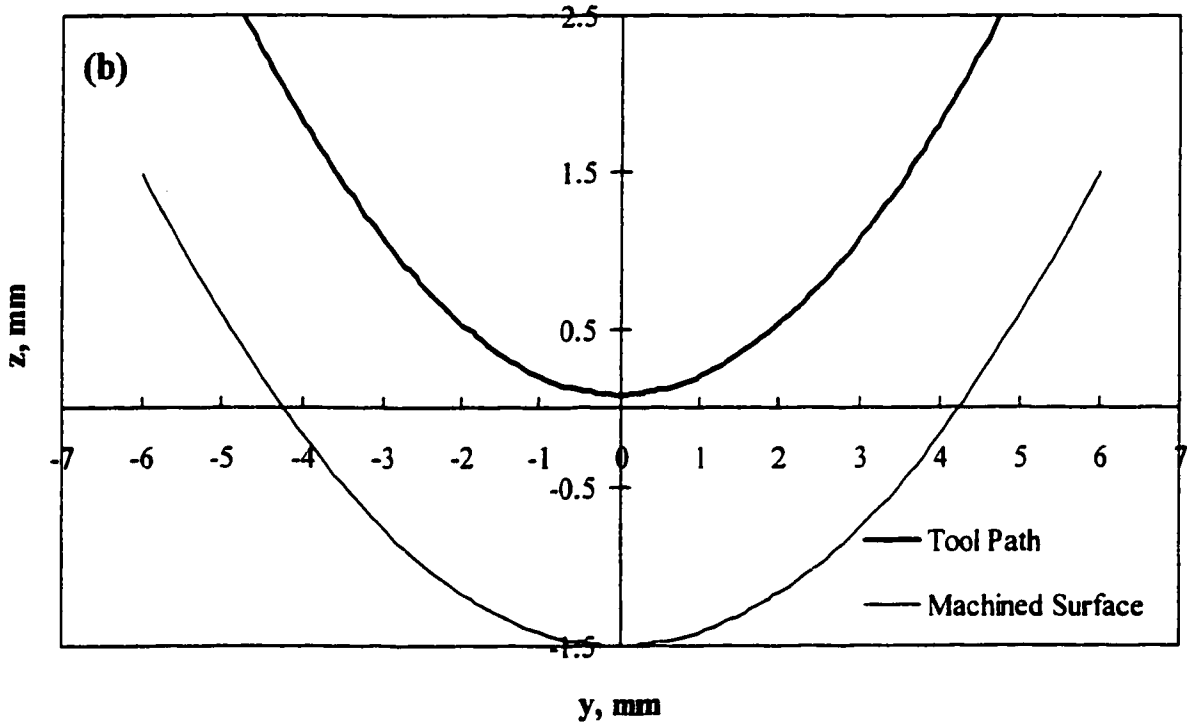

Figure 3.5 Production of the sinusoidal surface of the exit nozzle of figure 3.4; (a) Small perturbation; (b) Large perturbation

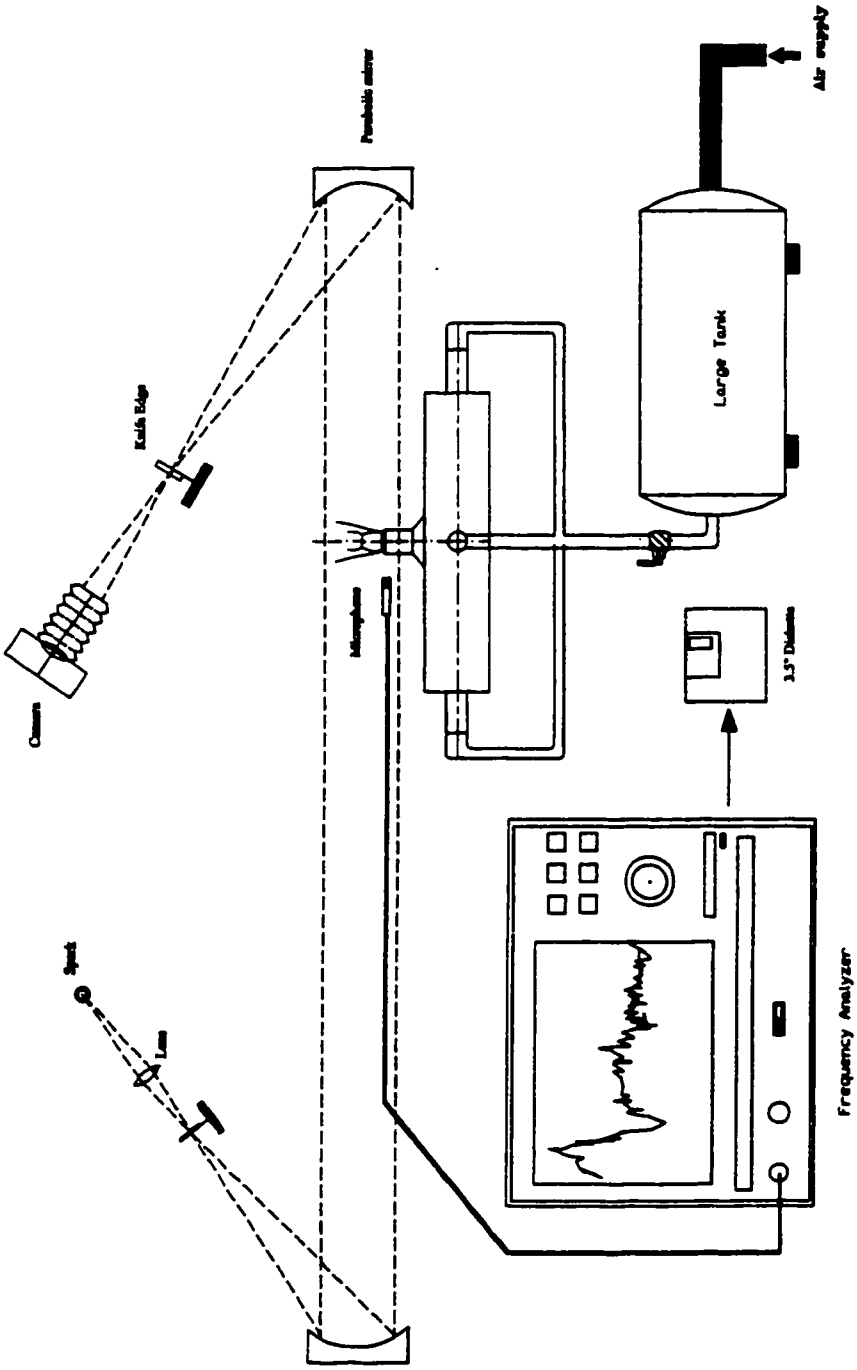

Figure 3.6 Expiremental setup of optical and acoustical equipment

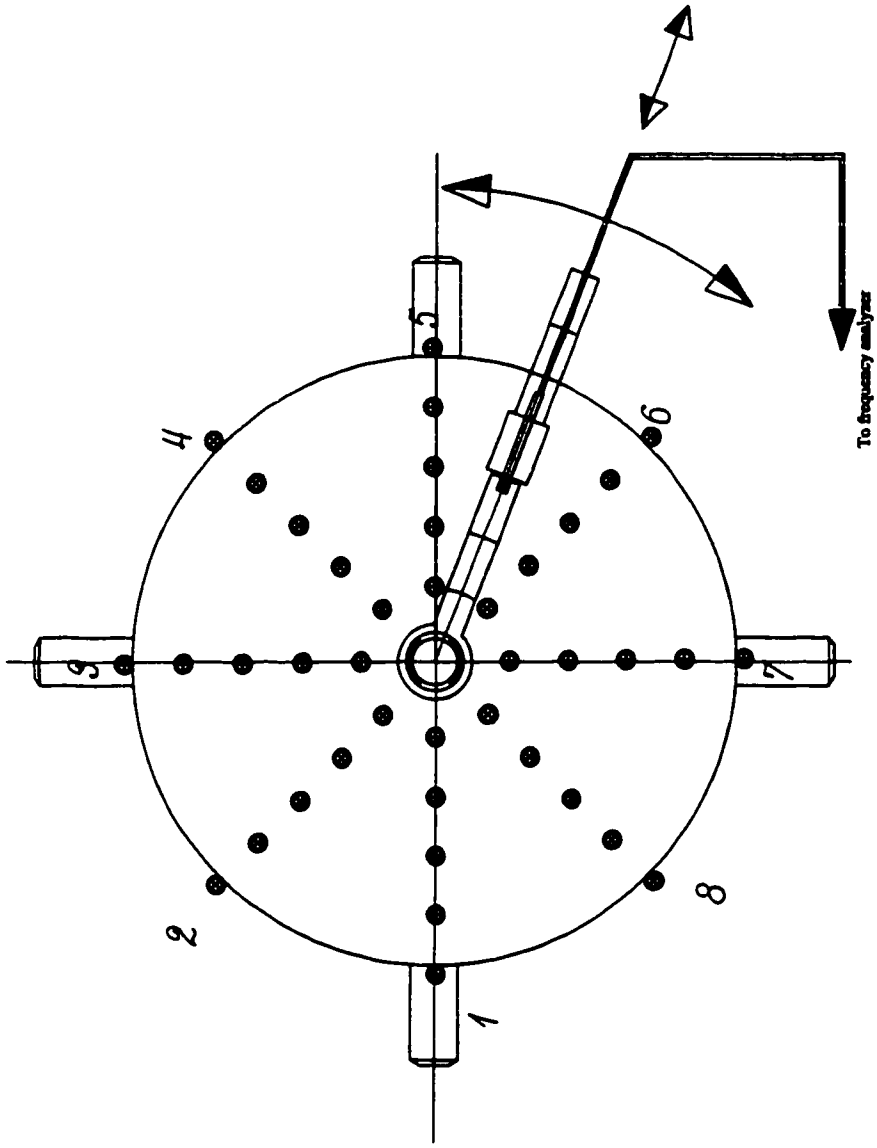

Figure 3.7 Schematic showing the various microphone positions

Chapter 4

Results and Discussions

4.1 Supersonic Jet with Fluid Rotation

Supersonic jets were produced using the vortex chamber apparatus described in the previous section. Moving radially, the four slabs inside the chamber varied the tangential component of the fluid velocity of the jet. Initially, the fluid emanates from four slots with a relatively low velocity. The fluid then accelerates to higher velocities as it approaches the nozzle exit. The results obtained from the detailed pressure and velocity measurements are presented in the next section followed by those from the schlieren photography and acoustic noise measurements.

4.1.1 Pressure and Tangential Velocity Measurements in the Vortex Chamber

The total pressure of the flow, P_o, entering the swirl chamber, was measured by means of a Pitot tube placed at one of the four slots exit plane. The static pressures P_1, P_2 and P_3 were measured from the three static taps located at the three radial locations mentioned above. From the total and static pressure measurements, the velocity of the jet exiting the slots and those at the two smaller radii were calculated from the following relation:

$$V = \sqrt{2(P_o - P)/\rho}$$

where V is the fluid velocity, P_o is the total pressure, P is the static pressure and ρ is the fluid density. The results for a jet total pressure ranging between 10 kPag and 250 kPag and for three different slot sizes of 16 mm, 13 mm and 9.5 mm, respectively, are presented in figure 4.1. As noted in the figure, using a larger slot size (16-mm) produces a weaker velocity than the use of a smaller slot size (9.5-mm). The jet velocity is also found to increase monotonically with the jet total pressure until choking condition is reached. With fluid rotation, choking of the jet does not take place at the same value of P/P_o as that measured in jets without rotation. To find the exact pressure where choking takes place, another pressure tap was inserted near the nozzle exit plane, as shown in figure 3.3. The static pressure at the nozzle exit was measured for every jet total pressure

for the three jet rotation cases mentioned above. The results are presented in figure 4.2. To determine the jet total pressure at which choking takes place, another graph was plotted for the exit pressure, P_e, normalized to the jet total pressure, P_o, versus the jet total pressure. As noted in figure 4.3, the ratio of the static to total pressure gradually decreases to reach a constant value at which point the choking condition has been reached. This critical pressure ratio is found to decrease with the decrease in the slot size or the increase in the degree of initial jet tangential velocity introduced to the flow. To analyze these results one has to first understand the nature of the flow emanating from the four slots and how it varies with the chamber radius. At large radii, the flow velocity is small and can therefore be analyzed using incompressible 2-D Navier-Stokes equations. These equations indicate that the flow is irrotational (Γ = constant) and that

$$V_1.r_1 = V_2.r_2 = V_3.r_3$$

This relation was verified for the three cases of jet rotation by presenting V * r, normalized to r_1, for taps 2 & 3. The results are presented in figure 4.4. From these results, it can be concluded that the fluid inside the chamber behaves as an irrotational vortex as it approaches the nozzle inlet.

4.1.2 Exit Velocity Profile

The fluid enters the nozzle with irrotational flow conditions, then propagates in a constant area tube before exiting to the atmosphere. Without fluid rotation inside the

cylindrical chamber, and assuming frictionless flow, the fluid exiting the nozzle is uniform. With fluid rotation, one may assume that swirl is being imposed on the flow exiting the nozzle and the tangential component of the velocity behaves in a similar fashion as those shown in figure 3.2. The tangential component of the velocity was determined indirectly using schlieren photographs of the flow at the nozzle exit plane. A very light nylon string was placed at the nozzle lip. Without fluid rotation the string takes the axial direction. With fluid rotation, the string takes the flow direction, which makes an angle θ with the nozzle axis. The ratio of the tangential velocity to the axial velocity is equal to:

$$V_\theta / Va = M_\theta / Ma = \tan(\theta)$$

and the total Mach number M is equal to :

$$M^2 = M_a^{\,2} + M_\theta^{\,2}$$

where M_a and M_θ are the axial and the tangential Mach numbers, respectively. The swirl Mach number, M_ϕ, is defined as

$$M_\phi = \frac{V_\theta}{c_c}$$

where c_c is the critical sound speed.

Assuming isentropic conditions, the total Mach number was calculated from the ratio of the static pressure, measured at the nozzle exit, to the jet total pressure measured at the cylindrical chamber inlet. Using the value of θ, measured from the schlieren photographs, the two components of the Mach numbers are then determined. The axial

and tangential components of the fluid velocity are obtained by multiplying the Mach number by the local sound speed, c, where,

$$c = \left(\frac{p_e}{P_o}\right)^{\frac{\gamma-1}{2\gamma}} c_o$$

and c_o is the sound speed of the air supply and γ is the specific heat ratio.

For the three cases tested, the measured angles of the flow are as shown in figure 4.6. The calculated values of the swirl Mach number are shown in figure 4.7. As noted in the figure, the swirl Mach number, M_ϕ, increases with the increase in the jet pressure until it reaches a maximum value after which it remains constant. The figure also shows that for any given jet pressure, M_ϕ increases with the decrease in the slot exit area. The mass flow rate was calculated based on the axial component of the velocity and was compared with the measured inlet mass flow rate into the cylindrical chamber. The results are shown in figure 4.8, for the 16-mm case. Excellent agreement was noted between the experimental values and the theoretical one indicating the validity of our assumption that the circulatory flow is superimposed on the main uniform flow. To further verify our assumption, a theoretical value of the critical pressure ratio was calculated and compared with the experimental values presented in figure 4.3. The critical pressure ratio was calculated based on the axial Mach number being unity and the swirl Mach number is as given in figure 4.7. The results are presented in figure 4.9. As seen in the figure, the theoretical results are in close agreement with the experimental ones and the critical pressure ratio is dependent on the degree of the initial swirl. A higher swirl results in a lower critical pressure ratio.

4.1.3 Effect of Swirl on Shock Cell Structure

Separate tests were run for various jet Mach numbers, Mj, for optical and acoustical measurements. Optical tests were carried out to examine the jet structure. The jet exhausts to the atmospheric pressure, Pa. The jet Mach number is calculated using the following isentropic relation:

$$M_j = \left[\frac{2}{\gamma - 1} \left[\left(\frac{P_c}{P_a} \right)^{\frac{\gamma - 1}{\gamma}} - 1 \right] \right]^{\frac{1}{2}}$$

where γ is the specific heat ratio for air.

A sample of the schlieren photographs taken are presented in figures 4.10, 4.11, 4.12 and 4.13 for four cases: jets without swirl, jets with low swirl (16 mm slot size), jets with medium swirl (13 mm slot size) and jets with high swirl (9.5 mm slot size), respectively. As seen in the figures, a stronger swirl results in a shorter cell length and jet Mach numbers higher than 1.37 result in secondary internal shock formation. The cell length and the position of the secondary shocks were measured from these photographs and the results are shown in figure 4.14. The effect of swirl on jet growth is shown in figure 4.15, for a jet Mach number of 1.37. As noted in the figure, swirl increases the spreading rate. With low swirl, and at an x/D_e ratio of 3, the jet spreads approximately 2.8 times that without swirl. High swirl is found to double the spreading rate.

The jet boundary of the inviscid core was measured from the schlieren photographs. Great care was taken in these measurements to minimize the errors. The photographs

were first magnified digitally to about 30 times their actual size then projected onto a screen for measurements. The results are presented in fig. 4.16 for two discrete values of M_j, 1.28 and 1.57. Since swirl requires higher jet pressures to choke the flow, the effect of under expansion is found to be less noticeable in jets with swirl than jets without swirl for the same jet total pressures. In the low swirl case, at M_j = 1.28, the jet boundary exhibited a 3% diameter increase as opposed to an 8% increase in jets without swirl. Swirl is also found to decrease the degree of lateral flow expansion which is found to weaken the internal shock strength and the noise associated with it. This phenomenon will be demonstrated in the acoustic measurements of the next section.

4.1.4 Acoustical results

4.1.4.1. Background

Cell length measurement in screech tones is very important and is related to the frequency as demonstrated by Powell [13]. He found that the screech tone frequency increases with the decrease in the cell length and estimated the screech frequency as

$$f_s = \frac{V_c}{L(1+M_c)}$$

where V_c is the convection velocity of the eddies, and L is the average shock cell length and M_c is equal to Vc / a_0 where a_0 is the atmospheric speed of sound.

Using cross laser beams, Harper-Bourne & Fisher [17] found the connection between the velocity, V_c, and the jet velocity, V_j. Their findings showed that V_c can be approximated by:

$$V_c = 0.7\, V_j$$

The resonant frequency can be written in terms of a non-dimensional Strouhal number as

$$St = \frac{f_s D_J}{V_J} = \frac{0.7\,(D_J / D)}{L/D\,(1+M_C)}$$

Where D_J/D is given by Tam and Tanna (14):

$$\frac{D_J}{D} = \left[\frac{[1+(\gamma-1)/2M_J^{\,2}]}{1+(\gamma-1)/2M_d^{\,2}]}\right]^{(\gamma-1)4(\gamma-1)} \left(\frac{M_d}{M_J}\right)^{1/2}$$

4.1.4.2 Acoustic results

A series of tests were run repeatedly for each configuration in order to insure the accuracy of the results. A sample of the obtained results of the narrow band spectra is presented in figure. 4.17 for jets with and without swirl at jet Mach numbers Mj of 1.18, 1.28, 1.37 and 1.44. As seen in the figure, the screech tones without swirl exhibit marked peaks. These peaks represent the sound pressure levels, SPL, which are greater than 130 dB. With low swirl (16-mm slot size), the screech tone is suppressed and only the turbulent noise is observed. For high swirl (9.5-mm slot size) little improvement is noted in the sound pressure level. The maximum SPL recorded for a wider range of jet

pressures is shown in figure 4.18. At low pressures and subsonic jet Mach numbers, swirl is found to yield higher SPL values due to the better mixing ability of the jet fluid with the surrounding ambient air. This increases the turbulence level and the sound level associated with it. At a jet Mach number greater or equal to 1.18, swirl is found to suppress screech noise thus reducing the maximum SPL by as much as 15 dB when compared to the no swirl case. The maximum effect is found within jet Mach numbers of 1.18 and 1.44. At jet Mach numbers higher than 1.44, the SPL difference decreases monotonically with the increase in jet pressures until no difference exists. This occurs at M_j greater than 1.68.

The resonant frequency of the screech tone is shown in figure 4.19 together with the maximum SPL associated with it. As noted in the figure swirl results in a considerable decrease in the SPL while increasing slightly the frequency and the Strouhal number. The latter effect is expected due to the decrease in the shock cell length with magnitude of the swirl.

The over-all sound pressure levels as a function of the angular position from the centerline of the jet were also measured. The microphone was set at an arc position equal to 20 nozzle diameters extending from the centerline of the nozzle exit. Measurements were carried out at 10 degree intervals until the surface of the swirl chamber was reached (~100 degrees). A sample of the noise spectra, measured at an angle of 30 degrees is presented in figure 4.20 for both a jet with low swirl and a jet without swirl. As noted in the figure, the major effect of swirl is in the screech noise component. With swirl, screech noise is practically eliminated. Similar results were obtained at all angles measured. The results are presented in figure 4.21 for the overall sound pressure level as a function of

the angular position. As noted in the figure, swirl decreases the overall sound pressure level by about 3.1 dB. The maximum pressure level, however, decreases by as much as 15 dB.

Swirl also results in a thrust loss when comparison is made for the same jet total pressure, or jet Mach number M_j. In the present work, the introduction of the swirl into the jet stems from the jet total pressure. An increase in the swirl magnitude is expected to decrease the jet axial component of the velocity and hence the mass flow rates exiting the nozzle. For the low swirl case, a 1.6% thrust loss is found to take place. With medium swirl the loss increases dramatically to 6.5%.

Sound pressure measurements indicate that low swirl is as effective as high swirl as far as noise reduction is concerned. Combining this with the thrust loss results, the low swirl case is found to be the best alternative in terms of both noise reduction with minimal thrust loss.

4.2 Supersonic Jet with Nozzle Perturbation

Experiments were carried out for two different perturbations at the nozzle lip. The perimeter at the nozzle's exit was perturbed with a sinusoidal shaped perturbation along the periphery of the nozzle and in the direction of the nozzle axis (see figure 3.4). Schlieren photography was employed to determine the effect of the variation in the nozzle shape on the structure of the underexpanded jet. Sound pressure measurements

were taken at different angular positions around the nozzle in a plane perpendicular to the jet axis to determine the effect of the nozzle lip shape on the sound emitted.

Two series of schlieren photographs were taken; One to view the downstream end of the perturbation and the other to view the upstream end of the perturbation. Figure 4.22 shows a series of photographs taken to view the upstream end of the perturbation (i.e. 90^{o} to that shown in figure 3.4c). As noted in the figure, the lateral expansion of the jet is present at all supersonic jet Mach numbers. The other set taken, to view the downstream end of the nozzle is presented in figure 4.23. In the latter case, the jet boundary is seen different from that observed in figure 4.22. The cell length is longer and the jet boundary narrows as the flow propagates downstream of the nozzle exit. The narrowing of the jet boundary is due to the arrival of the expansion waves originating along the upstream part of the perturbed nozzle. This phenomenon was also observed through the schlieren photographs shown in figures 4.24 and 4.25 with a nozzle perturbation half that shown in the previous two figures (see figure 3.4b). This demonstrates the nonuniformity of the jet in the azimuthal direction and of the weakening of the oblique shocks compared to those produced using a plane nozzle exit (figure 3.4a). To verify the ability of perturbed nozzle in minimizing the sound emitted from supersonic jets, a microphone, connected to frequency analyzer, was placed at a fixed radial position equal to $15D_j$ and at different angular positions as shown in figure 3.7. The digital data was then recorded on 3 ½" diskettes for further analysis. A sample of the obtained results of the narrow band spectra, measured with highly perturbed nozzles, is presented in figure 4.26 for different angular positions, corresponding to those shown in figure 3.7. As noted in the figure, screech noise is eliminated with the use of perturbed

nozzles. The percentage decrease in the maximum SPL measured is demonstrated in the polar diagram of figure 4.27. As noted in the figure, the sound emitted from the perturbed nozzle case slightly varies with angle θ. Screech sound suppression reduced the maximum SPL by as much as 10 dB (see figure 4.26). Similar results were obtained for M_j = 1.44 (see figure 4.28). In this case, smaller percentage in noise reduction was found (5%). A comparison between the SPL measured with the highly perturbed nozzle and that measured with a flat nozzle is shown in figure 4.29 as a function of the jet Mach number and for three angular positions. From the results, it is clear that perturbed nozzles eliminate screech noise and decrease the sound pressure level for supersonic jet Mach numbers less than 1.37.

Sound pressure measurements were also carried out with the lower perturbation case. Figure 4.30 shows that screech noise is eliminated but the broadband component of the shock noise still remains. In figure 4.31, a comparison is made between the results obtained from the lower and the higher perturbation cases. The results show that the higher perturbation case nozzle produces noise lower than those measured with the lower perturbation case.

A comparison between the SPL measured with the lower perturbation case and that measured with a flat nozzle exit is shown in figure 4.32 as a function of the jet Mach number. The percentage decrease in the sound emitted from the nozzle is shown in figure 4.33.

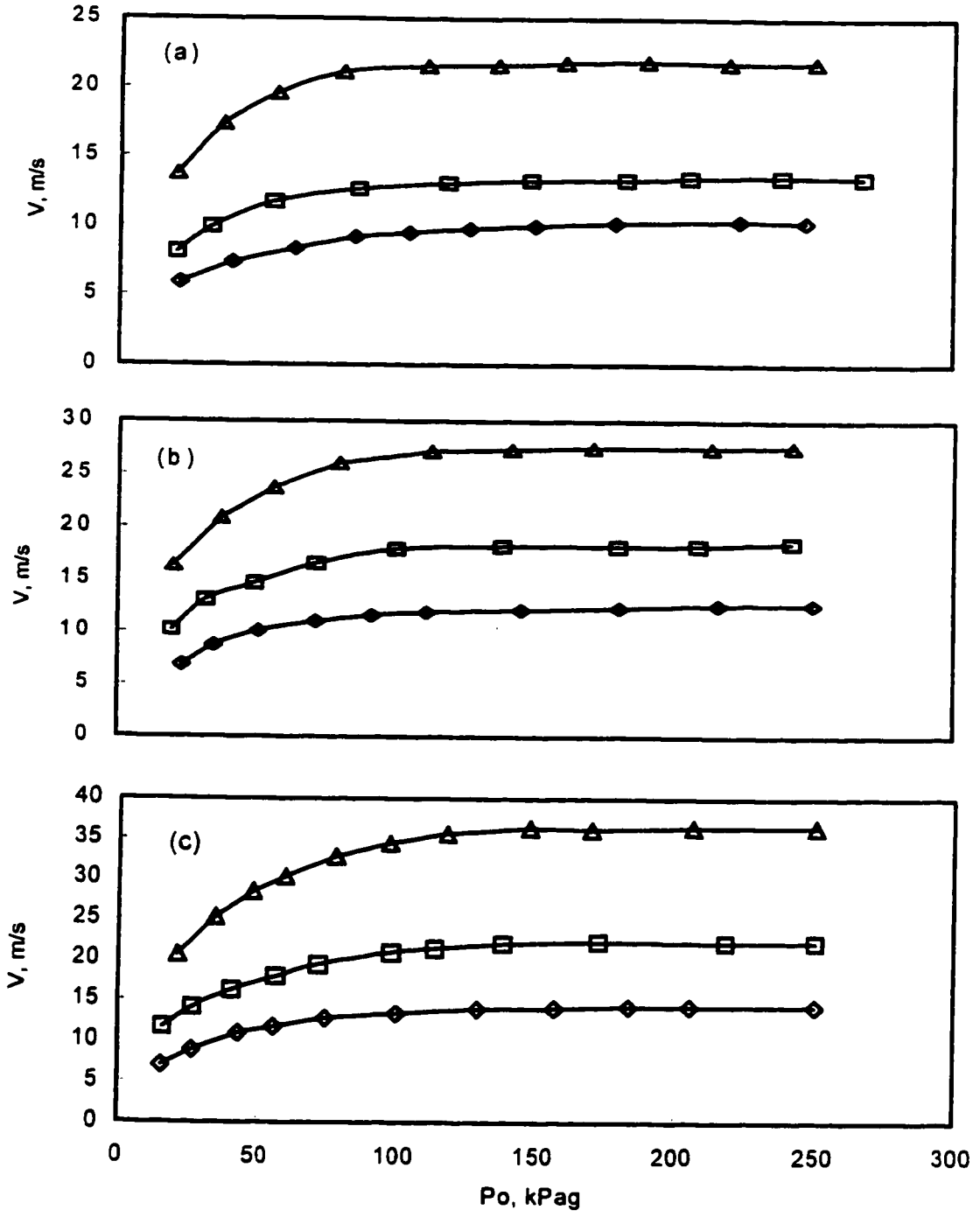

Figure 4.1 Fluid velocity v/s jet total pressure for various slot sizes; (a) slot size = 16 mm; (b) slot size = 13 mm; (c) slot size = 9.5 mm; ◊, V_1; □, V_2; Δ, V_3

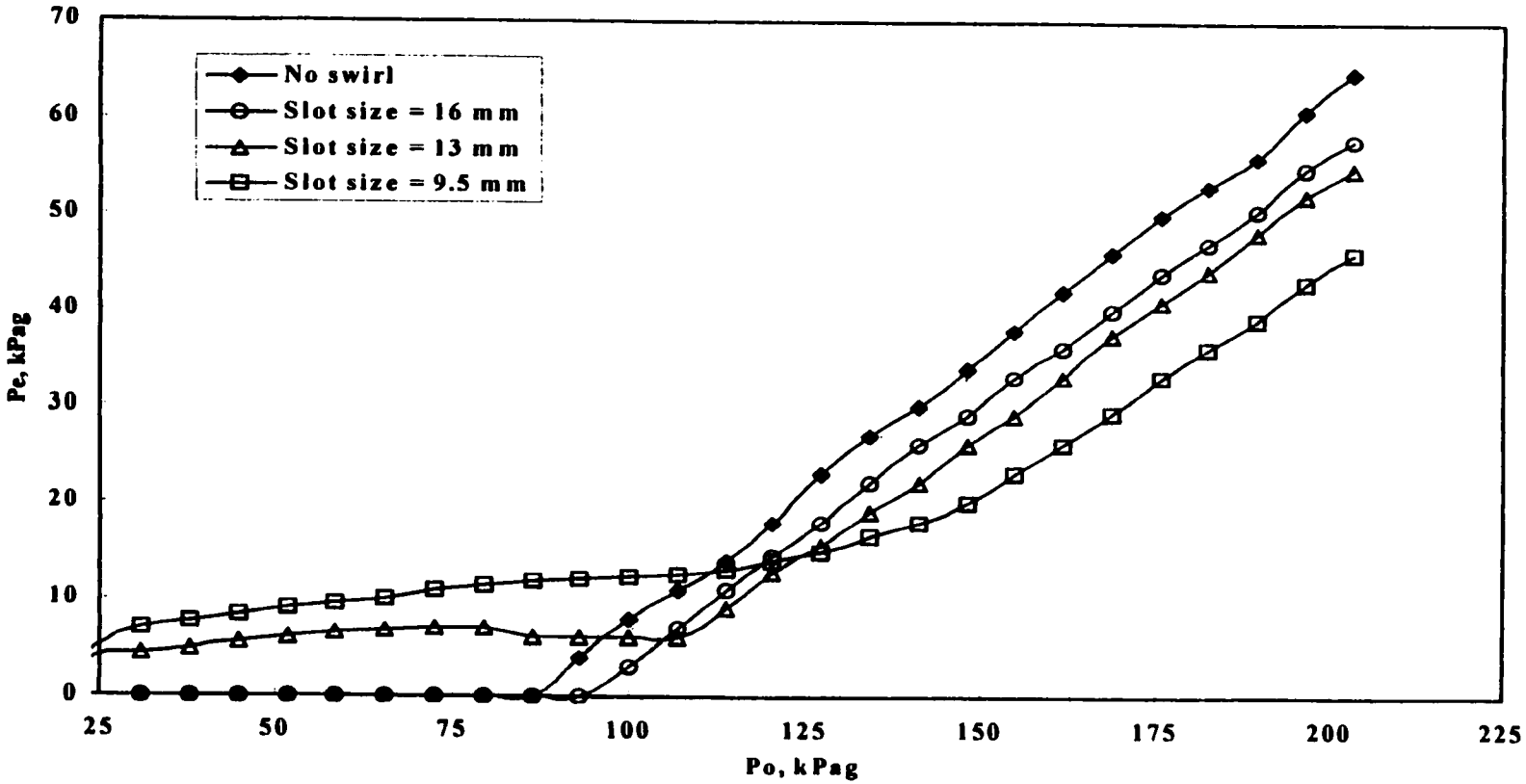

Figure 4.2 Static pressure at nozzle exit v/s jet total pressure; ♦, no swirl; o, slot size = 16 mm; Δ, slot size = 13 mm; □, slot size = 9.5 mm

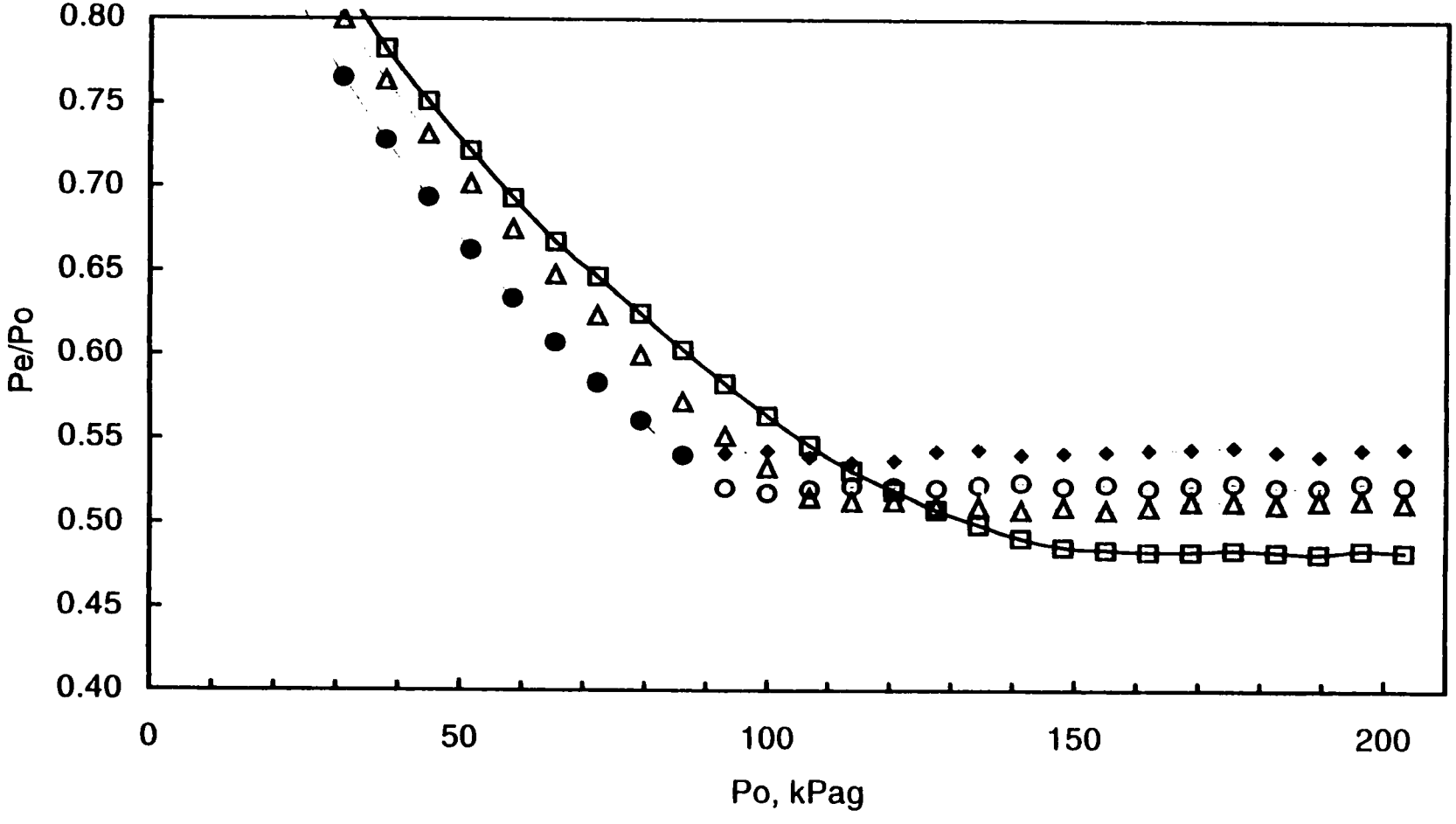

Figure 4.3 Static to total pressure ratio at nozzle exit v/s jet total pressure; ♦, no swirl; o, slot size = 16 mm; Δ, slot size = 13 mm; □, slot size = 9.5 mm

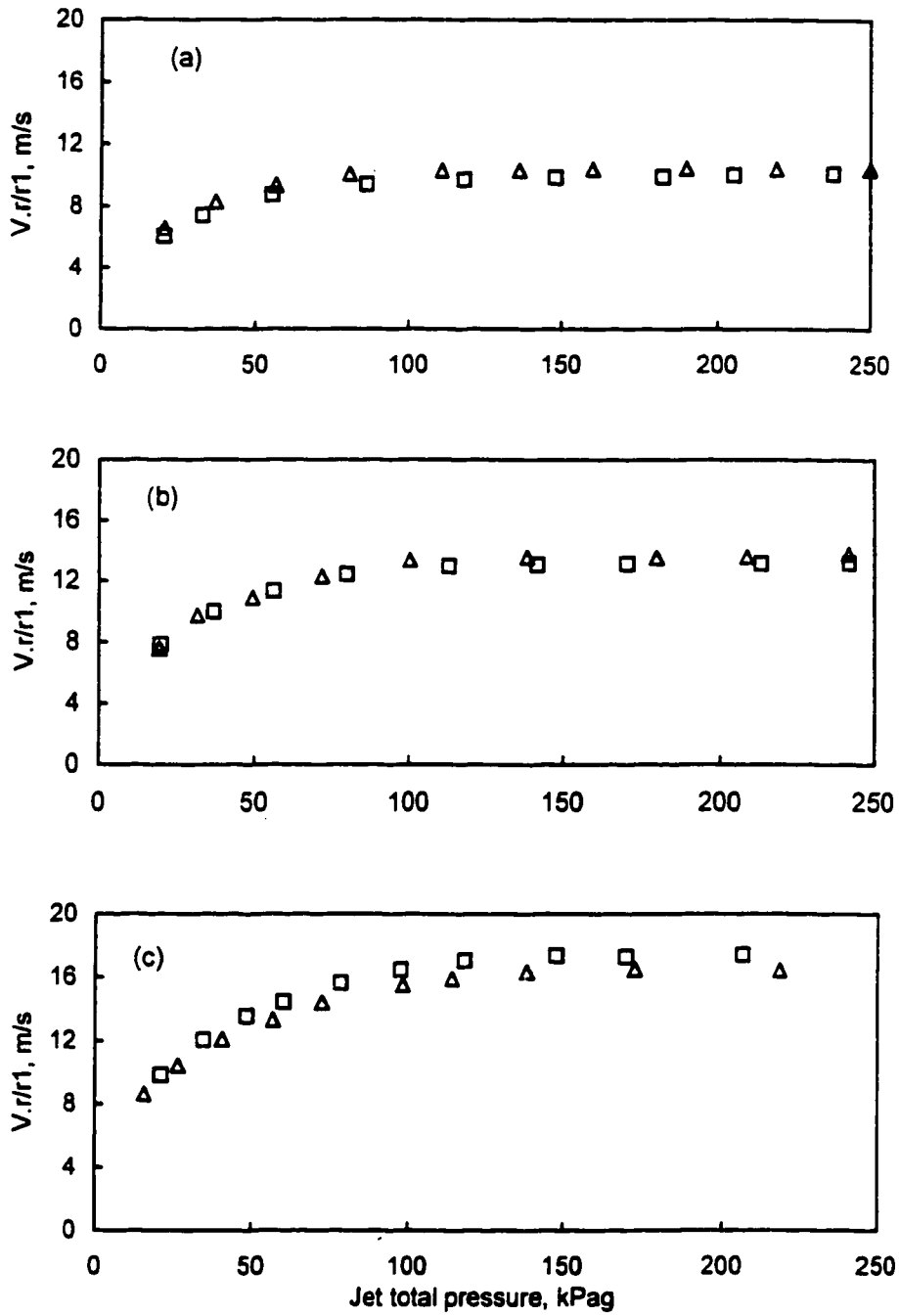

Figure 4.4 Experimental verification of fluid irrotationality inside the vortex chamber; (a) low swirl; (b) medium swirl; (c) high swirl. □, experimental, $r/r_1 = 0.48$; Δ, experimental, $r/r_1 = 0.75$

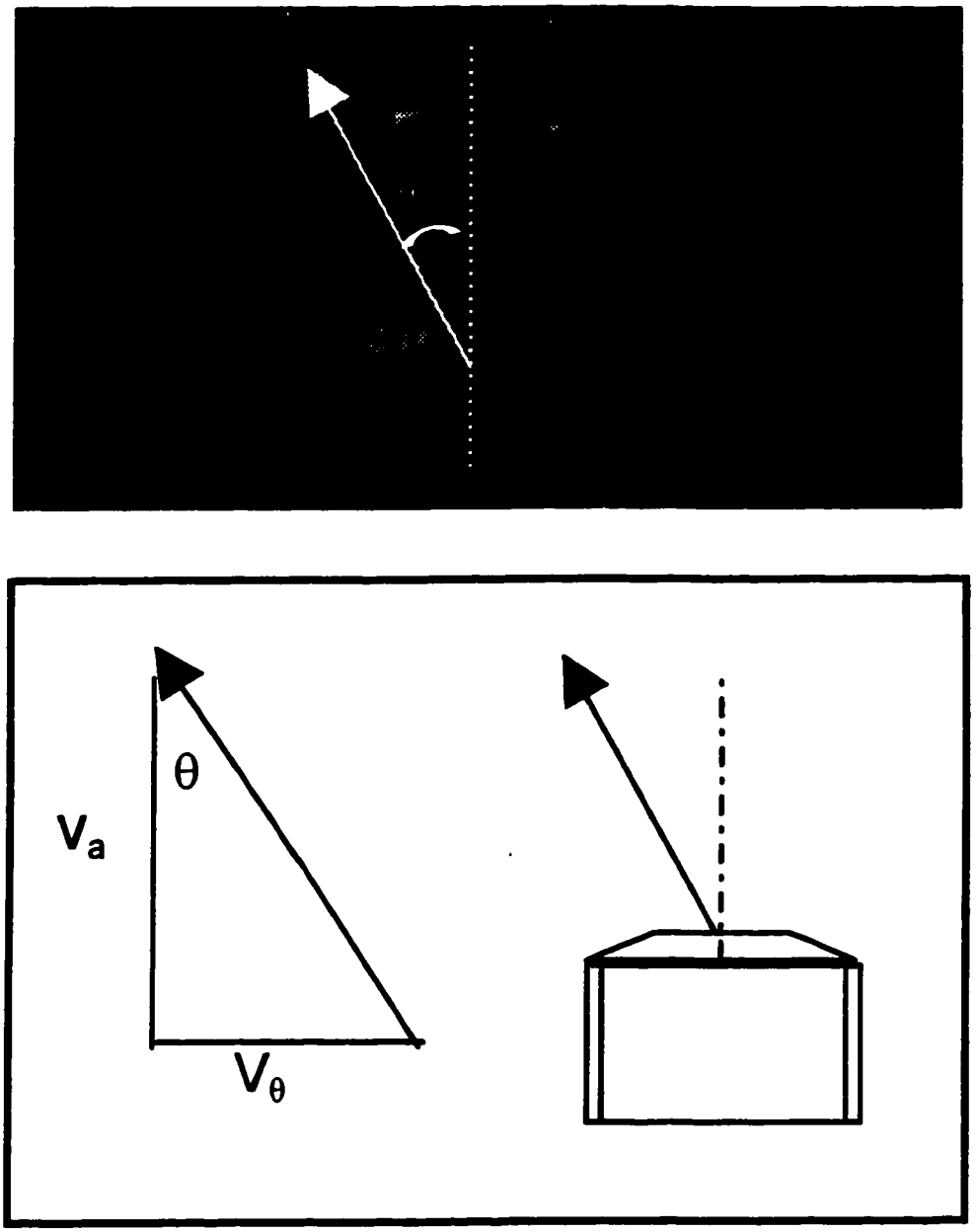

Figure 4.5 Schematic of the jet showing the tangential and axial velocity components

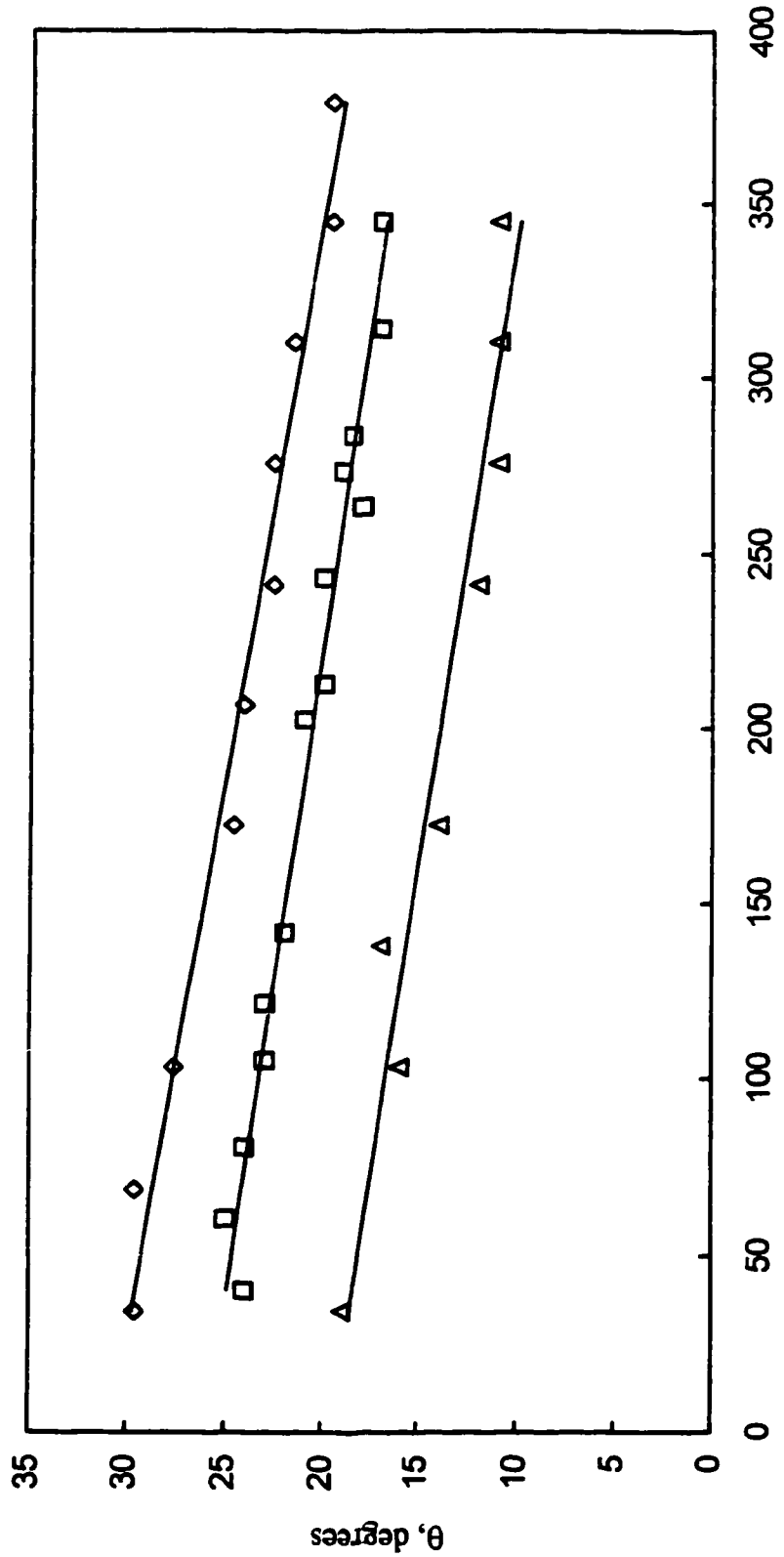

Figure 4.6. Flow angle with the nozzle axis at the nozzle exit; Δ, slot size = 16 mm; □, slot size = 13 mm; ◊, slot size = 9.5 mm

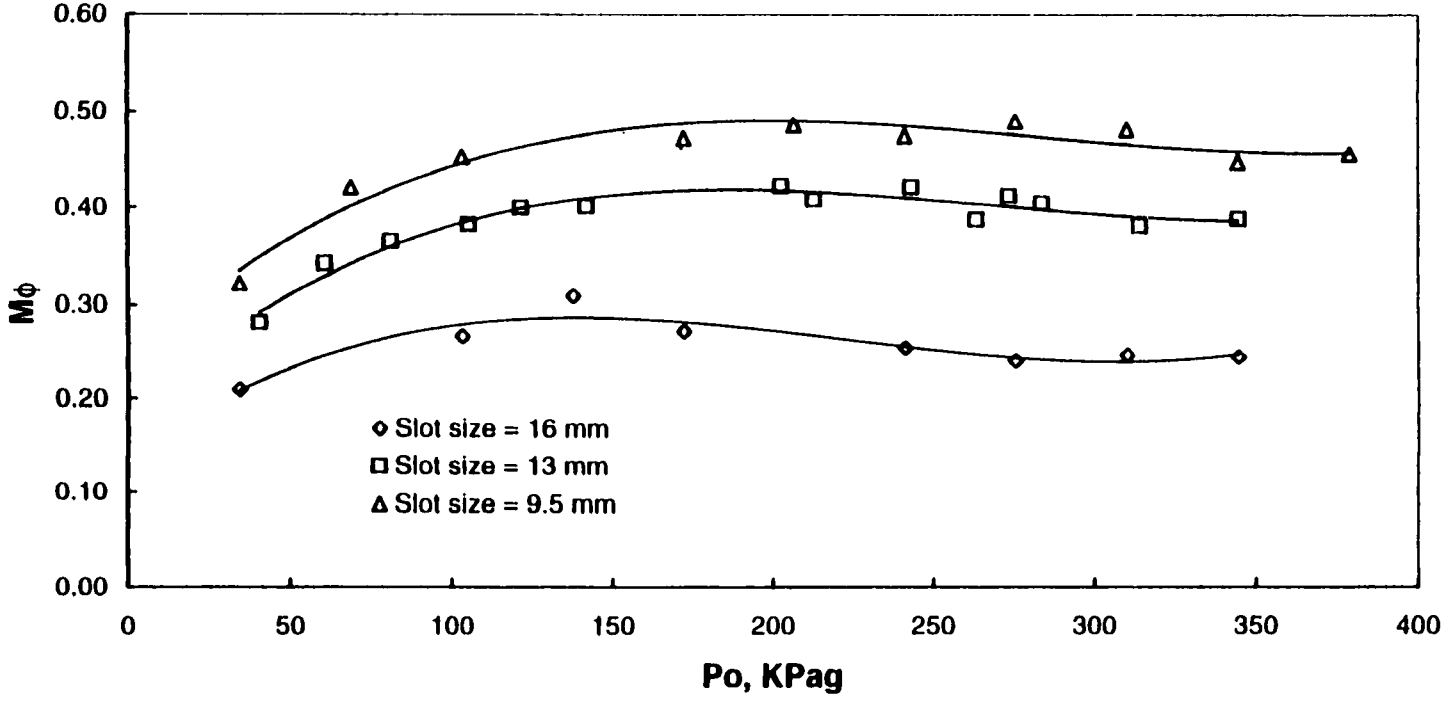

Figure 4.7 Calculated values of the swirl Mach number at the nozzle exit v/s jet total pressure for different slot sizes

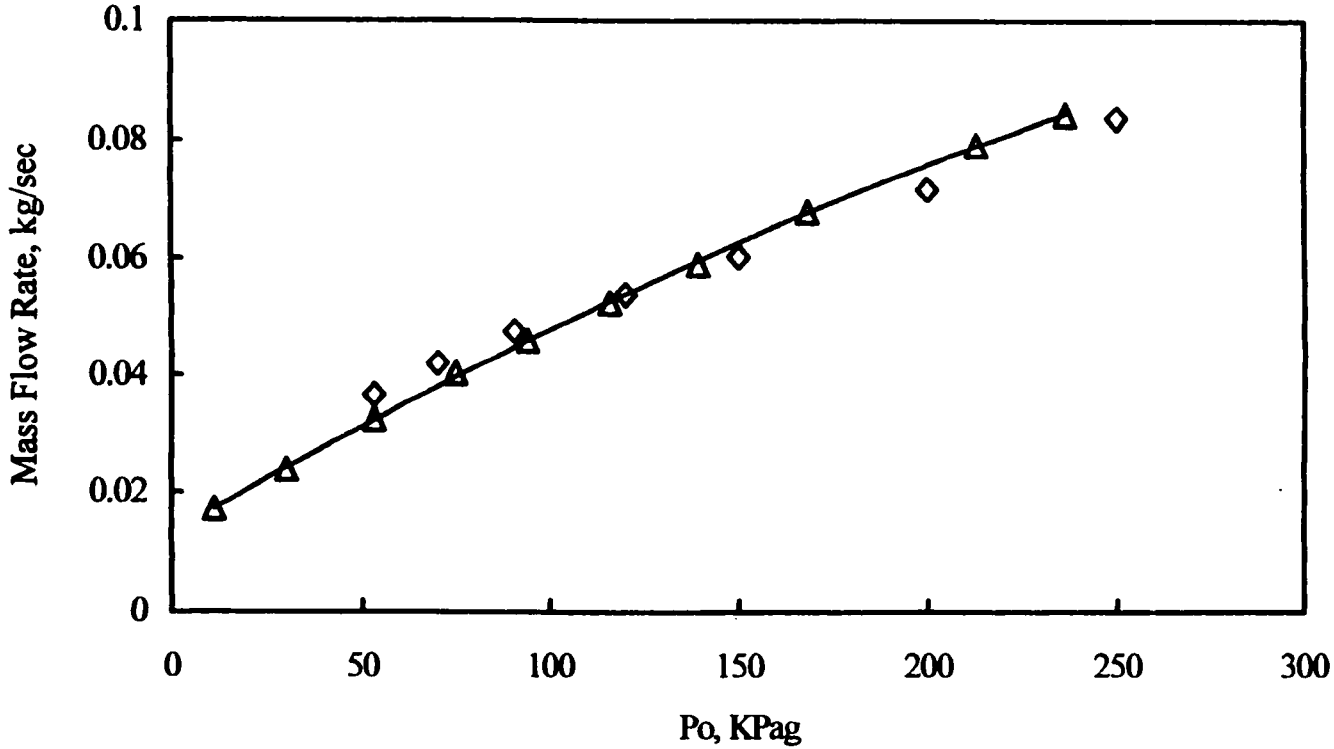

Figure 4.8 Mass flow rate v/s jet total pressure for the 16 mm slot size; Δ, experimental mass flow rate; ◊, theoretical mass flow rate

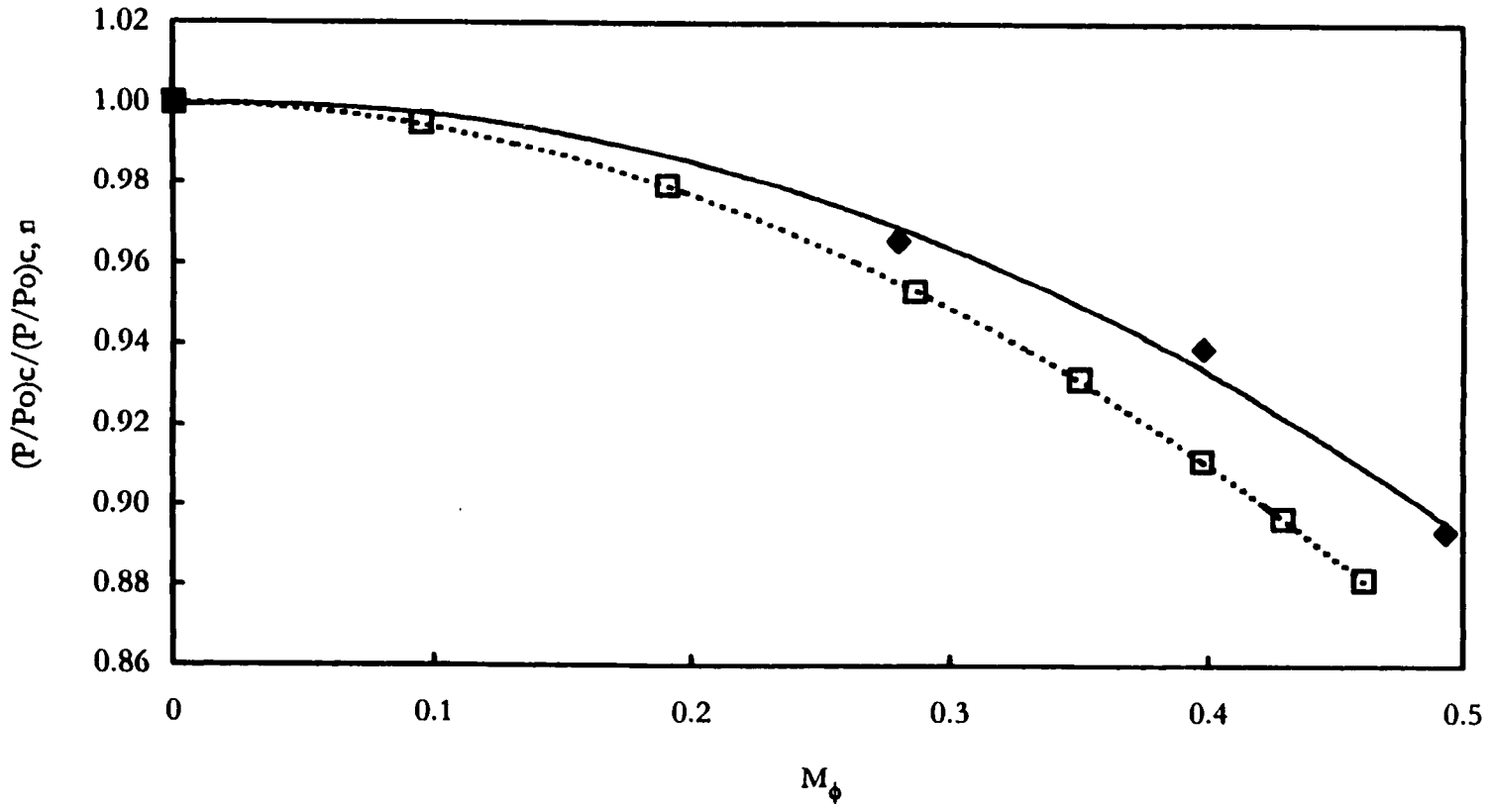

Figure 4.9 Critical pressure ratio with swirl normalized to that without swirl v/s the swirl Mach number; ♦, experiment; □, theory

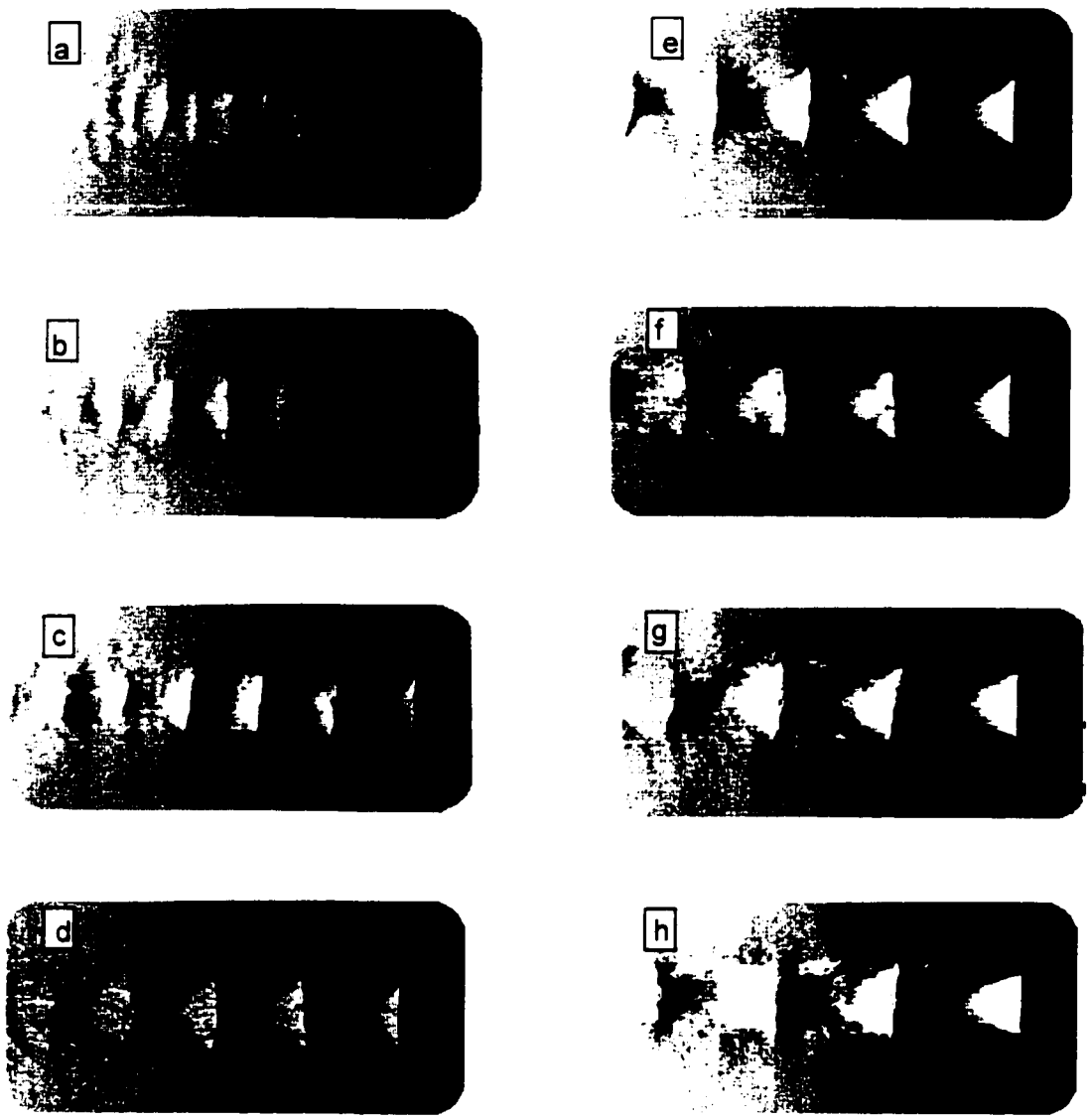

Figure 4.10. Schlieren photographs of supersonic jets without swirl: (a) Mj = 1.05; (b) Mj = 1.18; (c) Mj = 1.28; (d) Mj = 1.37; (e) Mj = 1.44; (f) Mj = 1.51; (g) Mj = 1.57; (h) Mj = 1.62

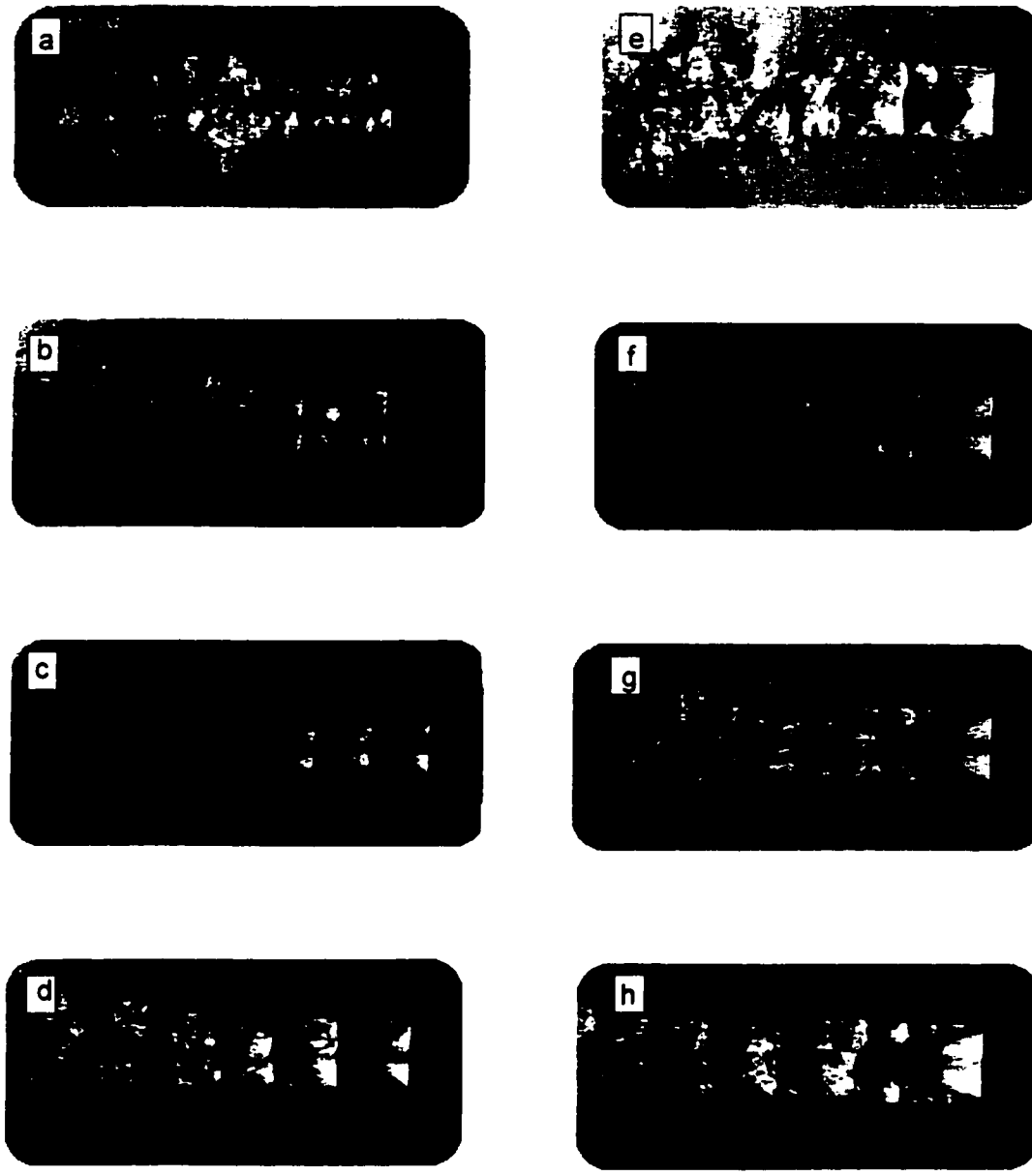

Figure 4.11. Schlieren photographs of supersonic jets with low swirl: (a) Mj = 1.05; (b) Mj = 1.18; (c) Mj = 1.28; (d) Mj = 1.37; (e) Mj = 1.44; (f) Mj = 1.51; (g) Mj = 1.57; (h) Mj = 1.62

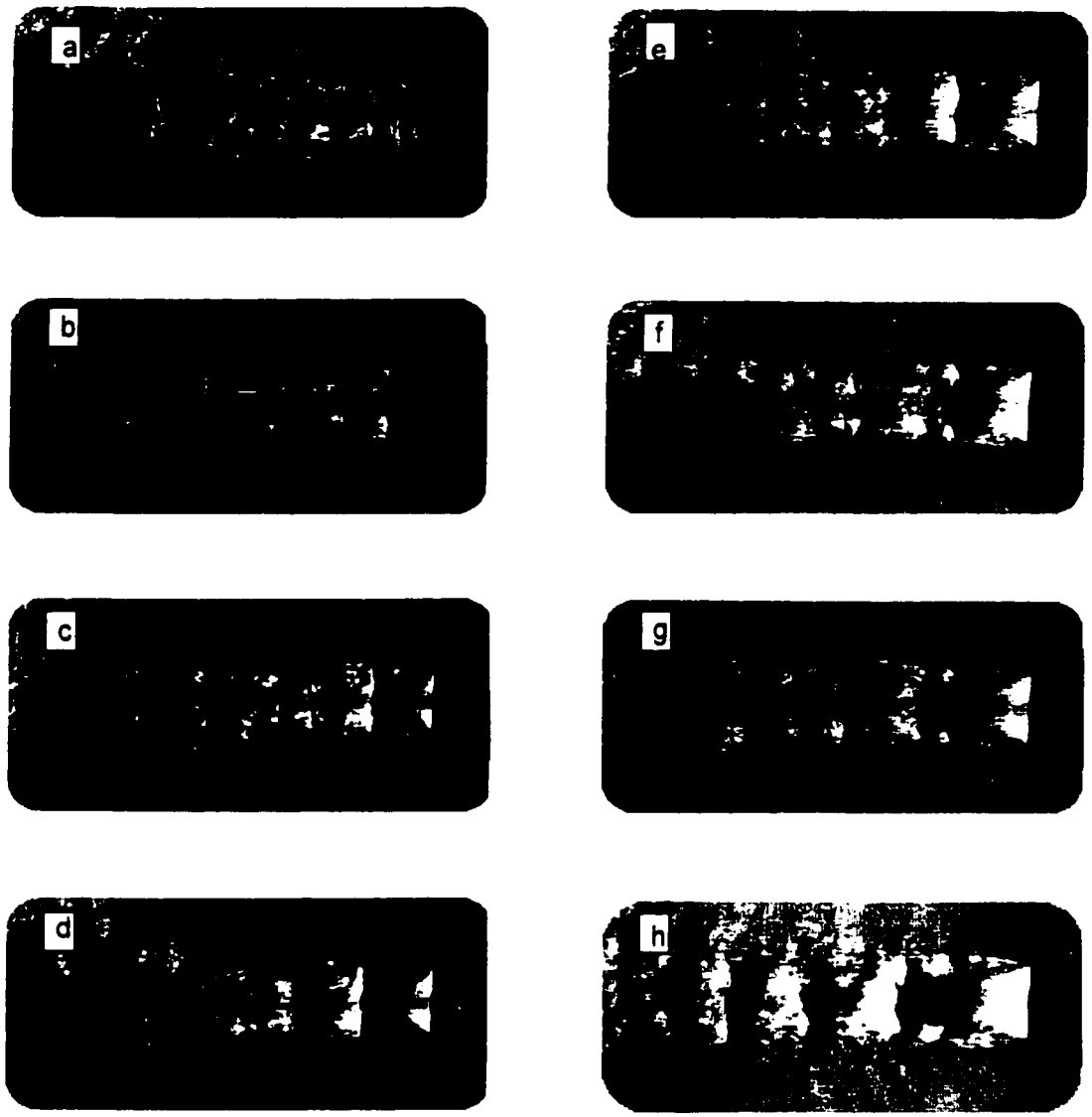

Figure 4.12 Schlieren photographs of supersonic jets with medium swirl: (a) Mj = 1.05; (b) Mj = 1.18; (c) Mj = 1.28; (d) Mj = 1.37; (e) Mj = 1.44; (f) Mj = 1.51; (g) Mj = 1.57; (h) Mj = 1.62

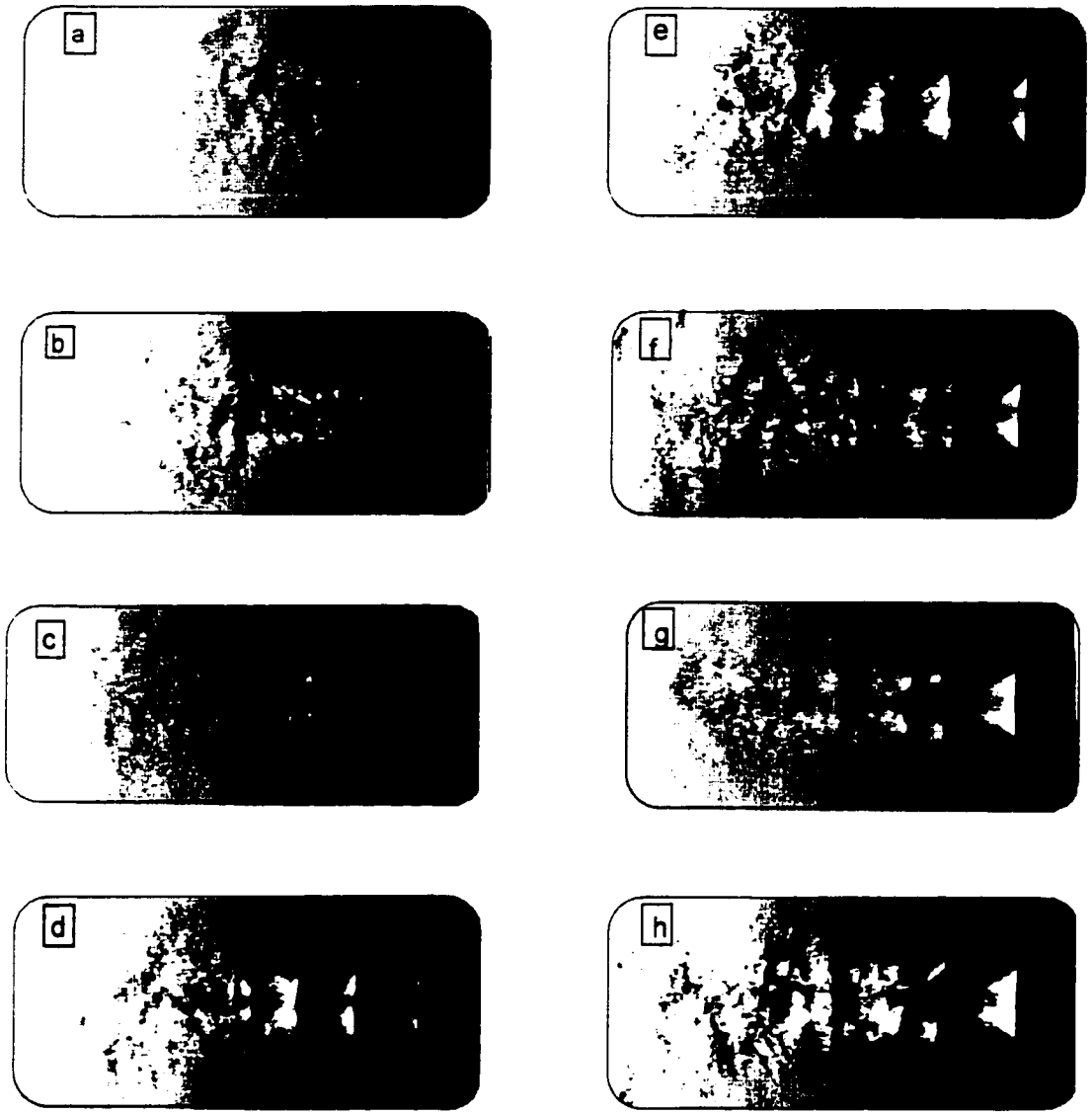

Figure 4.13 Schlieren photographs of supersonic jets with high swirl: (a) Mj = 1.05; (b) Mj = 1.18; (c) Mj = 1.28; (d) Mj = 1.37; (e) Mj = 1.44; (f) Mj = 1.51; (g) Mj = 1.57; (h) Mj = 1.62

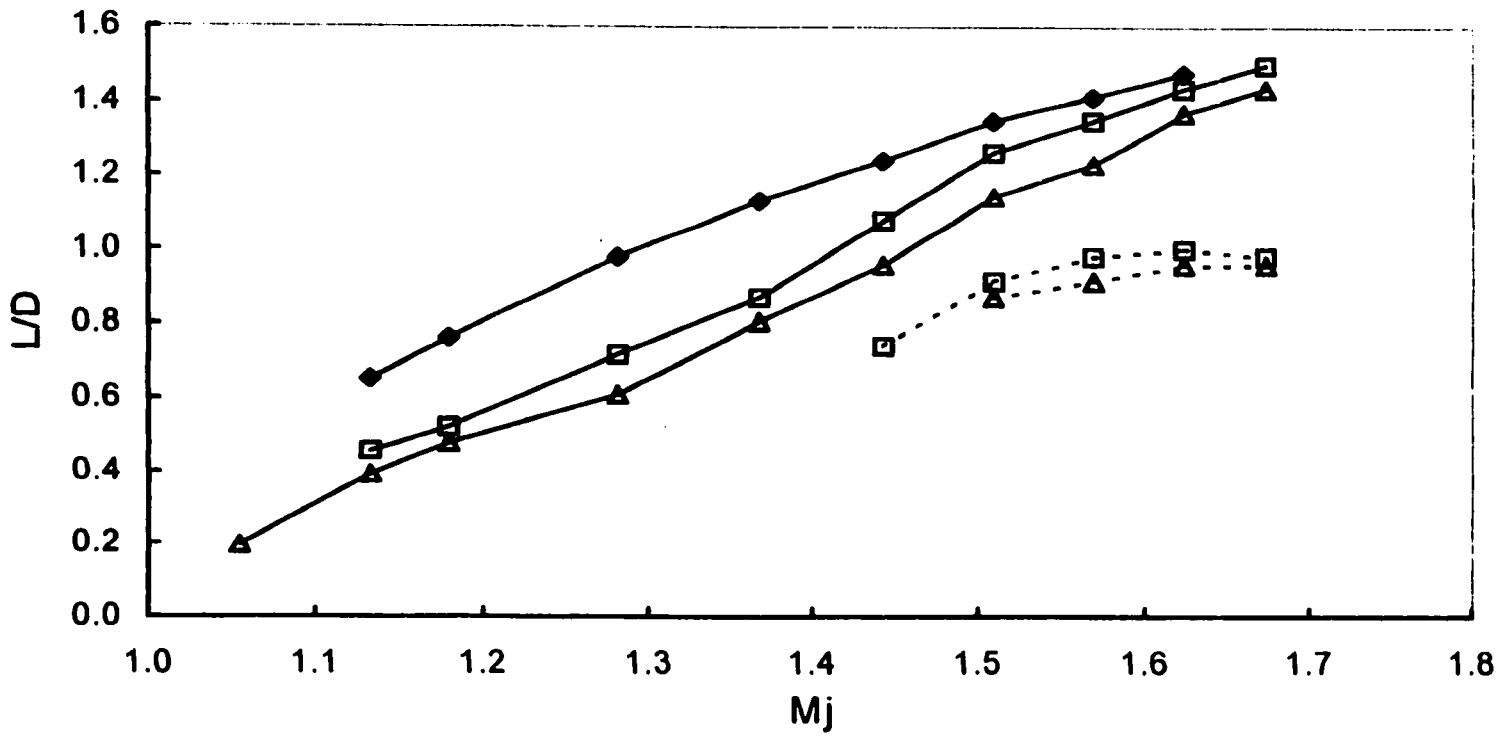

Figure 4.14 Cell length and secondary shock position v/s M_j with and without swirl; ♦ , no swirl; □ , low swirl; Δ, medium swirl; —— primary cell length; ---- secondary shock position.

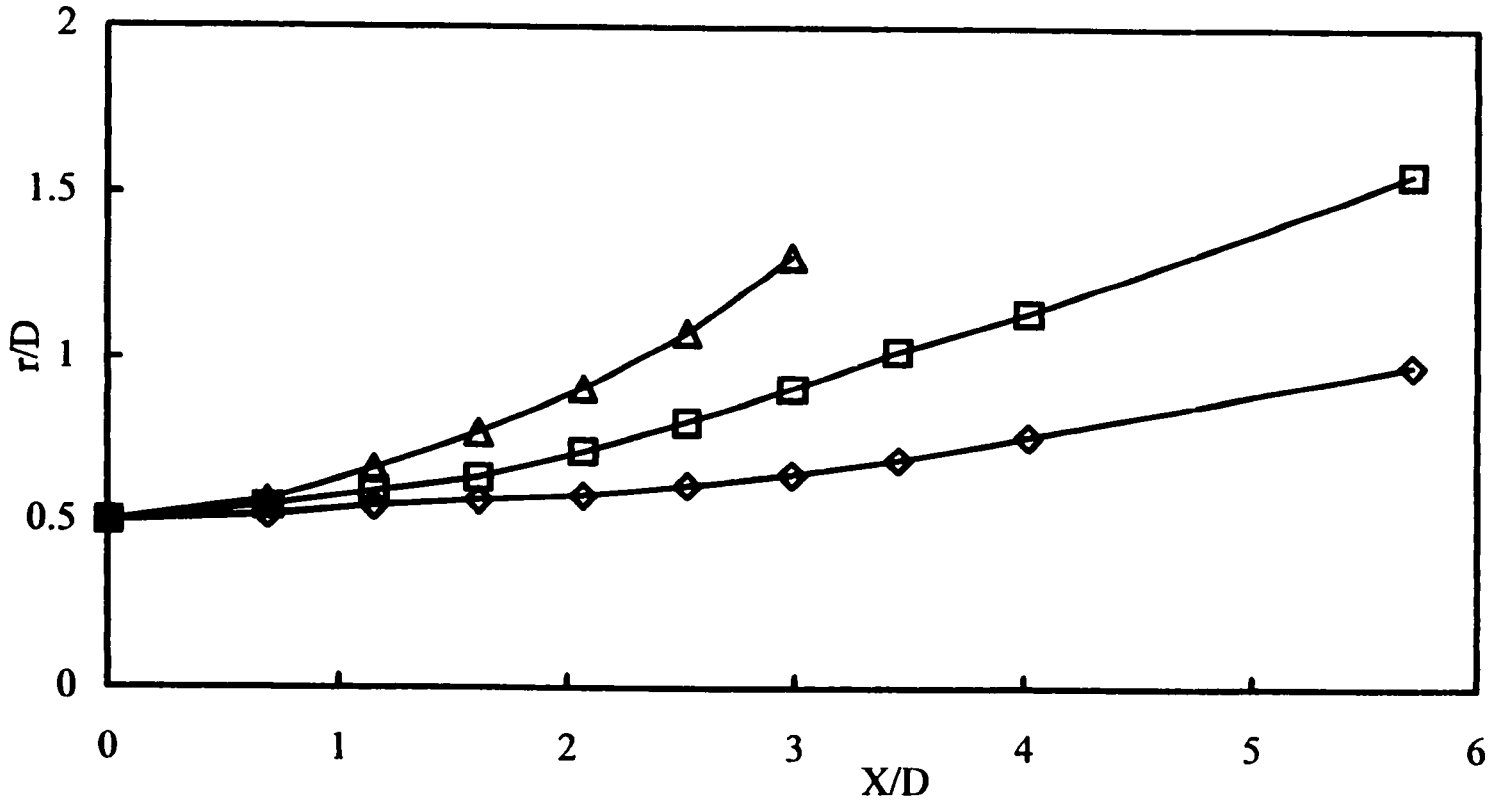

Figure 4.15 Growth of a circular jet with downstream distance; ◊, no swirl; □, low swirl; Δ, high swirl

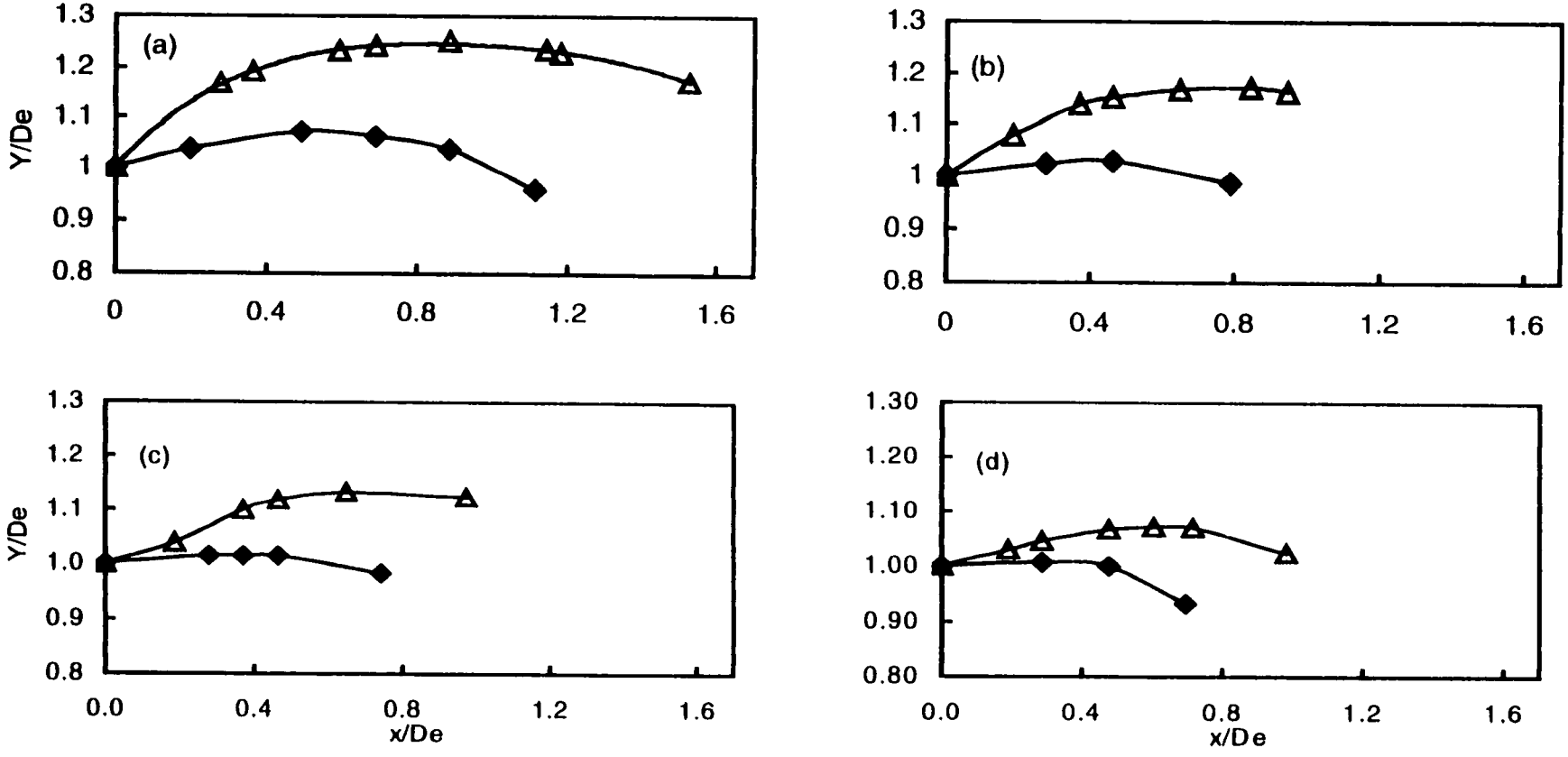

Figure 4.16 Jet boundary of the inviscid core with and without swirl; (a) no swirl; (b) low swirl; (c) medium swirl; (d) high swirl.

♦, M_j = 1.28; Δ, M_j = 1.57

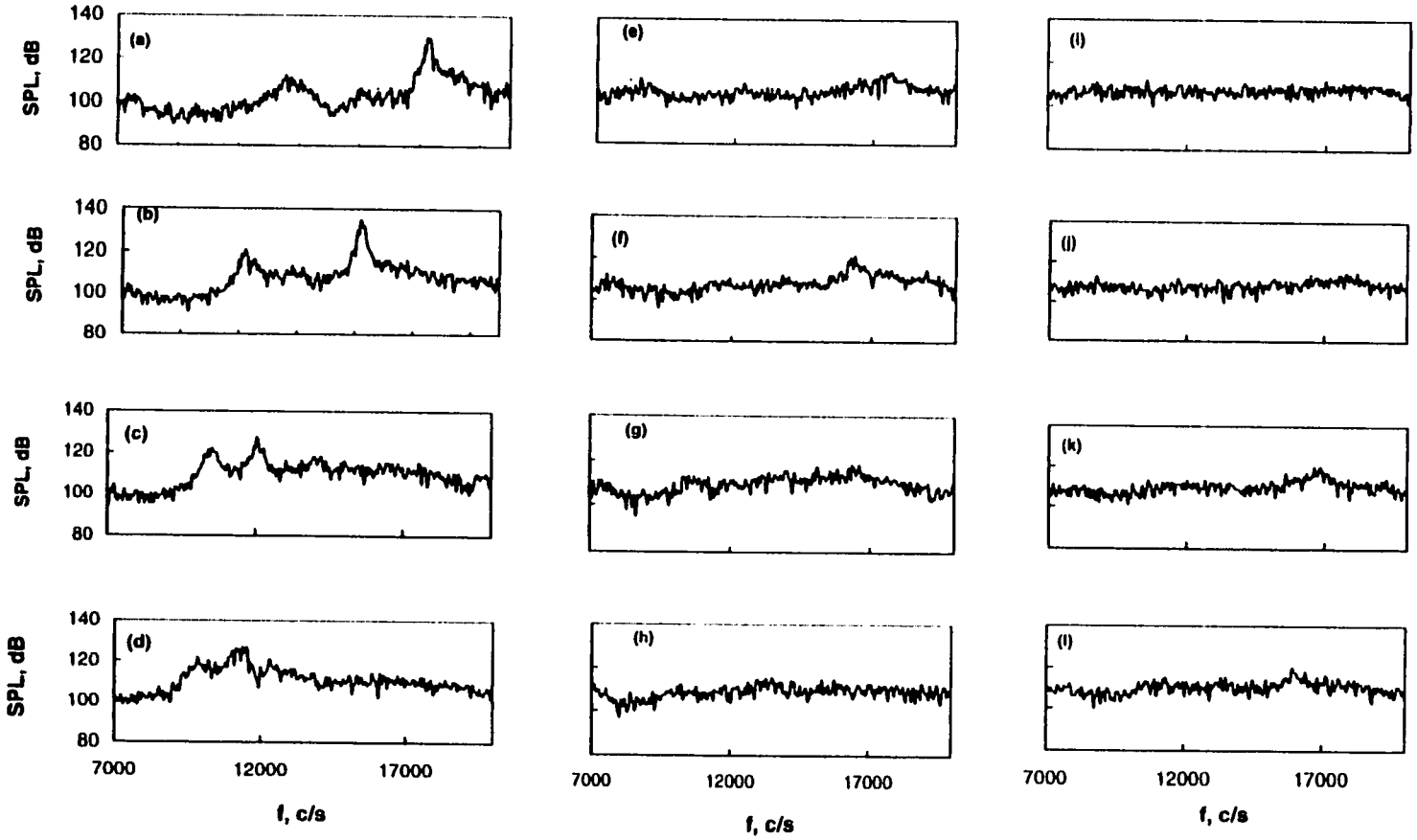

Figure 4.17 Typical narrow band spectra with and without swirl. No swirl: (a) Mj = 1.18; (b) Mj = 1.28; (c) Mj = 1.37; (d) Mj 1.44. Low swirl: (e) Mj = 1.18; (f) Mj = 1.28; (g) Mj = 1.37; (h) Mj 1.44. High swirl: (i) Mj = 1.18; (j) Mj = 1.28; (k) Mj = 1.37; (l) Mj 1.44.

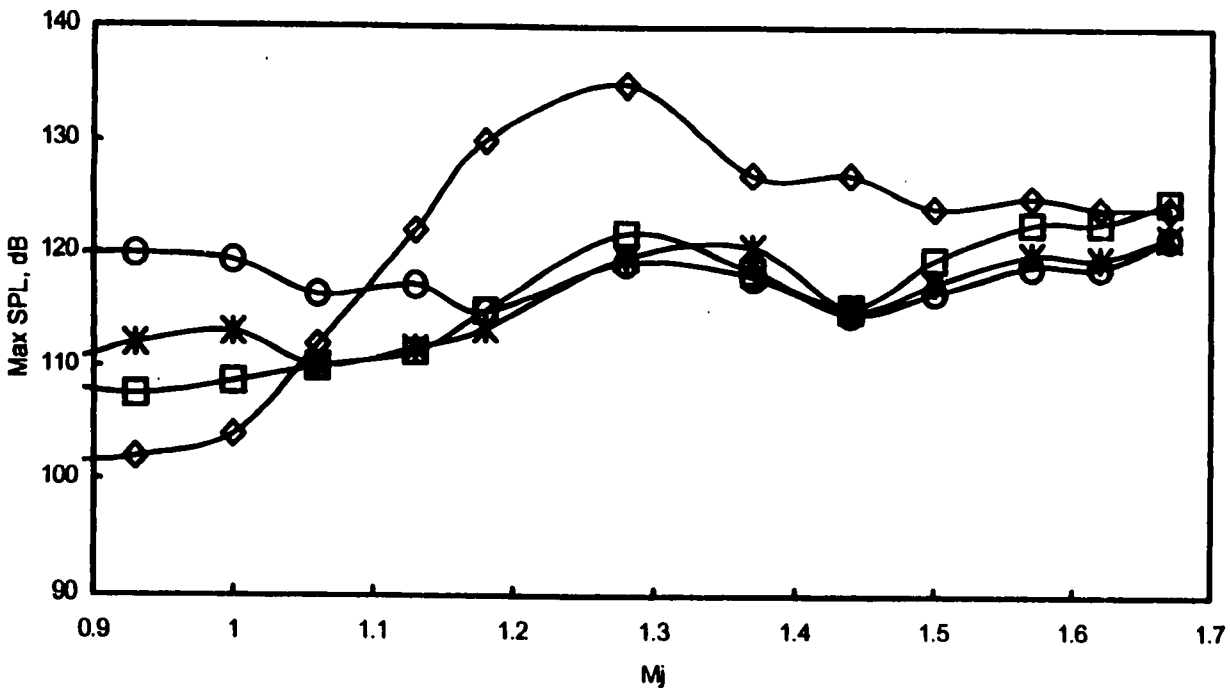

Figure 4.18 . SPL v/s Mj with and without swirl; ◊, no swirl; □, low swirl; ∗, medium swirl; o, high swirl

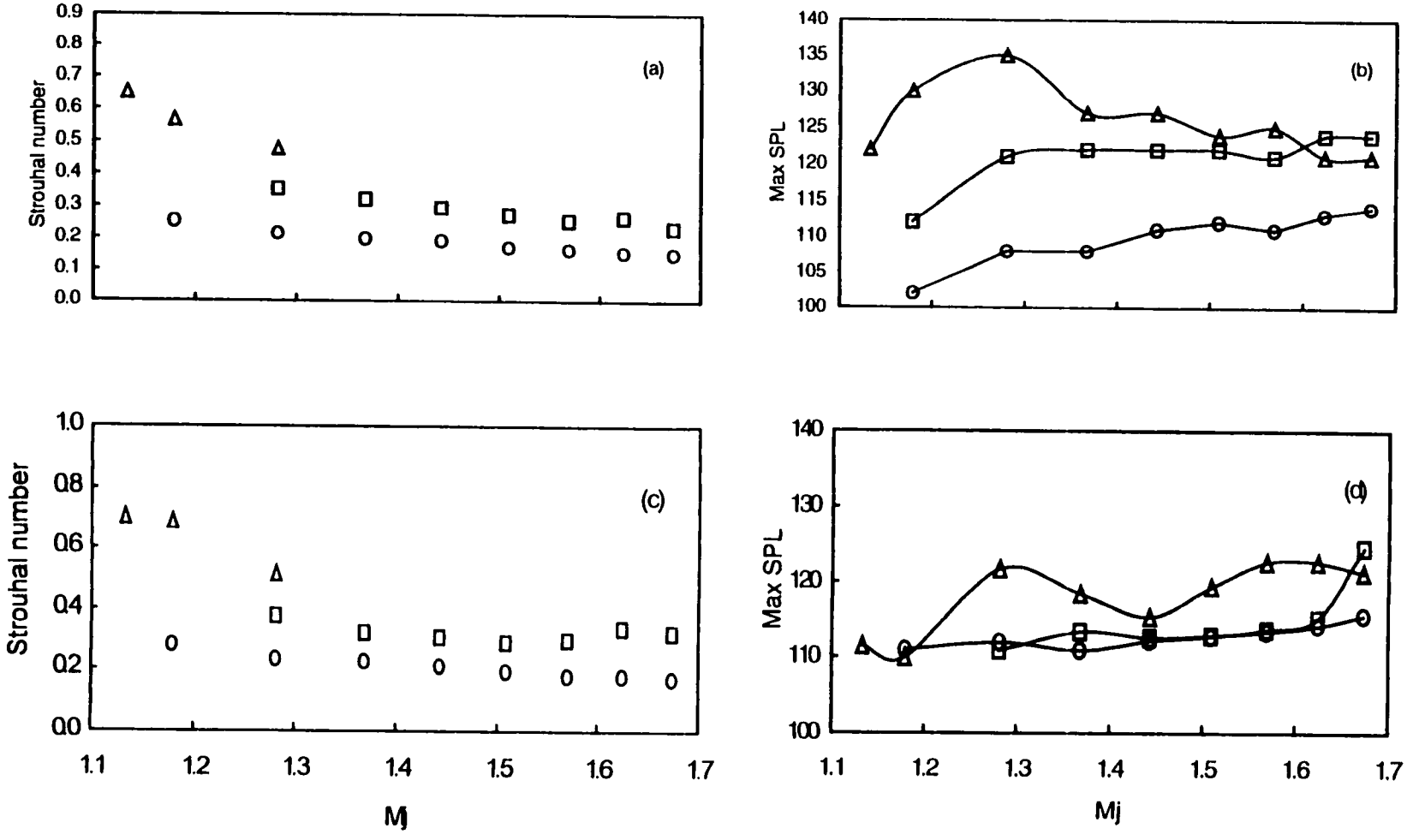

Figure 4.19. Strouhal number and SPL v/s Mj with and without swirl; (a), (b) no swirl; (c), (d) low swirl. Δ, A; □, B; o, C

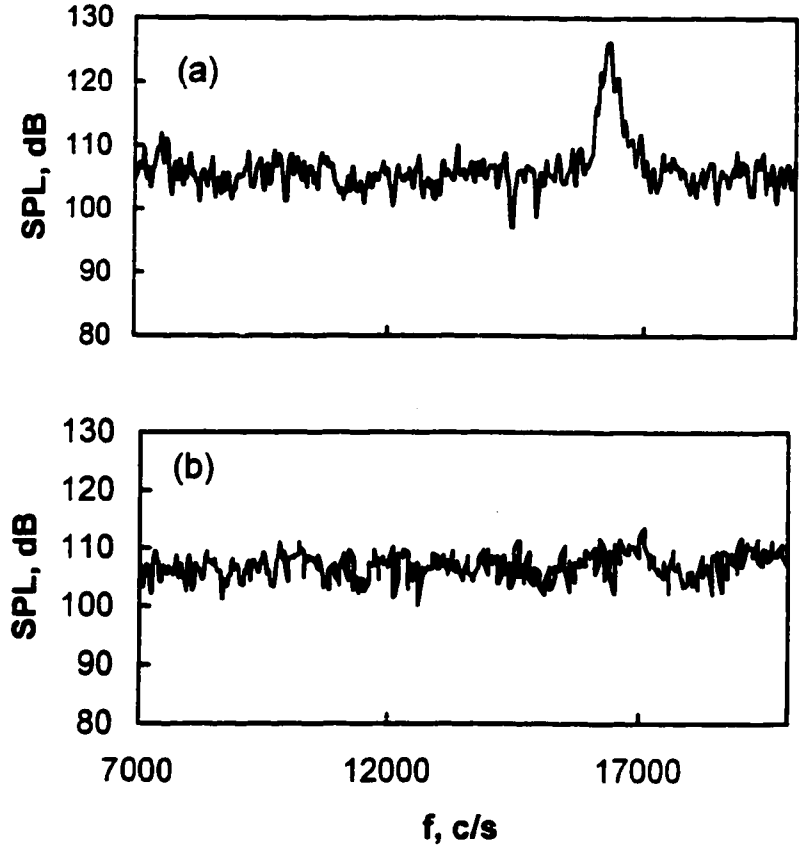

Figure 4.20 Noise spectra for a jet Mach number of 1.28 (30° from the centerline of exhaust nozzle); (a) no swirl; (b) low swirl

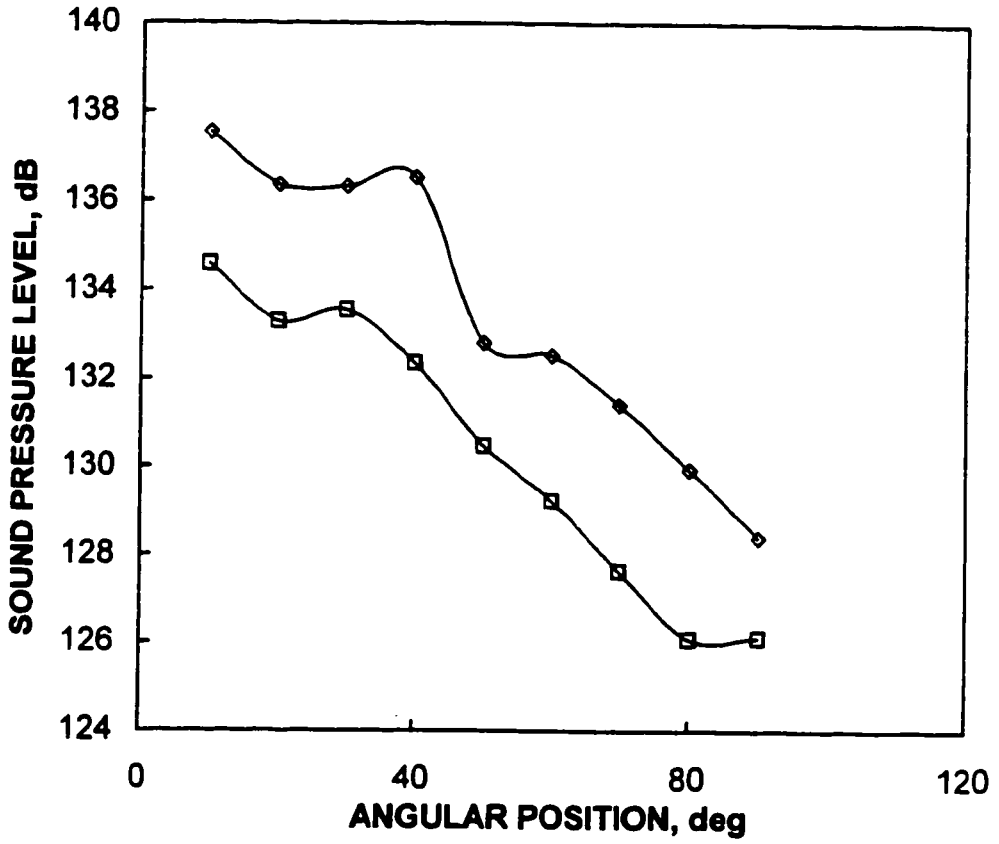

Figure 4.21 Over-all sound pressure levels as a function of angular position from the jet axis; ◊, no swirl; □, low swirl

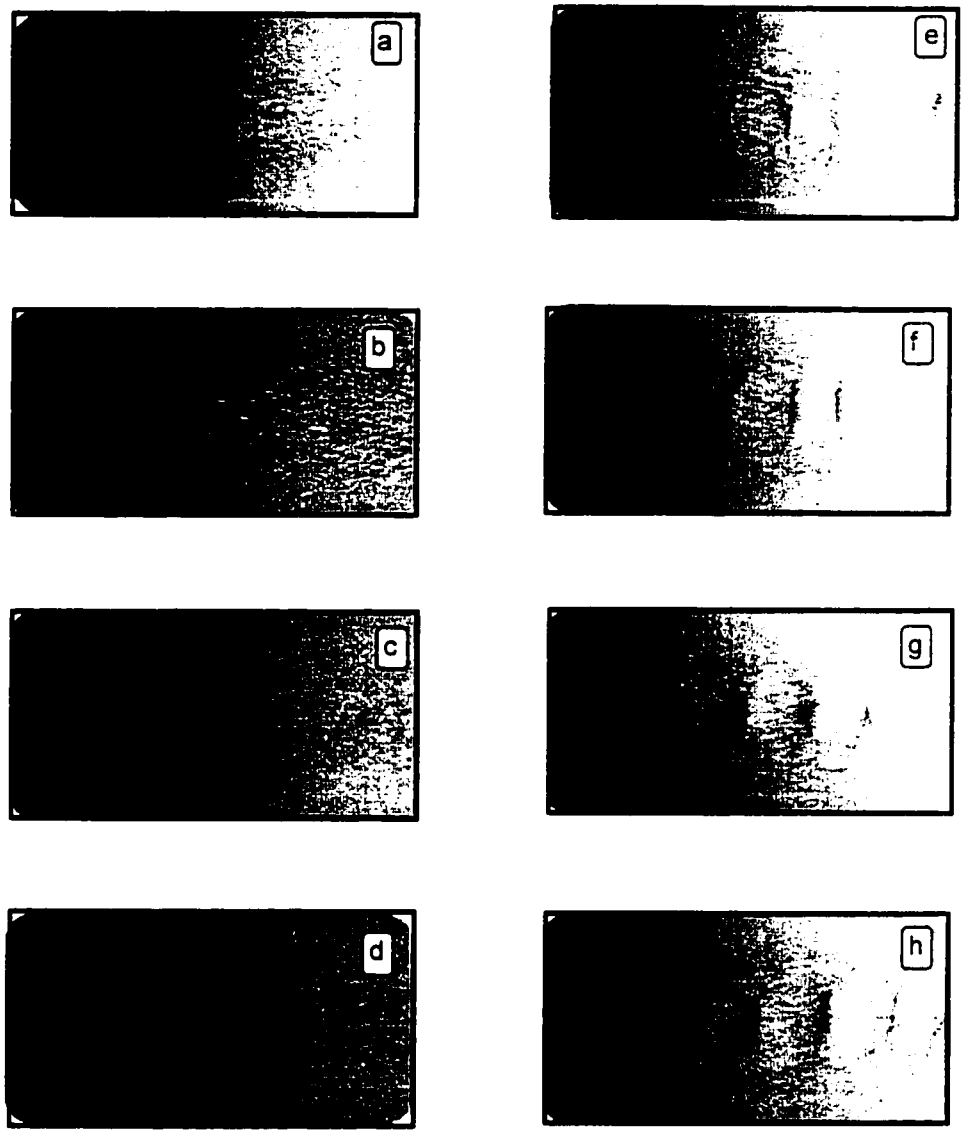

Figure 4.22 Schlieren photographs of supersonic jets with large perturbation at the nozzle exit (downstream side view); (a) Mj = 1.13; (b) Mj = 1.18; (c) Mj = 1.28; (d) Mj = 1.37; (e) Mj = 1.44; (f) Mj = 1.51; (g) Mj = 1.57; (h) Mj = 1.62

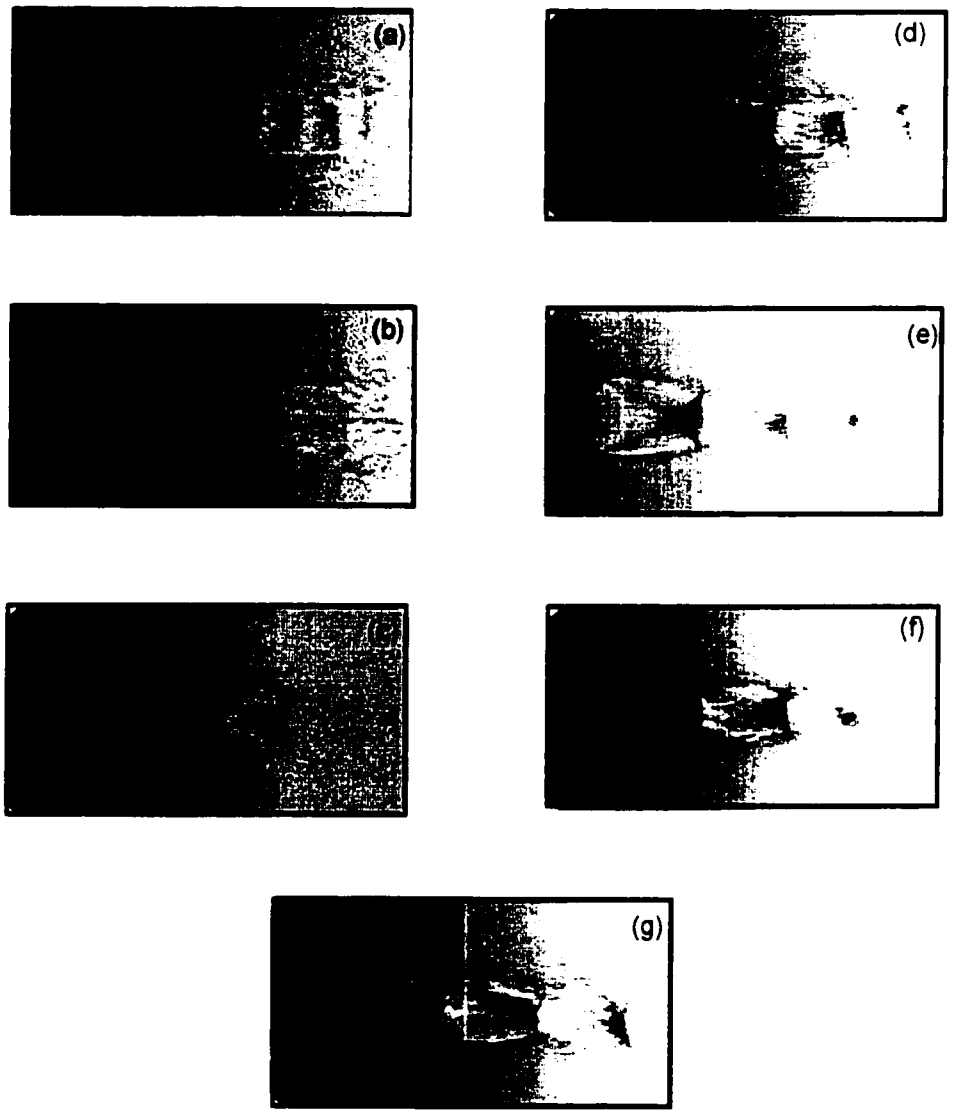

Figure 4.23 Schlieren photographs of supersonic jets with large perturbation at the nozzle exit (upstream side view); (a) Mj = 1.13; (b) Mj = 1.18; (c) Mj = 1.28; (d) Mj = 1.37; (e) Mj = 1.44; (f) Mj = 1.51; (g) Mj = 1.57; (h) Mj = 1.62

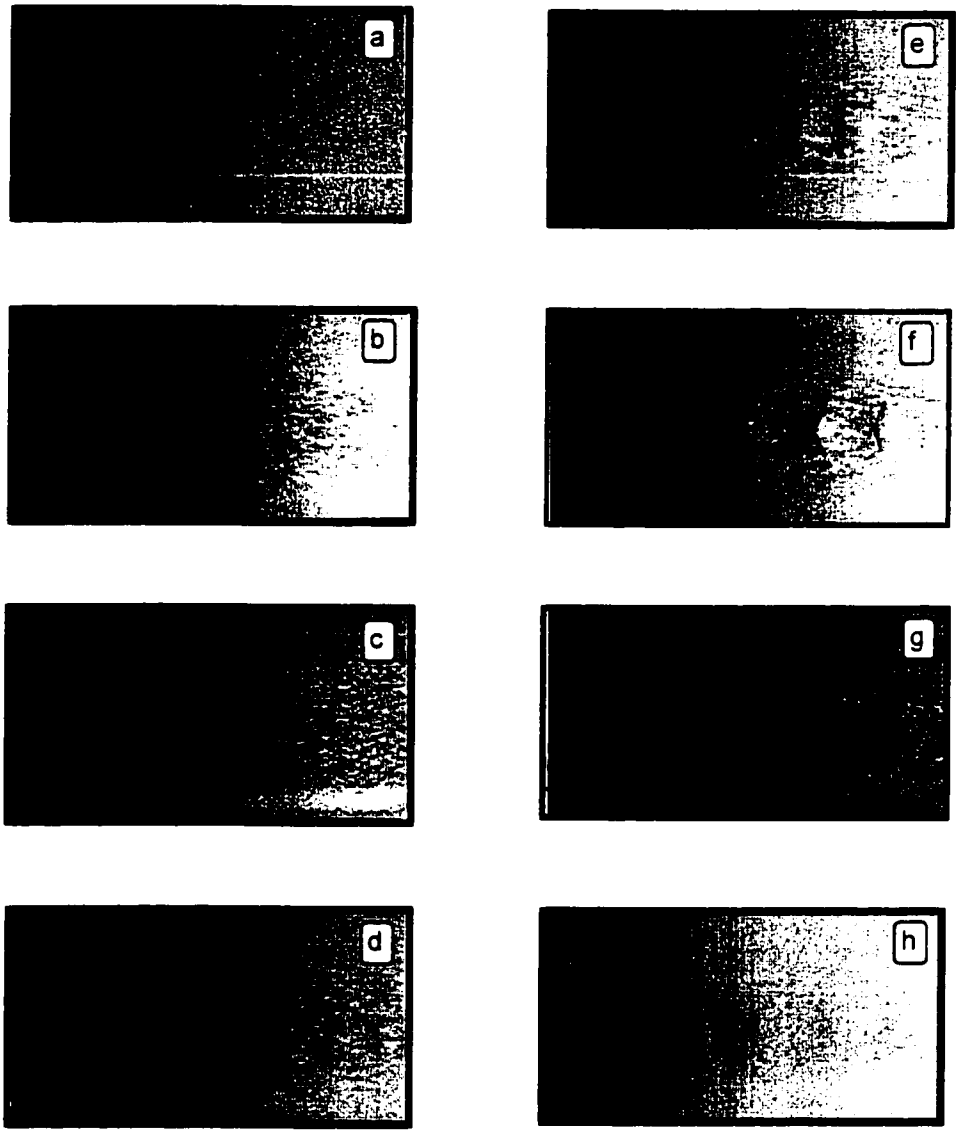

Figure 4.24 Schlieren photographs of supersonic jets with small perturbation at the nozzle exit (downstream side view); (a) Mj = 1.13; (b) Mj = 1.18; (c) Mj = 1.28; (d) Mj = 1.37; (e) Mj = 1.44; (f) Mj = 1.51; (g) Mj = 1.57; (h) Mj = 1.62

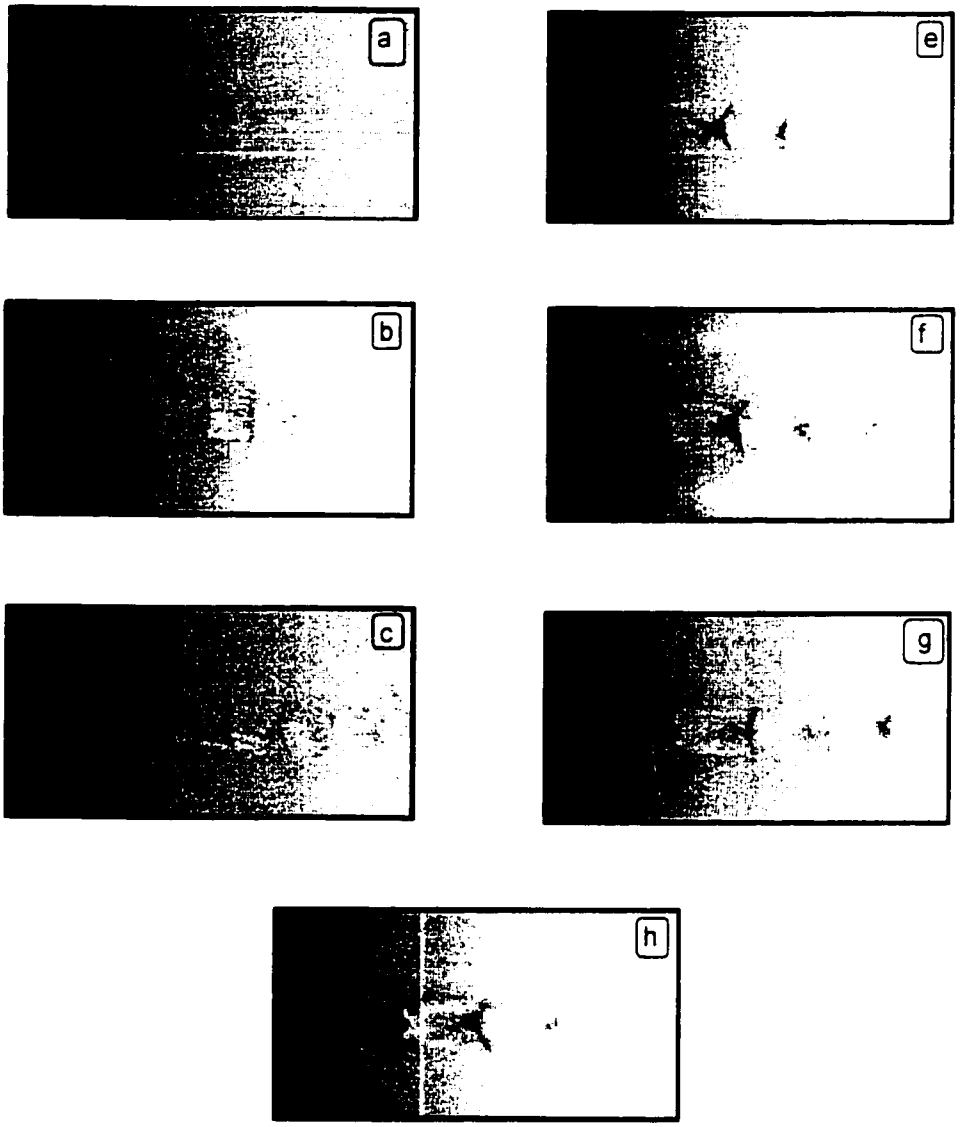

Figure 4.25 Schlieren photographs of supersonic jets with small perturbation at the nozzle exit (upstream side view); (a) Mj = 1.13; (b) Mj = 1.18; (c) Mj = 1.28; (d) Mj = 1.37; (e) Mj = 1.44; (f) Mj = 1.51; (g) Mj = 1.57; (h) Mj = 1.62

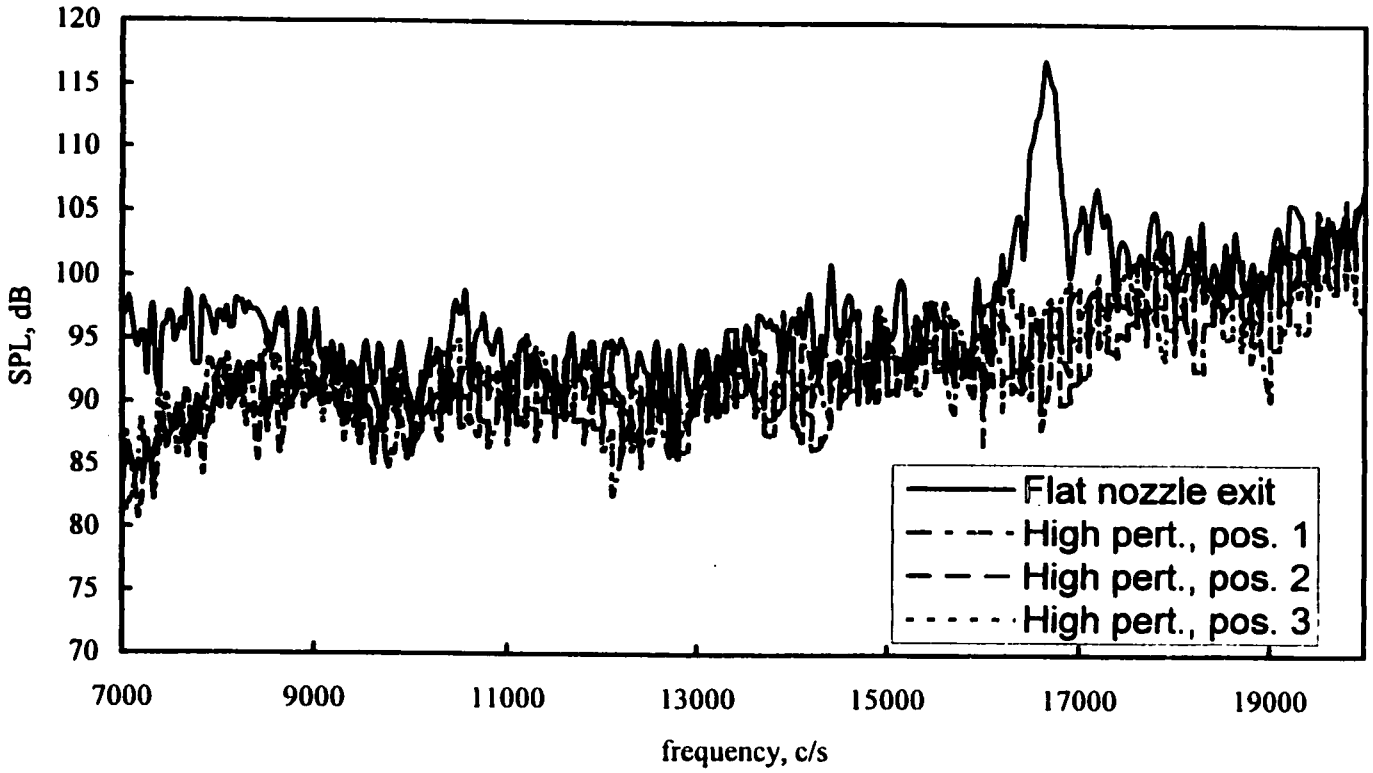

Figure 4.26 Spectrum obtained with highly perturbed nozzle exit compared to that obtained with a plain nozzle exit. Mj = 1.28; microphone located radially 15 Dj from the jet centerline

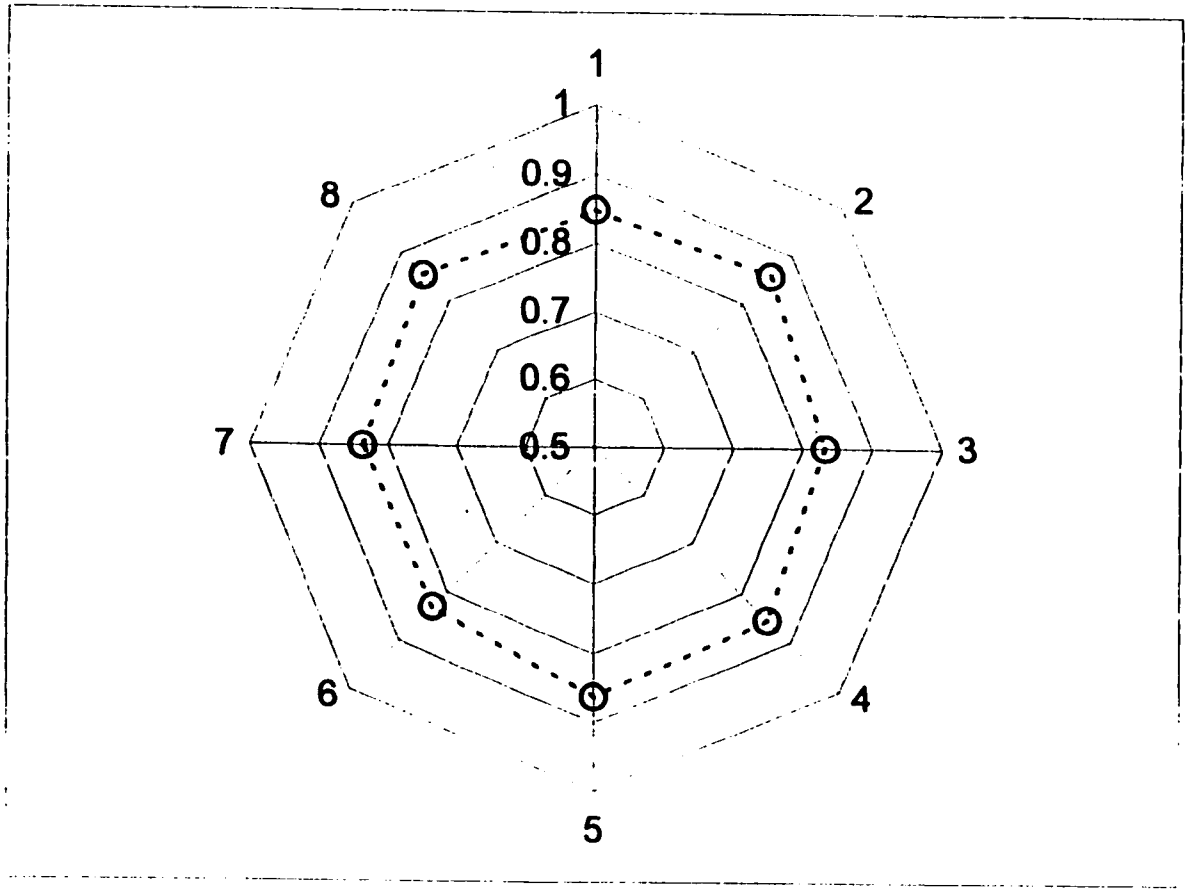

Figure 4.27 Percetage noise reduction with Highly perturbed nozzle. Mj = 1.28; microphone placed at a fixed radial location (15 Dj) and at different angular positions

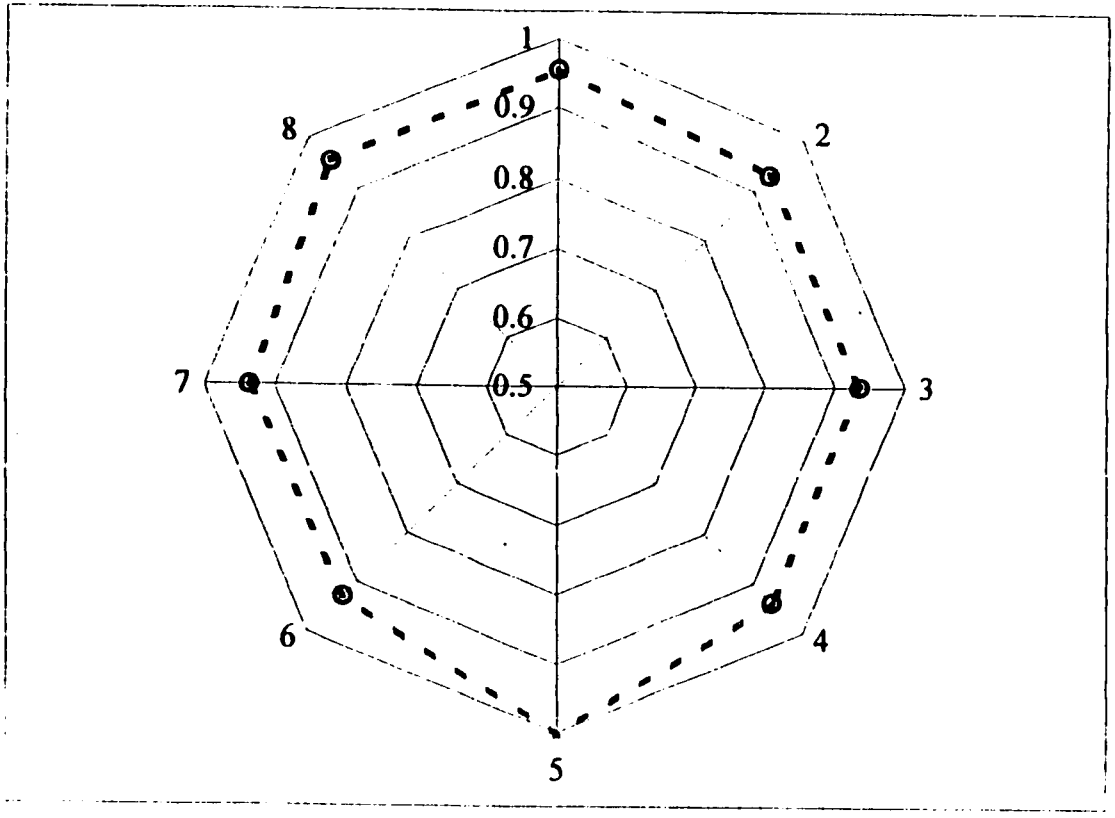

Figure 4.28 Percentage noise reduction with Highly perturbed nozzle. Mj = 1.44; microphone placed at a fixed radial location (15 Dj) and at different angular positions

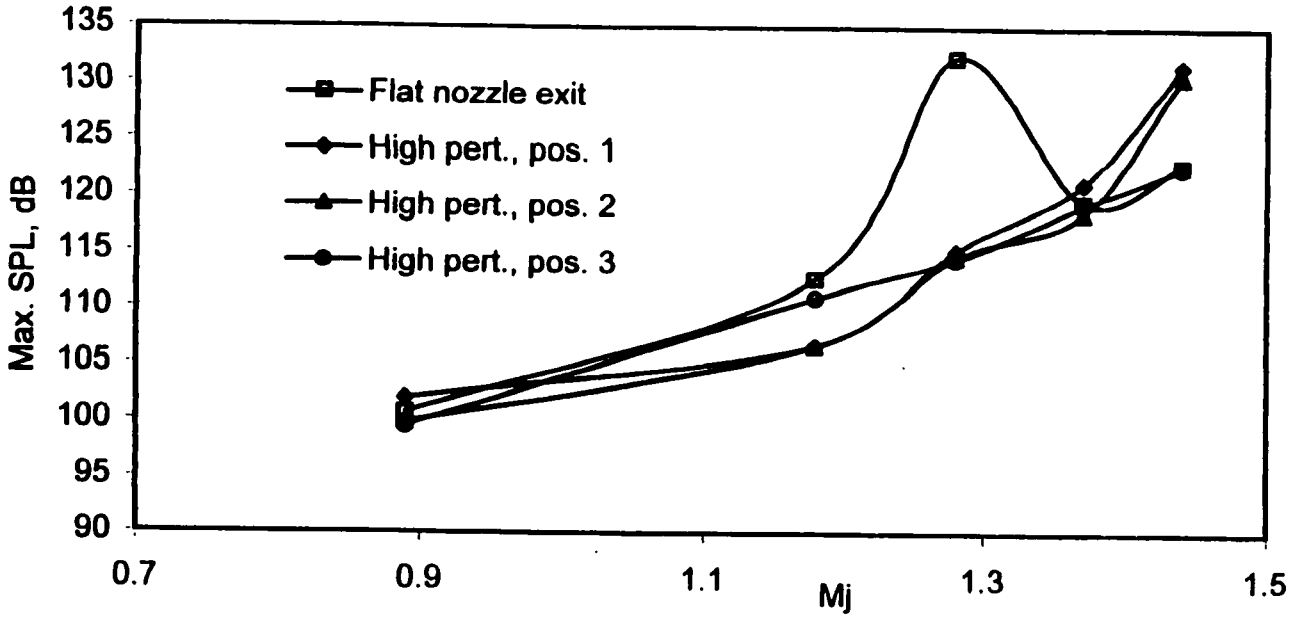

Figure 4.29. Comparison between SPL obtained with highly perturbed nozzle exit and flat nozzle exit

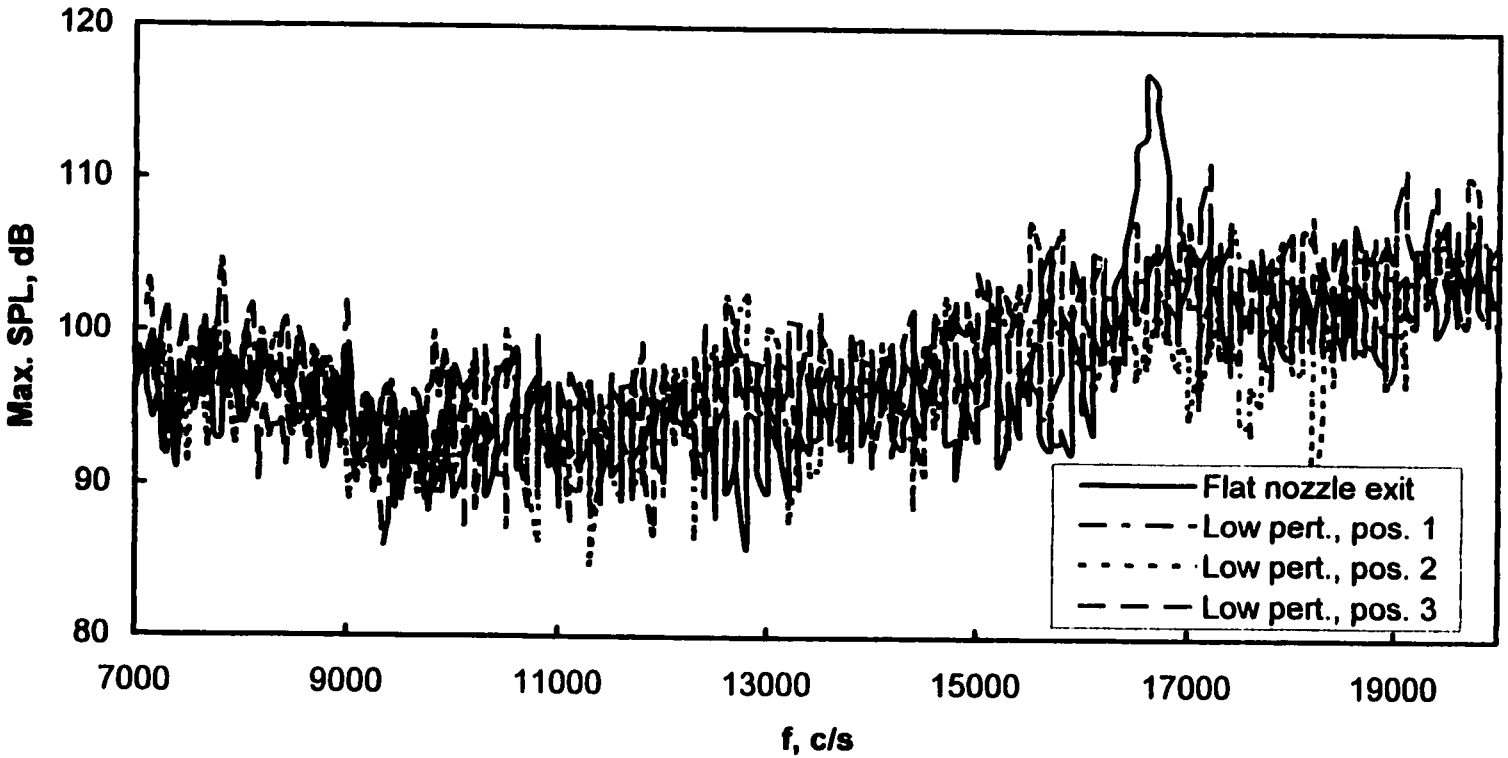

Figure 4.30 Spectrum Obtained with lower pertubation at the nozzle exit compared to that obtained with a plain nozzle exit. Mj = 1.28; microphone located radially 15 Dj from the jet centerline

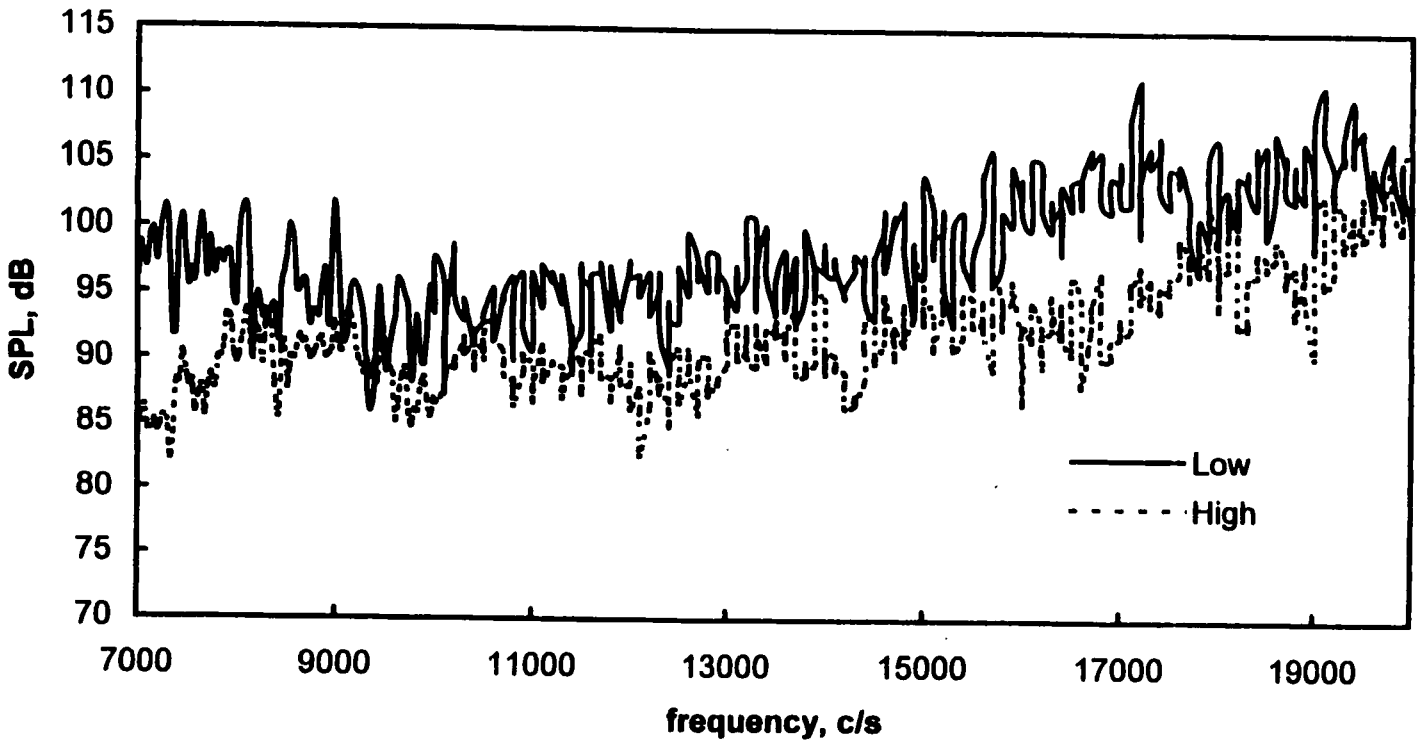

Figure 4.31. Comparison between the spectrum obtained with the two perturbed nozzles. Microphone located at zero angular position and is 15 Dj away from the jet centerline

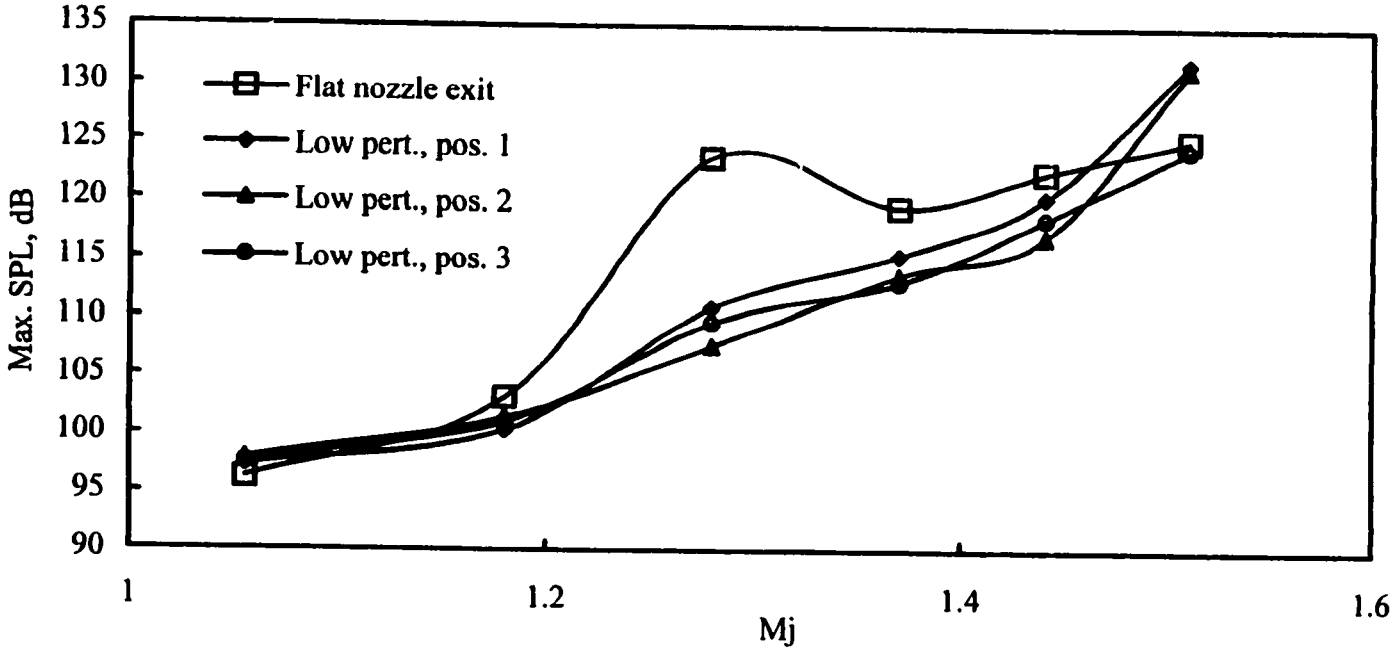

Figure 4.32. Comparison between SPL obtained with smaller perturbed nozzle exit and flat nozzle exit

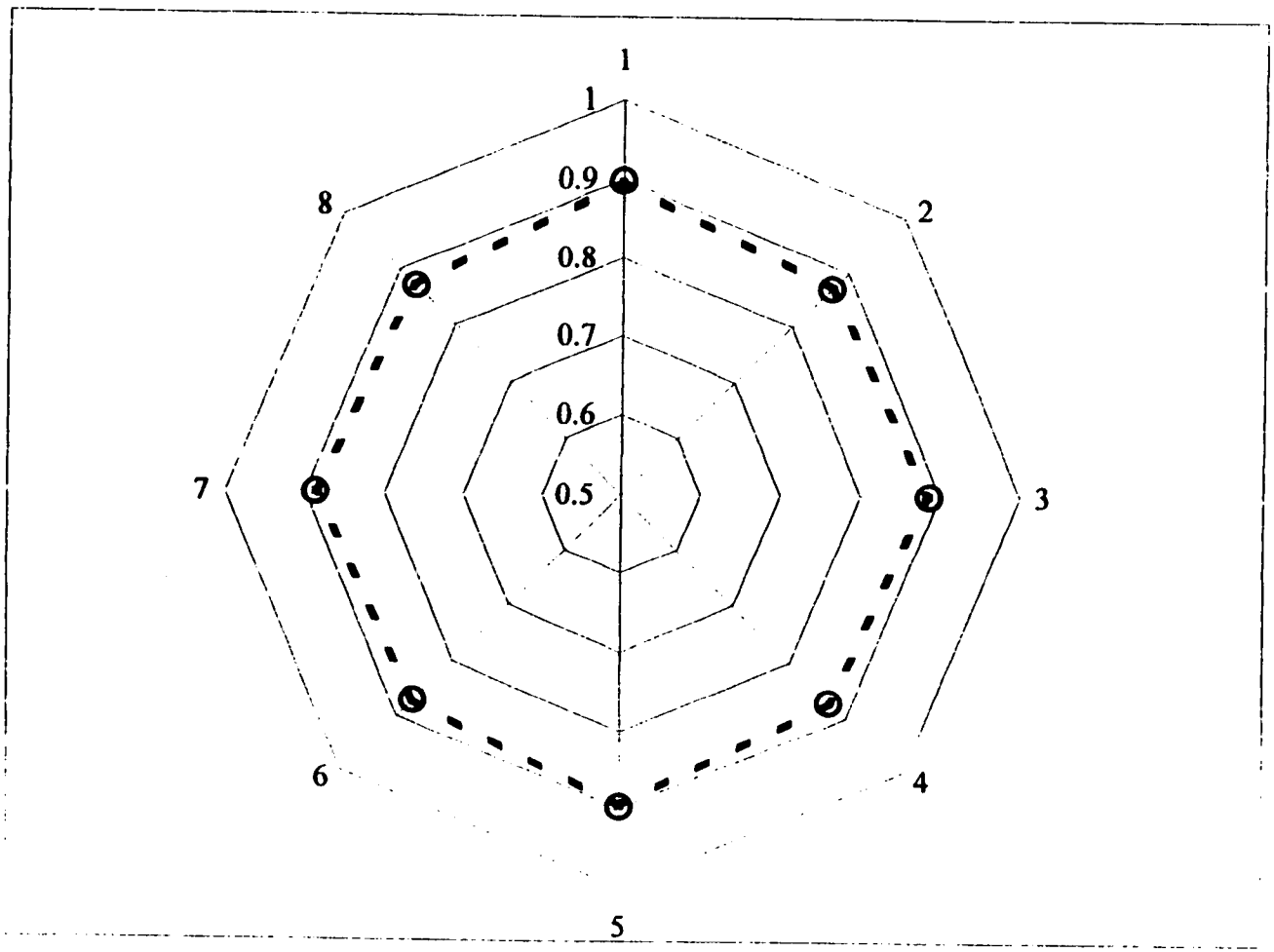

Figure 4.33 Percentage noise reduction with lower perturbation at the nozzle exit. Mj = 1.28

Chapter 5

Conclusions and Suggestions for Future Research

5.1.1 Noise Reduction by Swirl

The effect of swirl in noise reduction on supersonic jets was examined both optically, using Schlieren photography, and acoustically using a signal frequency analyzer. The results have shown that swirl behaves like an irrotational vortex as it approaches the nozzle. Using a large inlet area to the vortex chamber (slot size = 16 mm) resulted in a maximum value of the swirl Mach number, M_s, of 0.31 at the jet boundary. Decreasing the area was found to increase the swirl Mach number to a maximum measured value of 0.49.

The results obtained from the Schlieren photographs show that swirl does indeed affect the jet structure. As seen in the photographs, an increase in swirl yields a decrease in shock cell length, a decrease in the number of cells due to the increase in mixing with the surrounding fluid as well as the production of secondary shocks at higher pressures. Acoustically, for supersonic jets, low swirl is found to reduce the maximum SPL level as good as high swirl and by as much as 15 dB for M_j ranging between 1.18 and 1.4.

Swirl in supersonic jets was experimentally proven to reduce screech noise. However, in subsonic jets, it is better to use low swirl in order to minimize the turbulence effect resulting from the swirl [42].

5.1.2 Noise Reduction by Exit Modification

Perturbations on the nozzle exit were found to have a considerable effect on the screech noise. With a perturbed nozzle exit, the internal shock lost its symmetry and strength, resulting in noise suppression in both the broadband and screech noise. Maximum screech noise suppression was noted at a jet Mach number of 1.28. With the large perturbation case, the maximum SPL was found to decrease by as much as 15 dB from that measured with a plane nozzle exit. The effect was found to decrease monotonically with higher or lower jet Mach numbers.

5.2 Future work

With the existing apparatus and materials, the author may propose to extend this study in the future to cover the following:

- The bypass ratio of turbofan has been known to produce less noise. The addition of swirl to the secondary jet can be examined to reduce the noise even further.
- This study also can be extended to include the effect of swirl in twin jets. In this case the flow in one jet will be rotating in an opposite direction to the flow in the other jet.
- The use of more sophisticated equipment such as a high speed video camera will definitely help in obtaining a better understanding of any flow interaction and stability.
- The use of ejectors is found to eliminate screech noise as shown in figure 5.1 for a jet Mach number of 1.28. In this case, measurements were made 90 degrees to the jet axis and the microphone was placed near the jet exit. This method is found to be very effective in controlling screech noise. Future work in this area is, however, required to find the effect of the ejector's diameter, length and the distance it extends from the nozzle exit plane on screech noise suppression.

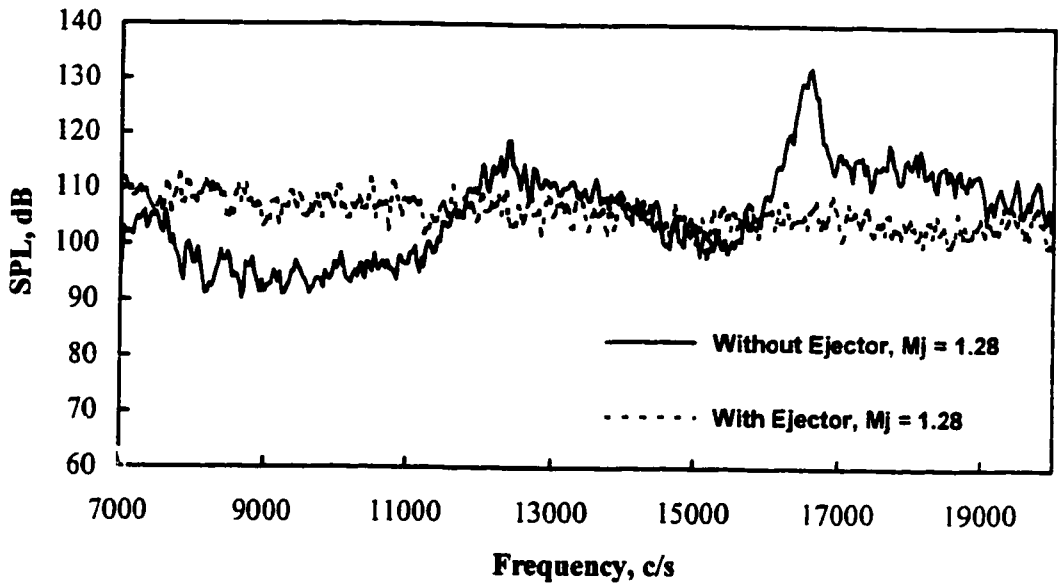

Figure 5.1 Comparison between the sound spectrum measured with and without ejector, $M_j = 1.28$

Bibliography

1. Tanna, H.K., " An experimental study of jet noise ", Part II: " Shock associated noise", *Journal of sound and vibration*, no. 50, 1977, pp. 429-444.
2. Crow, S. C. and Champagne, F. H. "Orderly Stuctures in Jet Turbulence", Journal of Fluid Mechanics, Vol. 28, 1971, pp. 547-591.
3. Browand, F. K. and Laufer, J., "The role of Large Scale Structuresin The Initial Development of Circular Jets", Proceedings of The 4th Biennial Symposium on Turbulence in Liquids, University of Missouri-Rolla, Science Press, 1975, pp. 333-344.
4. Hussain, A. K. M. F. and Zamman, A. B. M. Q., "Vortex pairing in circular Jet Under controlled Excitations", Part 2. Coherent Structure Dynamics", Journal of Fluid Mechanics, Vol. 101, 1980, pp. 493-544.
5. Kiebens, V., "Discrete Noise Spectrum Generated by an Acoustically Excited Jet", AIAA Journal, Vol. 18, 1980, pp. 434-441.

6. Laufer, J. and Yen, T., "Noise Generation by a Low-Mach Number Jet", Journal of Fluid Mechanics, Vol. 134, 1983, pp. 1-31.

7. Bridges, J. E. and Hussain, A. K. M. F., Roles of Initial Conditions and Vortex Pairing in Jet Noise", Journal of Sound and Vibrations, Vol. 117, 1987, pp. 289-311.

8. Hussain, A. K. M. F., Coherent Structures-Realityand Myth", Physics of Fluid, Vol. 26, 1983, pp. 2816-2850.

9. Yule, A. J. "Large Scale Structures in the Mixing Layerof a Round Jet", Journal of Fluid Mechanics, Vol. 89, 1978, pp. 413-432.

10. Van Dyke, An Album of Fluid Motion, 1982, Parabolic Press.

11. Ko, N. W. M. and Tang, S. K., "A Study on the Noise Generation Mechanism in a Circular Air Jet", Transactions of the ASME, Vol. 115, 1993, pp. 425-435.

12. Gutmark, E., Shadow, K. C. and Bicker, C. J., "Mode Switching in Supersonic Circular Jets", *Phys. Fluids A*, Vol. 1, No. 5, May 1989, pp. 868-873.

13. Powell, A., "On the mechanism of choked jet noise", *Proceeding of phy. Soc.*, Part B, No. 66, (1953), pp. 1039-1056.

14. Davies, M. G. and Oldfield, D. E. S., "Tones from a Choked Axisymmetric Jet," *Acoustica*, Vol. 12, 1962, pp. 257-277.

15. Poldelvaart, L. J., Vink, A. T., and Wijnands, A. P. J., "The Photographic Evidence of the Feedback Loop of a Two Dimensional Screeching Supersonic Jet of Air, " *The 6th International Congress on Acoustics*, Tokyo, Japan, Aug. 1968, F101-F104.

16. Lighthill, M. J., " Jet noise ", *AIAA Journal*, vol. 1, no. 7, 1963, pp.1507-1517.

17. Harper-Bourne, M. and Fisher, M. J., "The Noise from Shock Waves in Supersonic Jets", *AGARD-CP-131,* 1973, pp. 11-1-11-3.

18. Seiner, J. M and Norum, T. D., "Experiments on shock associated noise of supersonic jets", *AIAA Journal*, no. 79, pp. 1526-1979.

19. Tam, C.K.W, " On the noise nearly ideally expanded supersonic jet", *Journal of fluid Mech.*, no. 51, (1982), pp. 69-95.

20. Tam, C. K. W. and Chen, K., "A statistical model of turbulence in two dimensional mixing layer", *Journal of fluid Mech.*, no. 92, (1985), pp. 303-326.

21. Smith, Michael J. T., "Aircraft Noise", Cambridge University Press, 1989

22. Laurence, J. C. and Benninghoff, J. M., "Turbulent measurements in multiple interfering Air Jets", NASA TN 4029.

23. Ahuja, K.K. and Steven, J. C., "Recent advances in active noise control", *AIAA Journal*, Vol. 29, no. 7, 1990, pp. 1058-1065.

24. Kuhlman J.M., "Variation of entrainment in annular jets", *AIAA journal*, May 1987, pp. 374-378.

25. Ahuja, K.K. and Brown, W.H., "Shear flow control by mechanical tabs", *AIAA Paper No. 89-0994,* 1989.

26. Bradbury, L. and Khadem, A., "The distortion of a jet by tabs", *Journal of fluid Mech.*, vol. 70, no. 4, 1975, pp. 801-813.

27. Samimy, M., "Effect of tabs on the flow and noise field of an axisymmetric jet", *AIAA journal*, vol. 13, no. 4, April 1993, pp. 609-619.

28. Seiner, J.M. and Manning, J. C., "Model and full scale study of twin supersonic plume resonance", *AIAA Paper No. 87-0244,* Jan. 1987.

29. Shaw, L., " Twin jet Screech suppression ", *Journal of Aircraft*, Vol. 27, No. 8, 1990, pp. 708-715.

30. Neemeh, R. and Roshanzamir, A., "Experimental studies of single and twin supersonic jets noise and stability", *Proceedings of the 3rd International Congress on Air and Structure Born Sound and Vibration, Montreal, Canada,* June 1994, pp. 1177-1184.

31. Longmire, E. K., Eaton, J. K. and Elkins, C. J., "Control of Jet Structure by Crow-Shaped Nozzles", *AIAA journal*, no. 2, Feb. 1992, pp. 505-512.

32. Reynolds, A., "Similarity in Swirling Wakes and Jets", *Journal of Fluid Mechanics*, Vol. 14, 1962, pp. 241.

33. Rose, W. G., "A Swirling Round Turbulent Jet", *Journal of Applied Mechanics*, Vol. 29, 1962, pp. 615-625.

34. Smith R., "An investigation of Supersonic Swirling Jets", *Aeronautical Quarterly*, vol. 24, 1973, pp. 167-178.

35. Carpenter, W. P., "A linearized theory for swirling supersonic jets and its application to shock cell noise", *AIAA Journal* **23**, 1985, pp. 1902-1909.

36. Carvalho, I. S. and Heitor, M. V., "Visualization of Vortex Breakdown in Turbulent Unconfined Jet Flows", *Optical Diagnostics in Engineering*, vol. 1(2), 1996, pp. 22-30.

37. Y. Yu and R.-H. Chen 1997 *Jounal of Sound and Vibration* **205**(5), 698-705. A study of screech tone noise of supersonic swirling jets.

38. W. S. Janna, Introduction to Fluid Mechanics, 3rd ed., Boston: PWS - Kent, 1993, pp. 434-440.

39. Saad, M. A., "Compressible Fluid Flow", 2nd ed., Prentice-Hall, 1993.

40. Feyedelem, M. S. and Sarpkaya, T., "Free- and Near-Free-Surface Swirling Turbulent Jets", AIAA Journal, vol. 36, March 1998, pp. 359-364.

41. Gupta A.K., Lilley D.G. and Syred N., "Swirl flows", Abacus Press, Energy and Engineering Series, Tunbridge Wells, UK, 1984.

42. Neemeh, R. A., AlGattus, S. and Neemeh, L., "Experimental Investigation of Noise Reduction in Supersonic Jets due to Jet Rotation", Journal of Sound and Vibrations, vol. 222 (3), April 1999, pp. 505-524.